Institut für Wasserbau · Universität Stuttgart

Mitteilungen

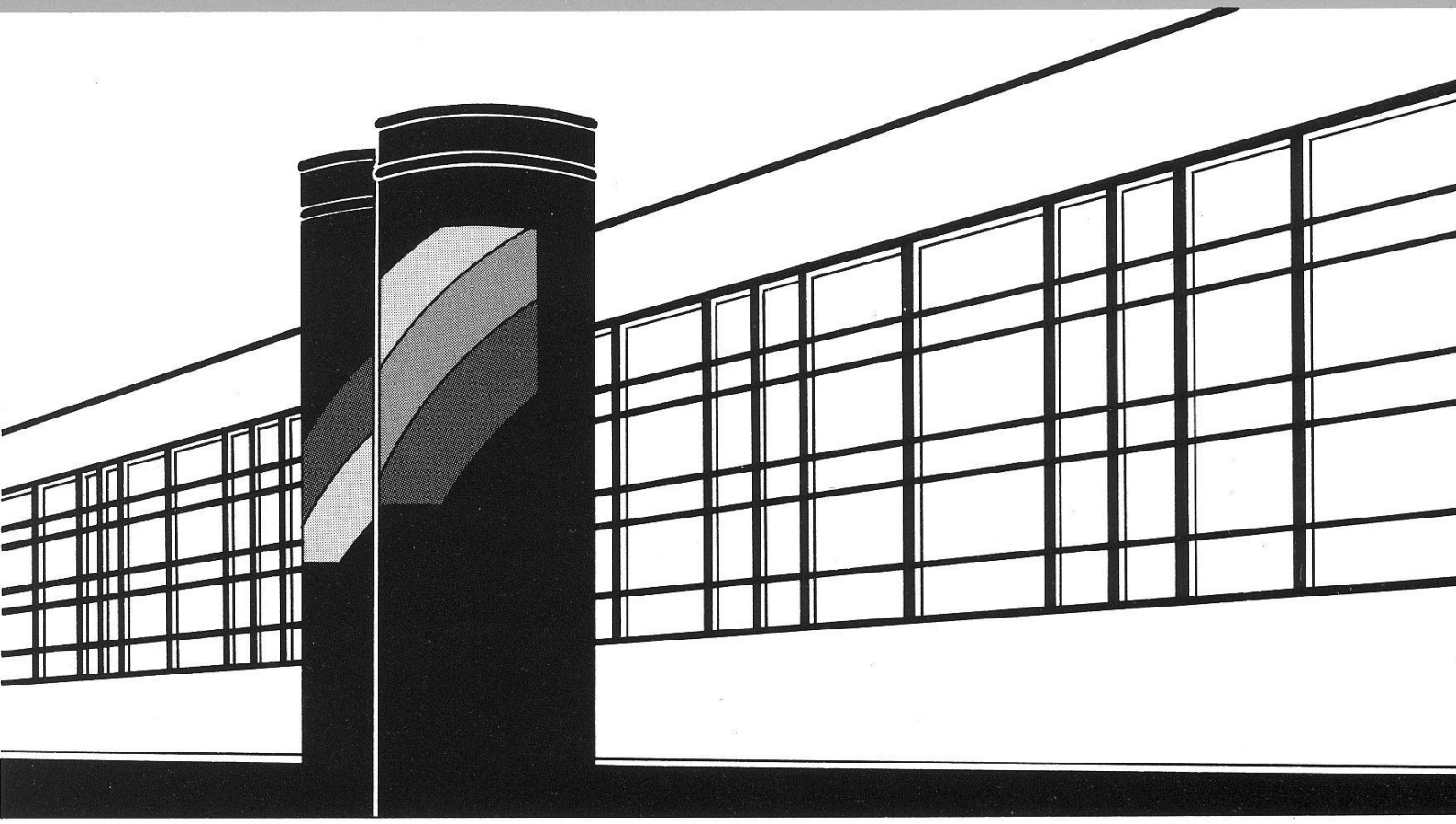

Heft 192

Jochen Fritz

A Decoupled Model for Compositional Non-Isothermal Multiphase Flow in Porous Media and Multiphysics Approaches for Two-Phase Flow

A Decoupled Model for Compositional Non-Isothermal Multiphase Flow in Porous Media and Multiphysics Approaches for Two-Phase Flow

Von der Fakultät Bau- und Umweltingenieurwissenschaften der Universität Stuttgart zur Erlangung der Würde eines Doktor-Ingenieurs (Dr.-Ing.) genehmigte Abhandlung

Vorgelegt von

Jochen Fritz

aus Tübingen

Hauptberichter:	Prof. Dr.-Ing. Rainer Helmig
Mitberichter:	Prof. Dr. ir. S. Majid Hassanizadeh
	Prof. Ivar Aavatsmark, PhD

Tag der mündlichen Prüfung: 07.06.2010

Institut für Wasserbau der Universität Stuttgart
2010

Heft 192

A Decoupled Model for Compositional Non-Isothermal Multiphase Flow in Porous Media and Multiphysics Approaches for Two-Phase Flow

von

Dr.-Ing.
Jochen Fritz

Eigenverlag des Instituts für Wasserbau der Universität Stuttgart

D93 A Decoupled Model for Compositional Non-Isothermal Multiphase Flow in Porous Media and Multiphysics Approaches for Two-Phase Flow

Bibliografische Information der Deutschen Nationalbibliothek
Die Deutsche Nationalbibliothek verzeichnet diese Publikation in der Deutschen Nationalbibliografie; detaillierte bibliografische Daten sind im Internet über http://www.d-nb.de abrufbar

Fritz, Jochen:
A Decoupled Model for Compositional Non-Isothermal Multiphase Flow in Porous Media and Multiphysics Approaches for Two-Phase Flow / von Jochen Fritz. Institut für Wasserbau,
Universität Stuttgart. - Stuttgart: Inst. für Wasserbau, 2010

(Mitteilungen / Institut für Wasserbau, Universität Stuttgart: H. 192)
Zugl.: Stuttgart, Univ., Diss., 2010
ISBN 978-3-933761-96-5
NE: Institut für Wasserbau <Stuttgart>: Mitteilungen

Herausgegeben 2010 vom Eigenverlag des Instituts für Wasserbau
Druck: Document Center S. Kästl, Ostfildern

Danksagung

Die vorliegende Arbeit entstand im Rahmen des Internationalen Graduiertenkollegs NUPUS, finanziert durch die Deutsche Forschungsgemeinschaft DFG (GRK 1398) und die Nederlandse Organisatie voor Wetenschappelijk Onderzoek NWO (DN 81-754).

Ich möchte allen danken, die zum Gelingen dieser Arbeit beigetragen haben. Zuvorderst sei hier mein Betreuer Prof. Rainer Helmig genannt. Seine Begeisterung und Entdeckungsfreude haben mir gezeigt, was Wissenschaft bedeuten muss und seine Ratschläge und sein nie endender Optimismus waren von unschätzbarem Wert. Prof. Majid Hassanizadeh und Prof. Ivar Aavatsmark danke ich für die Übernahme des Mitberichts und die Begutachtung in Rekordzeit. Mein ganz besonderer Dank gilt auch allen Kollegen am Lehrstuhl und im Graduiertenkolleg, die dieses ganz besondere Arbeitsklima entstehen ließen, das es an keinem zweiten Ort der Welt gibt. Prudence Lawday und Maria Costa danke ich für ihre Geduld und Hilfe in allen Lebenslagen; Anozie Ebigbo und Bernd Flemisch dafür, dass sie all die Charakterstärke aufgebracht haben, derer es bedarf um sich ein Bürozimmer mit mir zu teilen, und dass Sie ihre Erfahrungen und ihr Wissen mit mir geteilt haben (*Die Massenbilanz lügt nie!* – A. Ebigbo); Benjamin Faigle danke ich für die Hilfe beim Programmieren und das Lektorat dieser Arbeit; Irina Komarova, Anna Kuhlmann und Florian Doster für die Gute Zeit bei NUPUS-Veranstaltungen und bei gemeinsamen Abenden und Holger Class für die Erklärungen der nicht-isothermen Strömungen und die Selbstversuche zu denselben.

Ganz besonders hervorheben will ich meine Familie. Ohne sie wäre ich nicht da, wo ich bin. Meinen Großeltern Else und Hans Beck danke ich für ihre grenzenlose Liebe, meinen Großeltern Hildegard und Erwin Fritz für die Unterstützung meines Studiums. Meiner Mutter Gabriele Fritz danke ich für all ihr Vertrauen, ihre bedingungslose Unterstützung und dass Sie immer zu mir hält. Leider starb mein Vater Jürgen Fritz zu früh, nicht nur um das Ende meiner Promotion zu erleben. Im Geiste sehe ich Ihn, wie er am Tag meiner Doktorprüfung mit geschwellter Brust durch das Institut geschritten wäre. Danken möchte ich auch meinem Schwiegervater Harald Budelmann. Er verstand es, in manchem Gespräch die Zweifel zu vertreiben, die zuweilen an mir nagten.

Mein größter Dank gebührt meiner Frau Lina. Sie ertrug meine Zerstreutheit und richtete mich wieder auf, wenn ich schwarz sah. Danke, für jeden einzelnen Tag! In der Schlussphase der Promotion war mir die freudige Erwartung unserer Tochter Emma der größte Ansporn, meine Arbeit zu Ende zu bringen. Ihr sei diese Arbeit gewidmet.

Ever tried. Ever failed. No matter. Try again. Fail again. Fail better.
– Samuel Beckett

Contents

Contents I

Nomenclature VI

Abstract XI

Zusammenfassung XIII

1 Introduction 1
- 1.1 Literature . . . 3
- 1.2 Structure . . . 5

2 Physical Model 8
- 2.1 Definition of scales and domains . . . 8
- 2.2 Representative elementary volume concept . . . 9
- 2.3 Fluid properties . . . 10
  - 2.3.1 Phase composition . . . 10
  - 2.3.2 Density . . . 11
  - 2.3.3 Viscosity . . . 12
  - 2.3.4 Internal energy and enthalpy . . . 13
  - 2.3.5 Phase equilibria . . . 15
- 2.4 Permeability and Darcy's law . . . 17
- 2.5 Multi-phase flow in porous media . . . 19
  - 2.5.1 Saturation . . . 19
  - 2.5.2 Capillarity . . . 20
  - 2.5.3 Relative permeabilities and extended Darcy's law . . . 21
- 2.6 Balance equations . . . 22
  - 2.6.1 Multi-phase flow and transport . . . 23
  - 2.6.2 Compositional multi-phase flow and transport . . . 23
  - 2.6.3 Non-isothermal Systems . . . 24
- 2.7 Model formulations . . . 26
  - 2.7.1 Fully coupled formulations . . . 27
  - 2.7.2 Decoupled formulations . . . 29
- 2.8 Multiphysics concepts . . . 33
  - 2.8.1 Multiphysics concept for isothermal systems . . . 34

2.8.2 Multiphysics concept for non-isothermal Systems 37
2.9 Summary 39

3 Numerical Implementation 40
3.1 General remarks 41
3.2 Time discretization 42
3.3 Isobaric flash calculation 45
3.3.1 Rachford-Rice equation 45
3.3.2 Equilibrium ratios 48
3.3.3 Isothermal isobaric flash 52
3.3.4 Isoenergetic isobaric flash 56
3.4 Spatial discretization: Finite Volumes 58
3.4.1 Pressure equation 58
3.4.2 Transport equations 64
3.4.3 Determination of coefficients by full upwinding 65
3.4.4 Evaluation of derivatives of total specific volume 66
3.5 Adapted time discretization 68
3.6 Multiphysics Implementation 68
3.6.1 Multiphysics implementation for isothermal two-phase two-component systems 70
3.6.2 Multiphysics implementation for non-isothermal two-phase two-component systems 72
3.6.3 Subdomain adaptivity 73

4 Test cases 77
4.1 Non-isothermal single-phase flow 77
4.2 Single-component two-phase flow 82
4.3 Non-isothermal two-phase two-component flow 86
4.4 Isothermal three-phase three-component flow 91
4.5 Discussion - Model applicability and oscillating pressures 93

5 Examples for applications 96
5.1 Injection of CO_2 into the Johansen formation 96
5.2 Enhanced remediation of subsurface contaminations 99

6 Summary and Outlook 102

Bibliography 106

List of Figures

1.1 Flow regimes in a porous medium. 2
1.2 Vertical and horizontal model coupling. 4
1.3 Exemplarily overview of horizontal and vertical coupling methods. . . . 6

2.1 Definition of model domain and subdomains. 8
2.2 Relation between an averaged quantity and the size of the averaging volume (after Bear [1972]). 10
2.3 Angular velocity and shear stress. 12
2.4 Selected viscosities at atmospheric pressure. 14
2.5 Vapor pressures of water and xylene 16
2.6 Applicability of Henry's law and Raoult's law for a binary gas–liquid system (after Lüdecke and Lüdecke [2000]). 18
2.7 Contact angle between solid surface and fluid interface. 20
2.8 Example for a possible multiphysics application and decomposition of the model domain. 34
2.9 Multiphysics decomposition of the model domain for non-isothermal models. 38

3.1 Examples for computational grids. 40
3.2 IMPES / IMPESC solution technique. 43
3.3 Phase mass fractions and internal energy per unit mass of a water air mixture. 56
3.4 Two-phase isoenergetic flash calculations for moderate (left) and very low concentrations (right) of gas component. 58
3.5 Vector and interface notation in FVM scheme. 61
3.6 Non-Cartesian, regular grid with constant inclination. 63
3.7 Tangent and secant method for numerical derivatives. 67
3.8 Program cycle of the decoupled compositional model. 69
3.9 Example setup for isothermal 2p2c multiphysics model. 73
3.10 Breakthrough curves of 2p2c model and multiphysics model. 74
3.11 Saturations in full 2p2c model and multiphysics model with fixed and adaptive 2p2c-subdomain. 75

4.1 Setup of single-phase non-isothermal flow flume experiment. 78

4.2 Initial concentration distribution of the non-isothermal single-phase experiment. . . . 80
4.3 Comparison of measured and simulated temperatures for 2-D heat well experiment. . . . 81
4.4 Comparison of measured and simulated tracer concentrations for 2-D heat well experiment. . . . 83
4.5 Comparison of simulation results for steam injection into a water-saturated 1-D domain. . . . 85
4.6 Comparison of simulation results for steam injection in a water-saturated 2-D domain. . . . 86
4.7 Sketch of the setup of the 1-D column experiment. . . . 87
4.8 Measurements and simulation results for steam injection into dry horizontal column. . . . 89
4.9 Measurements and simulation results for injection of hot air into residually saturated sand column. . . . 92
4.10 Setup of 3p3c soil vapor extraction example. . . . 93
4.11 Simulation results of 3p3c soil vapor extraction after 13 hours. . . . 94

5.1 Permeability and porosity inside the Johansen formation. . . . 97
5.2 Model results after 25 years of carbon dioxide injection into the Johansen formation. . . . 97
5.3 Transient model results of full 2p2c-model and multiphysics model for carbon dioxide injection into the Johansen formation. . . . 98
5.4 Isosurfaces of permeability, initial contamination and position of wells and heat wells for enhanced subsurface remediation example. . . . 100
5.5 Contaminant mass and extend of subdomains in course of simulation of enhanced subsurface remediation example. . . . 101
5.6 Extend of subdomains during the simulation of enhanced subsurface remediation example with the non-isothermal multiphysics model. . . . 101

List of Tables

2.1 Conservation equations for fluid flow in porous media. 28
2.2 Pressure equations for flow and transport in porous media. 39

3.1 Equilibrium ratios for a two-component gas / liquid system. 50
3.2 Equilibrium ratios for a three-component gas / liquid / liquid system. . 52

4.1 Model parameters for 2-D single-phase non-isothermal setup. 79
4.2 Model parameters for steam injection in one-dimensional domain. . . . 84
4.3 Model parameters for injection of steam and hot air into the glass column. 88

Nomenclature

Symbol	Description	Dimension
G	Control volume	
Γ	Control volume boundary	
Ω, Ω_i	Model domain, i-th subdomain.	
$\partial\Omega$, $\partial\Omega_{ij}$	External boundary, internal boundary between i-th and j-th subdomain	
Scalars		
ε	Error term	$[s^{-1}]$
ϕ	Porosity	$[-]$
φ^κ	Fugacity coefficient of component κ	$[-]$
ϱ_α	Density of phase α	$\left[\mathrm{kg/m^3}\right]$
ϱ_s	Density of solid	$\left[\mathrm{kg/m^3}\right]$
λ_α	Mobility of phase α	$[1/(\mathrm{Pa}\cdot\mathrm{s})]$
λ_{pm}	Heat conductivity of the porous medium	$[\mathrm{W}/(\mathrm{m}\cdot\mathrm{K})]$
τ	Shear stress	$\left[\mathrm{Pa/m^2}\right]$
μ	Dynamic viscosity	$[\mathrm{Pa}\cdot\mathrm{s}]$
μ^κ	Chemical potential of component κ	
ν	Kinematic viscosity	$[\mathrm{m^2/s}]$
ν_α	Mass fraction of phase α	$[-]$
ν_α	Mole fraction of phase α	$[-]$
$\sigma_{\alpha\beta}$	Surface tension between phases α and β	$[\mathrm{N/m}]$
A	Area	$[\mathrm{m^2}]$
a	Coefficient for timestep control	$[-]$
C_α^κ	Concentration of component κ in phase α	$\left[\mathrm{kg/m^3}\right]$
C^κ	Total concentration of component κ	$\left[\mathrm{kg/m^3}\right]$
C_v	Total heat capacity per unit volume	$[\mathrm{J}/(\mathrm{kg}\cdot\mathrm{K})]$
c_p, c_v	Isobaric and isochoric specific heat capacity, respectively	$[\mathrm{J}/(\mathrm{kg}\cdot\mathrm{K})]$

Symbol	Description	Dimension
c_s	Specific heat capacity of solid phase	$[\mathrm{J}/(\mathrm{kg}\cdot\mathrm{K})]$
c_t	Total compressibility	[1/Pa]
E, e	Extensive and intensive conserved quantity	
f_α	Fractional flow factor of phase α	$[-]$
f^κ	Fugacity of component κ	[Pa]
H, h	Enthalpy and specific enthalpy, respectively	[J], [J/kg]
Δh_{sol}	Specific enthalpy of solution	[J/kg]
Δh_{vap}	Specific enthalpy of vaporization	[J/kg]
H_α^κ	Henry coefficient of component κ in phase α	$[Pa]$
K	Scalar permeability	$[\mathrm{m}^2]$
K_α^κ	Equilibrium ratio for component κ in phase α	$[-]$
$k_{r,\alpha}$	Relative permeability of phase α	$[-]$
$\bar{l}$	Mean discretization length	[m]
M^κ	Molar mass of component κ	[kg/mole]
$\bar{M}^\alpha$	Mean molar mass of phase α	[kg/mole]
m	Mass	[kg]
n_α^κ,n_α	Number of moles of component κ in phase α and total number of moles in phase α, respectively	$[-]$
p_α	Pressure in phase α	$[Pa]$
p_c	Capillary pressure	$[Pa]$
p_{vap}	Vapor Pressure	$[Pa]$
Q	Volumetric flux	$[\mathrm{m}^3/\mathrm{s}]$
q^α	Volumetric source of phase α	$[\mathrm{m}^3/(\mathrm{s}\cdot\mathrm{m}^3)]$
q^κ	Mass source of component κ	$[kg/(\mathrm{s}\cdot\mathrm{m}^3)]$
q^u	Heat source	$\left[\mathrm{W}/\mathrm{m}^3\right]$
R, R_s	Total and specific gas constant, respectively	$[\mathrm{J}/(\mathrm{mole}\cdot\mathrm{K})]$, $[\mathrm{J}/(\mathrm{kg}\cdot\mathrm{K})]$
S_α	Saturation of phase α	$[-]$
S_e	Effective saturation	$[-]$
$S_{r,\alpha}$	Residual saturation of phase α	$[-]$
T	Temperature	[K]
t	Time	[s]
Δt	Timestep	[s]

Symbol	Description	Dimension
U, u	Internal Energy and specific internal energy, respectively	[J], [J/kg]
u_t	Total internal energy per unit volume	$\left[\mathrm{J/m^3}\right]$
V	Volume	$[\mathrm{m^3}]$
$\lvert V\rvert$	Control volume cubature	$[\mathrm{m^3}]$
v_t	Total specific fluid volume	$[\mathrm{m^3/m^3}]$
X_α^κ	Mass fraction of component κ in phase α	$[-]$
x	Coordinate in first (horizontal) direction	[m]
Δx	Discretization length in x-direction	[m]
x_α^κ	Mole fraction of component κ in phase α	$[-]$
y	Coordinate in second (horizontal) direction	[m]
Δy	Discretization length in second (horizontal) direction	[m]
Z^κ	Feed mass fraction of component κ	$[-]$
z^κ	Feed mole fraction of component κ	$[-]$
z	Coordinate in third (vertical) direction	[m]
Vectors/Matrices		
$\mathbf{\Phi}$	Potential gradient	[Pa/m]
$\mathbf{A}$	Stiffness matrix	
$\mathbf{D}_{pm}$	Hydrodynamic dispersion tensor	$[\mathrm{m^2/s}]$
$\mathbf{g}$	Vector of gravity	$\left[\mathrm{m/s^2}\right]$
$\mathbf{J}$	Conductive heat flux	$\mathrm{W/m^2}$
$\mathbf{n}$	Unit normal vector on control volume surface	[m]
$\mathbf{r}$	Right hand side vector	
$\mathbf{s}$	Substitute for normal vector	[m]
$\mathbf{u}$	Vector of unknowns	
$\mathbf{u}_k$	Vector connecting cell center with center of k-th neighbor	[m]
$\mathbf{v}_\alpha$	Velocity of phase alpha	[m/s]
$\mathbf{w}$	Dispersive mass flux	$[\mathrm{kg/\left(m^2 \cdot s\right)}]$
Subscripts		
α, β	Phase	
w	Wetting phase	

Symbol	Description	Dimension
n	Non-wetting phase	
g	Gas phase	
r	Reference phase	
e	Phase eliminated from Rachford-Rice equation	
k	Neighbor cell	
Superscripts		
κ, ι	Component	
A, B, C	Discrete component	

Abstract

The demands of computational resources of a simulator and the necessary efforts in defining boundary and initial conditions increase with the physical complexity of a model. Thus, a trade-off between physical accuracy and computational demands of a model are made. In many practical applications of porous media flow simulators, the most complex processes are confined to a small part of the model domain. In such a case, either high complexities are neglected in favor of a slim model or all processes are captured with a complex model which is superfluous in large parts of the domain. As a compromise between both options, an interface coupling method is introduced. It couples simple and complex models and adapts the resulting multiscale model to the actually occurring physical processes. As a basis for this, a decoupled formulation for non-isothermal compositional multiphase flow is introduced. It provides the advantage that the size of the linear system of equations does not grow with the number of phases or components involved.

This work reviews the common concepts for the description of multiphase flow in porous media and provides a consistent derivation of the conservation equations of non-isothermal compositional flow and transport processes. Based on these equations, decoupled formulations for isothermal and non-isothermal compositional flow are derived using the concept of local conservation of total fluid volume. The implementation of the derived formulations into a finite volume method with an implicit pressure explicit concentration time discretization is presented. The resulting simulation tool is tested and verified with results from different experimental and computational investigations and its range of applicability is considered.

Based on the decoupled formulations derived before, an isothermal and a non-isothermal multiphysics concepts for the transition of complexity within a porous media domain is presented. Furthermore, a simple and robust subdomain control scheme is developed which assures optimal adaption of the model complexity to the occurring processes at any time. Both models are implemented and tested towards their accordance with the globally complex decoupled models. It is shown that computational demands of a simulator can be lowered by incorporation of the multiphysics schemes. Finally, further ideas for the extension of the multiphysics towards more complex systems and possible interfaces with multiscale methods are considered.

Zusammenfassung

Numerische Modelle zur Beschreibung von Mehrphasen-Mehrkomponentenströmungsprozessen in porösen Medien finden vielfältigen Einsatz bei der Lösung technischer oder umweltrelevanter Fragestellungen aus Wissenschaft und Industrie. Seit der Einführung erster Grundwassermodelle hat sich die Komplexität der Modelle und der beschreibbaren Prozesse enorm gesteigert. Die Anwendbarkeit hochkomplexer numerischer Modelle wird jedoch durch verfügbare Rechenkapazitäten und die finanzielen und technischen Möglichkeiten zur Messung entsprechend detailierter Eingangswerte begrenzt. Dies begründet eine Abwägung zwischen der physikalischen Genauigkeit eines Modells einerseits und seiner Aufwändigkeit andererseits. Zwar sollte die Auswahl des Modells so erfolgen, dass alle relevanten physikalischen Prozesse abgebildet werden, allerdings ist es möglich, dass die verfügbaren Rechenkapazitäten oder Messwerte den Anforderungen des Modells nicht gerecht werden. Wenn sich nun sehr komplexe physikalischen Prozesse auf einen kleinen Teil des zu untersuchenden Gebiets beschränken, eröffnen sich grundsätzlich die zwei Möglichkeiten, die komplexen Prozesse entweder zu vernachlässigen um ein schlankes Modell benutzen zu können oder ein detailiertes Modell zu verwenden, das in der Lage ist alle auftretenden Prozesse abzubilden, dessen Komplexität aber in großen Teilen des zu untersuchenden Gebiets überflüssig ist. Erstere Möglichkeit hat den Nachteil, dass eventuell wichtige Vorgänge nicht abgebildet werden können, Zweitere, dass hoher Aufwand erzeugt wird, der zu großen Teilen vermeidbar sein sollte. Aus diesem Konflikt heraus ergibt sich die Motivation, eine Mutliphysics-Methodik zu entwickeln, die die Modellkomplexität den tatsächlich auftretenden Vorgängen anpasst, um dadurch beide vorgenannten Nachteile zu überwinden und ein schlankes und gleichzeitig hinreichend genaues Modell zu erlangen.

Die Basis für jedes numerische Modell bilden mathematische Formulierungen der auftretenden Fluss- und Transportprozesse. Diese lassen sich im Fall der Mehrphasenströmungen in porösen Medien in voll Gekoppelte (auch voll implizit genannt) und Entkoppelte (oder sequentielle) unterteilen. Die Namensgebung rührt im Wesentlichen von der Lösungsmethodik des sich ergebenden Systems partieller Differentialgleichungen her. Während die Primärvariablen bei der voll gekoppelten Formulierung simultan in einem iterativen Prozess ermittelt werden, trennt die entkoppelte Formulierung die Drücke von den Erhaltungsgrößen um sie getrennt – oder eben entkoppelt – zu berechnen. Aufgrund der iterativen Lösungsstrategie sind voll gekoppelte Modelle im Allgemeinen flexibler bezüglich der Einführung neuer Prozesse in die mathematische Formulierung,

wohingegen dies bei entkoppelten Modellen in der Regel wesentlich mehr Aufwand erfordert. Es ist daher nicht verwunderlich, dass bisher keine einsatzbereiten Simulationsprogramme für die Berechnung von Mehrphasen-Mehrkomponentenströmungen in porösen Medien verfügbar sind, die auf entkoppelten Formulierungen basieren. Allerdings haben entkoppelte Modelle den entscheidenden Vorteil der weniger aufwändigen und schnelleren Lösung, was bei großen und komplexen Systemen in immensen Unterschieden zwischen voll gekoppelten und entkoppelten Modellen in der benötigten Rechenzeit resultieren kann. Aufgrund der klaren Trennung zwischen Fluidbewegung und Massen-/Energietransport in der entkoppelten Formulierung, eignet diese sich besonders gut für die Einbeziehung in das zu entwickelnde Multiphysics-Modell. Daher wird im Rahmen dieser Arbeit ein Beitrag zur Entwicklung eines entkoppelten Modells zur Modellierung von nicht-isothermen Mehrphasen-Mehrkomponentenströmungen in porösen Medien geleistet.

Entwicklung einer entkoppelten Formulierung für nicht-isotherme Mehrphasen-Mehrkomponentenströmungen Als Basis für die Umsetzung der angestrebten Multiphysicsmethoden wird eine entkoppelte Formulierung für nicht-isotherme Mehrphasen- Mehkomponentenströmungen in porösen Medien entwickelt. Dafür werden zunächst die relevanten physikalischen Prozesse beleuchtet und etablierte Methoden zu ihrer Beschreibung eingeführt. Diese dienen als Grundlage zur Formulierung von Erhaltungsgleichungen der Masse und Energie, die konstequent aus dem Reynold'schen Transporttheorem hergeleitet werden und die Systeme partieller Differentialgleichungen bilden, die die betrachteten Mehrphasenströmungen beschrieben. Zur Entkopplung dieser Differentialgleichungen wird für gewöhnlich die so genannte Fractional Flow Formulierung, welche auf Umformungen der Massenerhaltungsgleichung basiert, verwendet. Je nach Abwandlung wird Sie in der Literatur unterschiedlich benannt, wobei sich die Namen in der Regel auf die Behandlung der Phasendrücke beziehen. Lokale Änderungen des Fluidvolumens werden darin lediglich durch Kompressibilitäten berücksichtigt. In Mehrkomponentensystemen treten jedoch Lösungs- und Entmischungsprozesse auf, welche in nicht-isothermen Systemen durch Verdampfung und Kondensation ergänzt werden. Diese Prozesse können erheblichen Einfluss auf das Volumen haben, das ein Fluidgemisch einnimmt. Als Beispiel kann die Verdunstung oder Verdampfung einer Flüssigkeit genannt werden. Hierdurch kann sich das spezifische Volumen einer Komponente um mehrere Größenordnungen verändern, was sich auch bei kleinen Massenumsätzen merklich auf das Volumen einer Gas-Flüssig-Mischung auswirken kann. Diese Veränderungen werden von der Fractional Flow Formulierung jedoch nicht erfasst. Um die Nachteile der massenbasierten Formulierung zu umgehen wird ein Konzept aufgegriffen, das der Druckgleichung der entkoppelten Formulierung die lokale Erhaltung des Fluidvolumens zugrunde legt. Hierbei wird postuliert, dass innerhalb eines Kontrollvolumens immer dasselbe Volumen – nämlich das Porenvolumen – für Fluidphasen bereit steht. Dieses Volumen muss stets mit einer Fluidphase oder

einem Gemisch mehrerer Fluidphasen ausgefüllt sein. Verändert sich nun das Volumen des im Kontrollvolumen enthaltenen Gemisches, so muss zwangsläufig Masse zu- bzw. abströmen. Dieses Verhalten wird mittels Ableitungen des Fluidvolumens nach Masse, Druck und Energie in eine Druckgleichung umgesetzt.

Numerische Umsetzung des entkoppelten Modells Die eingeführte, entkoppelte Formulierung wird als numerisches Modell implementiert. Dies erfordert die räumliche und zeitliche Diskretisierung der entwickelten partiellen Differentialgleichungen, die es ermöglicht, Differential- durch Differenzenausdrücke und kontinuierliche Funktionen durch diskrete Werte zu ersetzen. Zur räumlichen Diskretisierung wird eine zellzentrierte Finite Volumen Methode verwendet. Obwohl sie lediglich ein Verfahren erster Ordnung darstellt, bietet sie die Vorteile, dass sie intuitiv, sehr robust und massenkonservativ ist. Die Zeitdiskretisierung wird mittels des IMPES-Verfahren (IMplicit Pressure Explicit Saturation) bewerkstelligt. Wie der Name bereits erahnen lässt, wird dabei die Druckgleichung zeitlich implizit und die Transportgleichung zeitlich explizit gelöst, was den mathematischen Eigenschaften beider Gleichungen (Druck: elliptisch, Transport: hyperbolisch, sofern advektionsdominiert) entspricht.

Bedingt durch die Formulierung kann am Ende eines jeden Zeitschritts nur die Gesamtmenge an innerer Energie und Masse der Komponenten in einem Kontrollvolumen ermittelt werden. Die Anzahl der Phasen und Aufteilung der Komponenten auf die Phasen ist daraus jedoch noch nicht ersichtlich. Um die Sättigungen und Massenbrüche in den Phasen zu berechnen bedarf es daher noch einer Phasengleichgewichtsberechnung oder Flash-Calculation. Dazu wird in der Regel die Rachford-Rice Gleichung herangezogen, welche noch zusätzlicher Parameter, der Gleichgewichtsverhältnisse, bedarf. Diese Gleichgewichtsverhältnisse werden oft aus thermodynamischen Zustandsgleichungen berechnet, was jedoch sehr komplex ist und im Rahmen dieser Arbeit nicht weiter behandelt wird. Stattdessen wird ein Vorschlag aufgegriffen, die Gleichgewichtsverhältnisse mittels einfacher Löslichkeitsgesetze, wie dem von Raoult oder Henry zu berechnen. Die Implimentierung der Flash-Calculation wird für bestimmte, in dieser Arbeit relevante, Kombinationen aus Phasen- und Komponentenanzahl für isotherme und nicht-isotherme Systeme behandelt.

Um ein robustes numerisches Modell zu erhalten, müssen die Koeffizienten für die Druck- und Transportgleichungen durch eine konsequente Oberstromgewichtung ermittelt werden. Dies ist insofern nicht trivial, als dass die Oberstromrichtung bei gravitativ beeinflussten Systemen je nach Phase unterschiedlich sein kann. Bei ebensolchen Systemen hat sich auch gezeigt, dass die mathematisch konsistente Art und Weise, den Durchfluss durch eine Kontrollvolumengrenzfläche zu bestimmen – dieser wird benötigt um am Kontrollvolumen die Massen- und Energieflüsse zu bilanzieren – bei bestimmten Gitterausformungen zu fehlerhaften Druckverteilungen führen kann. Daher wird eine alternative Berechnung vorgeschlagen, bei der die Filtergeschwindigkeit

nicht mit der Einheitsnormalen und dem Inhalt der Kontrollvolumengrenzfläche, sondern mit dem Verbindungsvektor der Zellmittelpunkte und einer korrigierten Fläche multipliziert wird.

Außer der Diskretisierung der entkoppelten Gleichungen stellt sich auch noch die Frage nach der Bestimmung der Ableitungen des Volumens nach Masse, Energie und Druck. Es wird vorgeschlagen, diese Ableitungen numerisch durch Vorwärtsdifferentiation (entspricht Taylor-Reihe erster Ordnung) zu ermitteln. Anstatt dafür einen sehr kleinen Schritt zu wählen um eine (mathematisch korrekte) Tangente an die Volumenfunktion anzunähern, wird vorgeschlagen, den Schritt entsprechend der im nächsten Zeitschritt zu erwartenden Veränderungen zu wählen, was einer Sekante entspricht. Um diese Veränderung abzuschätzen, wird jeder Zeitschritt durch eine vorgeschaltete Lösung der Transportgleichung mit altem Geschwindigkeitsfeld ergänzt.

Multiphysics Ansätze für zwei-Phasen, zwei-Komponenten Flüsse Der Kerngedanke des Multiphysics Ansatzes ist es, das Modellgebiet in Untergebiete zu teilen. Je nach auftretenden relevanten Prozessen im Untergebiet werden unterschiedliche Modelle angewandt. Die Kopplung der Modelle wir am internen Rand, der die Untergebiete voneinander abgrenzt, realisiert. Dadurch wird ein Übergang von Modellkomplexitäten geschaffen, der die Anpassung des Modells and die lokale Komplexität der auftretenden physikalischen Prozesse erlaubt. Dieser Ansatz wird sowohl für isotherme als auch nicht-isotherme Systeme zweier Komponenten realisiert.

Wo der Übergang einer Komponente von einer Phase in eine Andere durch Lösung, Ausgasung, Verdunstung oder Kondensation geschieht, muss ein zwei-Phasen zwei-Komponenten (2p2c) Modell angewandt werden, das ebenjene Prozesse abbilden kann. An Stellen, an denen lediglich ein-Phasen Fluss und Transport der gelösten Komponenten beobachtet wird, ist ein entsprechend einfacheres Modell ausreichend. Vergleicht man die volumenbasierte entkoppelte Formulierung mit der Fractional Flow Formulierung, so wird deutlich, dass diese für den Fall, dass eine einzelne Phase vorliegt, quasi identisch sind. Das bedeutet, dass sich zwei Modelle, die auf den unterschiedlichen Formulierungen basieren, an einem Rand, an dem nur ein-Phasen Fluss vorliegt, ohne besondere Schwierigkeiten koppeln lassen. Der daraus erwachsende Vorteil ist, dass im ein-Phasen Gebiet wesentlich einfachere Gleichungen angewandt werden können und die Ausführung von Phasengleichgewichtsberechnungen und Ableitungen des Fluidvolumens entfallen. Wenn im ein-Phasen Untergebiet eine Flüssigkeit vorliegt und daher von inkompressibler Strömung ausgegangen werden kann, so vereinfacht sich das mathematische Modell sogar soweit, dass lediglich eine Laplace-Gleichung zur Ermittlung des Druck- und Geschwindigkeitsfeldes gelöst werden und eine einzelne Massenbilanzgleichung für die gelöste Komponente ausgewertet werden muss.

Für die Gültigkeit des Multiphysics Modells ist die richtige Wahl der Untergebiete von entscheidender Bedeutung. Da a priori nur schwer oder überhaupt nicht festzustellen

ist, wo im Gebiet die relevanten Prozesse auftreten, die das 2p2c Modell erforderlich machen, ist eine adaptive Gebietsunterteilung notwendig. Es zeigt sich, dass Entmischungseffekte direkt unterstromig eines bereits bestehenden zwei-Phasen Bereichs am wahrscheinlichsten sind. Daher kann eine adaptive Gebietszerlegung unter Ausnutzung des Courant-Kriteriums für die explizite Zeitdiskretisierung (innerhalb eines Zeitschrittes kann Transport um maximal eine Maschenweite im Gitter stattfinden) derart umgesetzt werden, dass das 2p2c Untergebiet ein Element größer gewählt wird als der eigentliche zwei-Phasen Bereich. So wird gewährleistet, dass eventuell auftretende Entmischungen am Ende eines jeden Zeitschrittes erfasst werden. Nach Beendigung des Zeitschritts wird die Wahl des 2p2c Untergebietes überprüft und gegebenenfalls angepasst.

Im Allgemeinen ist davon auszugehen, dass der Zusammenhang zwischen Energie, Temperatur, Fluidvolumen und anderer Größen in einem Kontrollvolumen nichtlinear ist, was sich besonders bei zwei Phasen bildenden Gemischen oder am Siedepunkt einer Flüssigkeit zeigt. Allerdings kann dieser Zusammenhang innerhalb kleiner Bereiche durchaus als linear angenähert werden. Wenn nun eine maximale Veränderung der Temperatur gegenüber der Anfangstemperatur definiert wird, innerhalb derer eine lineare Annäherung hinreichend ist, so kann das Modellgebiet danach in zwei Untergebiete geteilt werden. In einem Untergebiet mit niedrigen Temperaturänderungen wird die isotherme Druckgleichung und isotherme flash-calculation angewandt. Die Temperatur wird über die Veränderung der internen Energie und der Wärmekapazität des Kontrollvolumens berechnet. Durch Überschneidung der Grenzen zwischen Bereichen niedriger und maßgeblicher Temperaturveränderung einerseits und Grenzen zwischen ein- und zwei-Phasen Bereichen andererseits, ergeben sich vier mögliche Untergebiete. Dabei wird das 2p2c-Untergebiet wie zuvor festgelegt, während die Grenze des Gebietes, wo nicht-isotherme Modelle anzuwenden sind, durch den angesprochenen Grenzwert der Temperaturveränderung definiert wird.

Bei der Implementierung der Multiphysics Ansätze wird der Umstand ausgenutzt, dass die Druckgleichungen in den verschiedenen Untergebieten letzlich dieselbe physikalische Bedeutung haben: die Erhaltung des Fluidvolumens. Durch Formulierung in den gleichen physikalischen Einheiten ist es somit möglich, die Beiträge aller Elemente (unbesehen des Untergebietes) in ein einzelnes, globales, lineares Gleichungssystem zu assemblieren und gleichzeitig zu lösen. Dazu muss lediglich sichergestellt werden, dass die Fließgeschwindigkeit der Phasen auf beiden Seiten einer Untergebietgrenze gleich berechnet wird. Wenn ebenfalls der Massentransport auf beiden Seiten gleich berechnet wird, so können auch die Transportgleichungen ohne weitere Vorkehrungen gemeinsam gelöst werden. Dadurch kann das Einschritt-Verfahren der IMPES Zeitdiskretisierung beibehalten werden. Dies ist ein wesentlicher Vorteil gegenüber anderen Multiphysics Ansätzen, bei denen die Erfüllung der Kopplungsbedingungen an den internen Rändern über eine Iteration bewerkstelligt wird, was eine mehrmalige Lösung der Modelle in den Teilgebieten notwendig macht.

Validierung des Entkoppelten Modells und Anwendung des Multiphysics Ansatzes an realistischen Beispielen Um die Verlässlichkeit des entwickelten nicht-isothermen Modells zu überprüfen, wurde es gegen die Ergebnisse mehrerer Experimente und Simulationsläufe des HYDROTHERM Programms validiert. Dabei wurde die Komplexität der Prozesse zunehmend gesteigert. Zunächst wurde ein zwei-dimensionales Experiment zur Untersuchung von statischen Wärmequellen in der gesättigten Bodenzone betrachtet. Mit einem Heizelement wird thermische Energie in Boden und Grundwasser eingebracht, was zu einer Erwärmung und – durch die damit einhergehende Dichteveränderung – zu auftriebsbedingtem Fluss und Transport von Gelöststoffen führt. Die dadurch erzeugte Verteilung des gelösten Tracers in der Versuchapparatur konnte mithilfe des Modells qualitativ vorausgesagt werden.

HYDROTHERM ist ein voll gekoppeltes Modell zur Simulation von nicht-isothermen Strömungsprozessen von reinem Wasser. Es wurde verwendet, um jeweils ein ein- und zwei-dimensionales Beispiel von Dampfinjektionen in voll wassergesättigte Böden zu simulieren. Die Ergebnisse wurden wiederum mit denen des in dieser Arbeit vorgestellten, entkoppelten Modells verglichen. Eine sehr gute Übereinstimmung von Druck-Sättigungs- und Temperaturwerten konnte festgestellt werden. Allerdings zeigten sich auch unphysikalische Druckoszillationen im entkoppelten Modell, die auf die schwierige Handhabbarkeit des starken Dichtekontrasts zwischen flüssigem und dampfförmigem Wasser zurückzuführen sind. Dabei zeigt sich auch, dass die Bestimmung der Kompressibilitäten sehr sorgfältig zu erfolgen hat, da diese am Siedepunkt einer Flüssigkeit – bedingt durch Verdampfung- und Kondensationseffekte – um einige Größenordnungen größer sein können, als die Kompressibilitäten über oder unter dem Siedepunkt und sich stabilisierend auf das Modell auswirken.

Nicht-isotherme zwei-Phasen zwei-Komponenten Prozessen wurden anschließend mithilfe der Ergebnisse zweier, quasi ein-dimensionaler Säulenexperimente betrachtet. Im ersten Experiment wurde Wasserdampf in eine horizontale, luftgesättigte Säule injiziert. Dabei wird Luft verdrängt und die Feststoffmatrix durch die latente Wärme des kondensierenden Wasserdampfs erhitzt. Im zweiten Experiment wird Heißluft in eine teilgesättigte, vertikale Säule injiziert. Wieder wird die Feststoffmatrix dadurch erhitzt und das in der Säule enthaltene Wasser verdunstet und wird von der vorbeiströmenden Luft aus der Säule ausgetragen. Beim Beispiel der Dampfinjektion wurden die zeitlichen Verläufe von Temperatur und Druckanstieg an mehreren Punkten mit guter Genauigkeit prognostiziert. Lediglich der absolute Wert des Druckveränderungen differierte zwischen Experiment und Simulation, was jedoch auf Unsicherheiten bei der Bestimmung der Permeabilität zurückgeführt wird. Bei der Heißluftinjektion wurden die Durchgangszeiten der Trocknungsfront und des Temperaturanstieges sehr gut vom Modell vorausgesagt, allerdings zeigte sich eine lokal wesentlich langsamere Erwärmung als im Experiment. Durch Veränderung der Berechnung der Wärmeleitfähigkeit dergestalt, dass sie durch das Vorhandensein von Wasser nicht erhöht wird, werden die experimentellen Ergebnisse sehr gut getroffen. In der Beschreibung des Säulenexper-

imentes in Färber [1997] wurde darauf hingewiesen, dass sich speziell bei langsamen Prozessen (die Heißluftinjektion wird dazugezählt) über den Querschnitt der Säule veränderliche Sättigungen und Temperaturen ausbilden können. Dies kann die lokale Erwärmung und Wärmeleitung durchaus beeinflussen und wird als Grund für die auffälligen Abweichungen zwischen Modell und Experiment vermutet. Somit kann auch bei den beiden Beispielen der nicht-isothermen zwei-Phasen zwei-Komponentenprozesse von einer erfolgreichen Validierung gesprochen werden.

Zuletzt wurde die drei-Phasen drei-Komponenten Implementierung der entkoppelten Gleichung am Beispiel einer Bodenluftabsaugung zur Sanierung einer Kontamination der teilgesättigten Bodenzone getestet. Die Ergebnisse wurden mit denen eines voll gekoppelten Modells aus Class [2001] verglichen. Das entkoppelte Modell zeigte eine qualitativ richtige Nachbildung des Systemverhaltens. Die Abweichungen im Fortschreiten der Trocknungsfront der nicht-wässrigen Flüssigphase werden hier nicht weiter erörtert, da das Beispiel lediglich die grundsätzliche Tauglichkeit der drei-Phasen drei-Komponenten Implementierung zeigen sollte.

Zwei drei-dimensionale Problemstellungen wurden herangezogen um die Anwendbarkeit der vorgestellten Muliphysics-Ansätze zu demonstrieren. Dabei wurden die Ergebnisse der Multiphysics-Modelle mit denen der jeweiligen global komplexen, entkoppelten Modelle verglichen. Das heißt, das isotherme Multiphysics-Modell wurde mit dem, auf dem ganzen Modellgebiet angewandten, zwei-Phasen zwei-Komponenten Modell und das nicht-isotherme Multiphysics-Modell mit dem nicht-isothermen zwei-Phasen zwei-Komponenten Modell verglichen. Das isotherme Multiphysics-Modell wurde am Beispiel einer Injektion von CO_2 in eine voll mit Wasser gesättigte, geologische Formation getestet. Die zeitlichen Verläufe der Masse des im Wasser gelösten CO_2 und des Gesamtvolumens des CO_2 in Phase waren dabei nahezu deckungsgleich. Am Ende der Simulationszeit, als sich die CO_2-Blase am weitesten ausgebreitet hatte, wurden im Multiphysics-Modell lediglich fünf Prozent des Modellgebiets vom 2p2c-Untergebiet abgedeckt. Dadurch ergab sich eine Veringerung der Anzahl an Phasengleichgewichtsberechnungen um einen Faktor von 46. Angesichts der Tatsache, dass in Simulationsprogrammen, die komplexe thermodynamische Zustandsgleichungen einbeziehen, bis zu 70 Prozent der Gesamtrechenzeit auf ebenjene Berechnungen entfallen, eröffnet dies eine Perspektive auf massive Zeiteinsparungen.

Das nicht-isotherme Multiphysics Modell wurde am Beispiel einer Schadstoffsanierung mithilfe von Bodenluftabsaugung und statischen Wärmequellen getestet. Auch hier waren die betrachtete Größe – die Masse des im Modellgebiet befindlichen Schadstoffes – in ihrem zeitlichen Verlauf deckungsgleich mit den in der Referenzsimulation ermittelten Werten. Aufgrund der zunehmenden Erwärung des Bodens durch die statischen Wärmequellen wuchs das nicht-isotheme Untergebiet stetig an, während das zwei-Phasen zwei-Komponenten Untergebiet durch fortschreitenden Schadstoffaustrag kontinuierlich schrumpfte. Mithilfe des Multiphysics Konzeptes konnte in diesem Fall die Anzahl an aufwändigen, nicht-isothermen Phasengleichgewichtsberechnungen

um einen Faktor von 22 verringert werden, was mit einer nahezu Verdoppelung der Berechnungsgeschwindigkeit einherging und im Fall von komplizierteren Materialgesetzen noch größere Vorteile verspricht.

Ausblick Sowohl das entkoppelte Modell für nicht-isotherme Mehrphasen-Mehrkomponentenflüsse als auch die eingeführten Multiphysics-Konzepte bilden die Grundlage für weitere Untersuchungen. So sollten für die Weiterentwicklung beider Ansätze weitere Anstrengungen unternommen werden.

- Das isotherme drei-Phasen drei-Komponenten Modell bedarf weiterer Verbesserungen und der Valididerung.
- Um eine möglichst große Bandbreite von umwelt- und industietechnischen Problemen der Strömungen in porösen Medien abdecken zu können, sollte anschließend eine Erweiterung zu einem nicht-isothermen drei-Phasen mehrkomponenten Modell vorgenommen werden.
- Dabei sollte die Implementierung flexibel für die Einbeziehung einer beliebigen Anzahl von Komponenten gemacht werden. Dies wirft die Notwendigkeit einer Schnittstelle zu externen Algorithmen zur Berechnung von Phasengleichgewichten auf, da es dadurch möglich wird die Stärken anderer akademischer Disziplinen, wie der Thermodynamik oder des Chemieingenieurwesens, miteinzubeziehen.
- Die vorgestellte Implementierung des drei-Phasen drei-Komponenten Modells kann bereits als Grundlage für einen weiteren Multiphysics-Ansatz genutzt werden. Bei der Sanierung einer Kontamination der teilgesättigten Bodenzone mittels Bodenluftabsaugung ist beispielsweise die Lösung von Luft in Wasser oder von Wasser in Luft nicht von Interesse. Vielmehr soll der Austrag des Schadstoffes mit der Luft und die Lösung des Schadstoffes im Wasser betrachtet werden. Daher bietet es sich an, das drei-Phasen drei-Komponenten Modell auf den Bereich zu beschränken, wo der Schadstoff in Phase vorliegt und Lösungs- und Verdampfungsprozesse zu beobachten sind. In anderen Teilen des Modellgebietes ist ein zwei-Phasen Modell, das den Transport des Schadstoffes berücksichtigt, ausreichend. Dort kann die Verteilung des Schadstoffes auf die Gas- und Wasserphase mittels eines einfachen Phasengleichgewichtskoeffizienten beschrieben werden.
- In Niessner and Helmig [2007] wurde angestoßen, ein Multiphysics-Modell mit einem Mehrskalen-Modell zu verbinden. Dabei wurde das Untergebiet, in dem komplexe Prozesse stattfinden fein diskretisiert, wohingegen in den Bereichen des Gebiets, wo einfache Prozesse ablaufen, mithilfe eines Upscaling-Ansatzes vergröbert wurden. Die Kopplung beider Modelle basierte auf der Annahme eines divergenzfreien Geschwindigkeitsfeldes. Da diese Annahme aufgrund Kompressibilitäten und Phasenübergangseffekten nicht allgemeingültig ist, erscheint es vielversprechend, die in der vorliegenden Arbeit vorgestellten

Multiphysics-Modelle inklusive adaptiver Gebietszerlegung mit dem vorgeschlagenen Mehrskalen-Ansatz zu verbinden.

1 Introduction

Originating from the simulation of groundwater flow, single-phase and multi-phase porous media flow models are used for the investigation and prediction of flow processes in numerous environmental and industrial materials. The complexity of such models has increased rapidly since the first groundwater flow modesl were developed, enabling an increasingly realistic description of the relevant physical processes. With increasing physical accuracy of a model, not only the computational costs but also the demand for input parameters specifying initial and boundary conditions increases. This will always motivate the choice of a model which is as simple as possible while still providing the complexity which is needed to represent the physical processes under consideration. Thus, the most complex relevant physical processes determine the complexity of the model.

In many applications, however, very complex processes only occur in a narrow region of the considered domain. In this case, basically two options can be considered: Either, for economic reasons, a simple model is chosen to the price of negligence of the complex processes, or the model which accounts for the complex processes is chosen accepting the fact that the complexity is superfluous in most parts of the model domain. This conflict motivates the use of a concept which couples both models to adapt the resulting *multiphysics* scheme to the occurring processes.

To implement such a multiphysics model, the occuring physical processes have to be described in such a way that they can be mathematically decoupled. This, in turn, creates the need of the development of according mathematical models concepts. The already available model concepts can in general be classified into two categories: fully coupled (fully implicit) and decoupled (sequential) models. The most important difference between these concepts are their temporal discretizations and – linked to that – the corresponding solution strategies. While the decoupled models commonly work with single step solution schemes, the fully coupled models incorporate an iterative solver. Due to the non-linear behavior of many coefficients involved in porous media flow formulations, the fully coupled models are generally easier to extend to represent highly complex physical processes. As an example, models for the simulation of realistic non-isothermal compositional multiphase flow phenomena in porous media only exist in a fully-coupled form. However, the decoupled models have the advantage of simpler solution schemes which take advantage of the formal resemblance of the decoupled formulations to single-phase flow formulations (Chen and Ewing [1997]). This

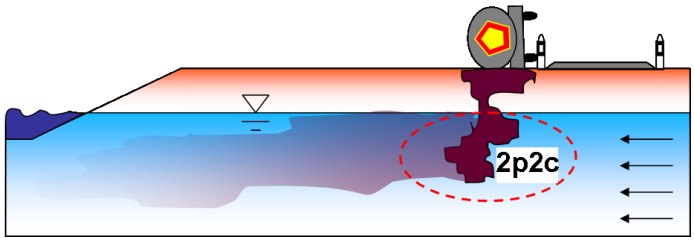

Figure 1.1: Flow regimes in a porous medium. Below the groundwater table, two-phase flow and mass exchange between phases is restricted to the marked area.

resemblance is achieved by splitting the governing equations for the flow phenomena in a (elliptic) pressure and a (hyperbolic/parabolic) transport equation. The splitting is the basis for a sequential solution scheme which can solve a timestep without iterations and with small systems of equations making the decoupled formulations much faster (Binning and Celia [1999]). A practical example for this advantage may be given by a comparison on a benchmark problem: carbon dioxide is injected into a 200 km long and 100 km wide aquifer which is discretized by about 100,000 cells. After an injection period of 25 years, the spreading and dissolution of the carbon dioxide is simulated by a decoupled simulator based on the concepts presented in this work and a fully coupled simulator, both being implemented in the simulating toolbox DuMuX. The decoupled model simulated a period of 30,000 years within two days. The fully coupled simulator implemented in the same numerical framework and running on a comparable machine was stopped after twelve days having simulated less than 3000 years.

For many environmental, technical and biological applications of porous media flow simulators, the representation of non-isothermal compositional multiphase processes is necessary. For most of these processes, the assumption of a local thermodynamic equilibrium holds. As an example, the thermal in-situ remediation of contaminated soils requires at least the representation of non-isothermal two-phase two-component processes.

To exemplify the multiphysics idea, consider Figure 1.1. A dense, non-aqueous phase liquid (NAPL) leaks into the subsurface and contaminates the groundwater. To capture the movement of the NAPL phase and the dissolution of the contaminants in the groundwater, a compositional two-phase simulator is necessary. However, these processes only happen inside the small area marked by the dashed line, while the movement of the contaminants inside the groundwater could as well be described by a simple, single-phase transport model. The goals of this work are the development of

- a multiphysics model that allows for the systematic application of simple and complex models at the same time inside one domain.
- the decoupled models needed for the representation of the respective physics under realistic conditions inside different parts of a domain in a multiphysics framework.

- a simple, efficient and robust scheme which provides optimal adaption of the multiphysics model to the occurring physical complexities.

To get an overview of existing decoupled and multiphysics methods, a literature review is given in the following section.

1.1 Literature

The first decoupled formulation for immiscible, two-phase flow was published in Chavent [1976] where the author called it *a new formulation*. In order to obtain a pressure equation, the velocities of the two phases were added to a total velocity which is separated to its fractions by so-called fractional-flow factors. These factors later on gave the approach the name "fractional flow formulation". However, this formulation could only be used for the description of immiscible and incompressible phases. A sequential model for compositional, compressible flow was introduced in Acs et al. [1985]. In this approach, the pressure equation is not derived from the fluid mass balance equations as the fractional flow formulations before, but rather from a volume conservation constraint. In Trangenstein and Bell [1989], the authors examine the proposed model for its mathematical structure and its formal adequacy for the established numerical methods to solve partial differential equations. In Chen et al. [2000], the authors study the mathematical properties of the volume conservation approach in terms of different pressure formulations for three-phase flow. The approach was also adapted in van Odyck et al. [2009], where a non-isothermal formulation for one-dimensional, two-phase systems under simplified physical conditions was considered.

Existing multiphysics approaches either have the aim of coupling porous media flow with other flow regimes or the transition of complexity within a porous medium. Multinumerics schemes have a certain relation to multiphysics methods. They couple subdomains with different solution approaches instead of different physics. The existing methods can, however, be classified into two categories. The first are double- or multicontinua models, where the model domain is projected on two or more overlapping continua with different properties. This means that a certain range of points in space exists in two or more continua and their physical state is described and influenced by two or more models. The coupling of the continua is usually realized via source and sink terms depending on the differences of one or more primary variables in the different continua. This is referred to as vertical coupling and is sketched in Figure 1.2, left. In the second category, every point in space only exists in a single domain. This model domain is divided into subdomains which are occupied by different models. The coupling is then realized at the interface between the subdomains by a set of continuity requirements as examplarily sketched in Figure 1.2, right. This is referred to as horizontal coupling.

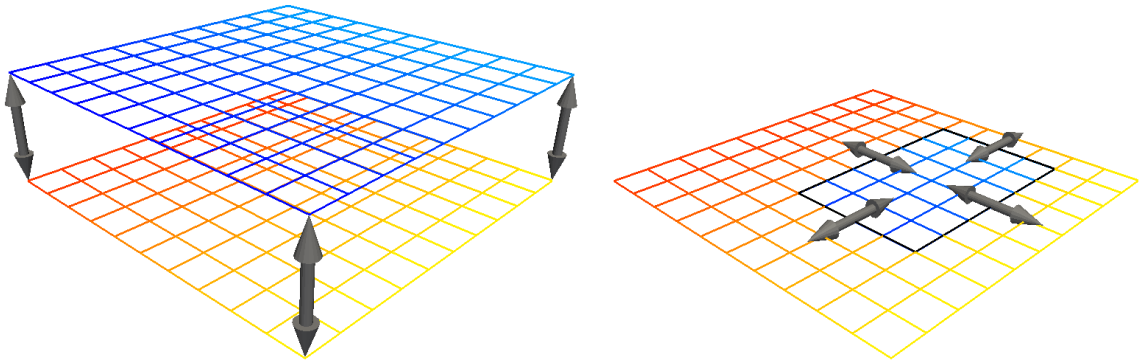

Figure 1.2: Vertical and horizontal model coupling.

Figure 1.3 examplarily sketches different vertical and horizontal concepts for model coupling in porous media flow.On the left, it shows vertical coupling methods starting with the double- or multi-continua approach for modeling flow and transport in fissured porous media. It approximates the randomly and evenly distributed fissures and fractures as an additional continuum with its own permeability and porosity which is connected to the porous medium matrix by source and sink terms. The method was introduced in Barenblatt et al. [1960] and has been adapted in numerous models, e.g. Moench [1984], Wang and Narasimhan [1985], Wang [1991]. A comprehensive introduction is given in Dietrich et al. [2005]. In Dogan et al. [accepted], the authors propose a hybrid model for the incorporation of discrete fractures into a double-continuum concept: while standard double-continuum concepts consider fractures on an equidimensional second domain, this approach confines the fluid movement in the second domain to flow along one-dimensional pipes. The MINC method (Multiple INteracting Continua) published in Pruess and Narasimhan [1982] and Pruess and Narasimhan [1985] regards the fact that, in a fractured porous medium, *any disturbance in reservoir conditions will travel rapidly through the network of interconnected fractures, while invading the matrix blocks only slowly* (Pruess [1992]). This is done by representing the medium by a continuum of fractures where flow and transport takes place, while the matrix is represented by several levels of disconnected blocks which exchange mass and energy with the fractures. An example for vertical coupling leading the way to multiphysics is the approach proposed in Niessner and Helmig [2006, 2007, 2009], where the model domain is projected on three continua: a fine-scale continuum to solve the pressure equation, and a coarse-scale continuum to solve a two-phase transport equation which is locally extended by a fine-scale continuum with a compositional three-phase transport equation. This method allows for the local adaption of the model complexity to the physical complexity and is related to the concept presented in this work. However, the method was developed under the assumption of a divergence-free velocity field at every point in space which is not valid under general conditions as will be discussed in Section 2.7.2.

The methods of horizontal coupling in the right column of Figure 1.3 begin with the non-overlapping domain decomposition concept published in Albon et al. [1999]. It considers the interface coupling of subdomains with different soil types and the coupling of porous media with lower dimensional fractures (discretized as a highly permeable porous medium), where the coupling conditions involve pressure continuity and mass conservation. The discrete fracture approach represents discrete single fractures equidimensionally or in lower dimensions and couples the different flow regimes inside the fractures and the porous medium at the fracture walls (e.g. Therrien and Sudicky [1996], Dverstorp and Andersson [1989], Reichenberger et al. [2006], Haegland et al. [2009]). In discrete fracture approaches, the fractures are often represented in a simplified way. For example, the fractures are considered as gaps between parallel plates and the equations of Hagen-Poiseuille are applied (e.g., Dietrich et al. [2005]) . Other coupling approaches for the interactions between free flow and porous media (e.g. at river beds or for technical filtration problems) solve Stokes or Navier-Stokes equations, see e.g. Discacciati et al. [2002], Layton et al. [2003], Vassilev and Yotov [2009]. At the interface between the free-flow subdomain and the porous medium, not only continuity of pressure and mass transfer are considered but also the velocities tangential to the interface (Beavers and Joseph [1967]). Instead of coupling different flow regimes, the authors of Wheeler et al. [1999] introduce a method to connect different solution schemes for porous media flow to each other. Subject to the dominating processes, decoupled or fully implicit model formulations are solved within different subdomains. Related to that, a multiphysics approach is presented in Peszynska [2002] which couples a black-oil, two-phase or single phase model, using a non-linear iteration algorithm at the interface.

Using the insights from the literature, a decoupled model for non-isothermal compositional multiphase flow has to be formulated. To be able to represent realistic systems, it is to be implemented for up to three dimensions regarding gravitational effects. Furthermore, a validation of the implemented model has to be made in order to obtain a simulator suitable for making predictions. A horizontal coupling using a non-linear iteration which requires the solution of a whole timestep in all subdomains for every iteration step is cumbersome. Therefore, a coupling concept which allows for a single-step solution of a timestep is to be developed.

1.2 Structure

In the following, an overview is given which shows the structure of this work:

Chapter 2 introduces the physical properties of fluids, models for the interaction between solids and fluids in porous media and the assumptions which are made in order to describe porous media flow. Additionally, the mathematical equations for flow and

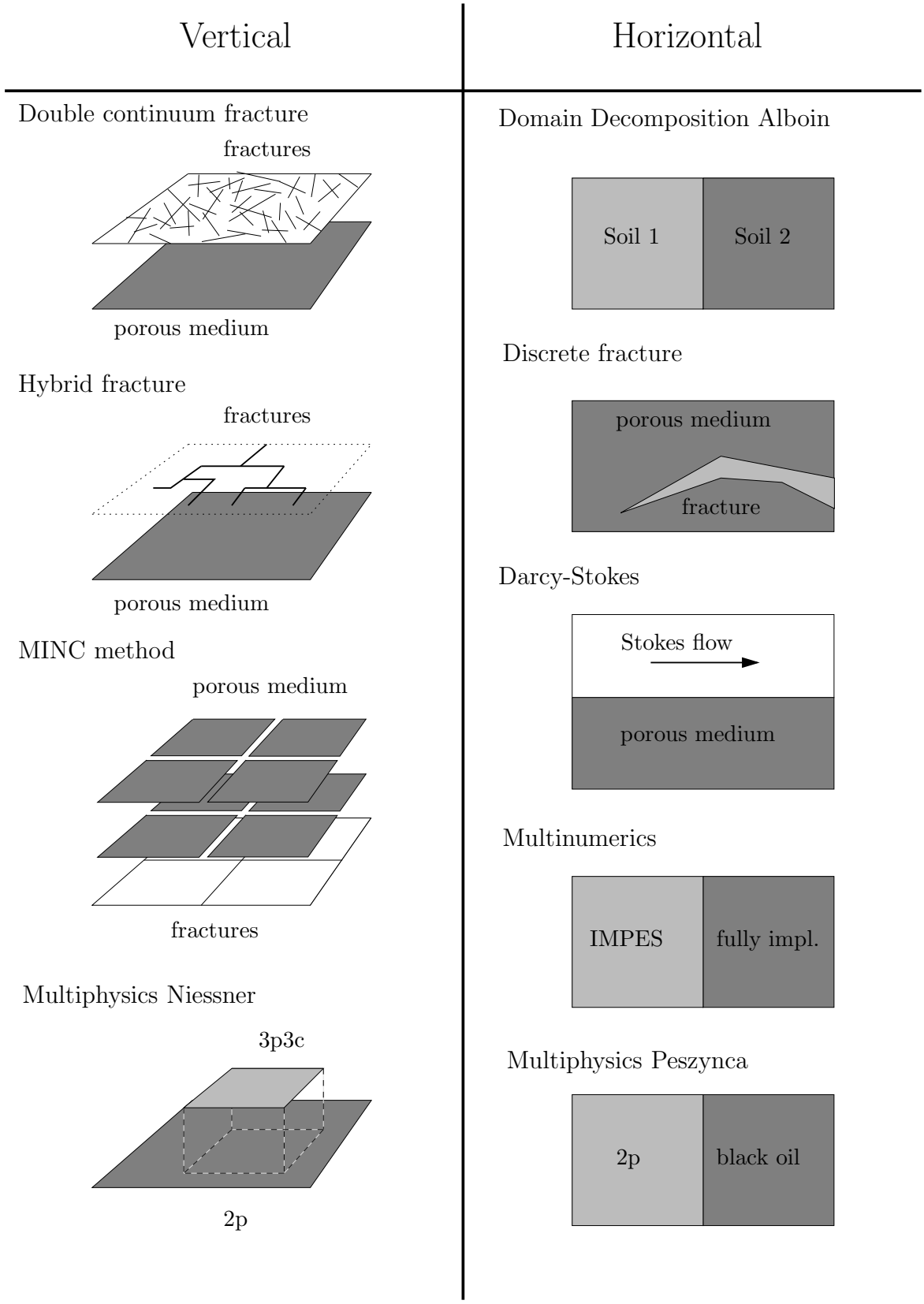

Figure 1.3: Exemplarily overview of horizontal and vertical coupling methods.

transport in porous media are introduced. Based on these equations, decoupled formulations for compositional and non-isothermal multiphase flow are derived before introducing two multiphysics concepts for transition of complexity in porous media flow simulation.

In Chapter 3, the main assumptions of this work are introduced and the spatial and temporal discretization of the flow and transport equations of Chapter 2 are derived. After the consideration of the implementation of the multiphysics schemes, the need for subdomain adaption is discussed and an associated method is presented.

The decoupled models are tested and validated on the results of several laboratory experiments and other numerical models in Chapter 4. To show practical applicability of both the decoupled models and the multiphysics schemes, two realistic examples of applications are presented in Chapter 5 before concluding in Chapter 6.

2 Physical Model

A general step in every engineering approach to solve a problem is to formulate a model describing the physical behavior of the considered system. In order to describe multiphase flow through porous media, many different models have to be combined to a complex system. The parts and concepts which constitute this system are introduced in the following section. A crucial precondition for the formulation of these concepts is the choice of an adequate scale of observation, which is in our case the continuum scale. That is, *matter is regarded as a hypothetical substance which is continuous in space and time and can be described by continuous in space variables* (Bear and Bachmat [1990]).

2.1 Definition of scales and domains

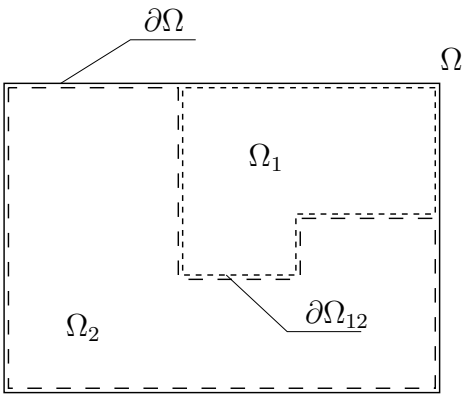

Figure 2.1: Definition of model domain and subdomains.

In order to design an appropriate modeling strategy for particular problems, it is important to consider the spatial and temporal scales involved, and how the physical processes and parameters of the system relate to these scales. A careful definition of relevant length scales can clarify any investigation of scale considerations, although such definitions are a matter of choice and modeling approach (Hristopulos and Christakos [1997]). In general, we define the following length scales of concern: the *molecular* length scale, which is of the order of the size of a molecule; the *microscale*, or the minimum continuum length scale on which individual molecular interactions can be neglected in favor of an ensemble average of molecular collisions; the *local scale*, which is the minimum continuum length scale at which the microscale description of fluid movement through individual pores can be neglected in favor of averaging the fluid movement over a representative elementary volume (REV, see Section 2.2); the *mesoscale*, which is a scale on which local scale properties (such as porosity or permeability, see Section 2.2) vary distinctly and markedly; and the *megascale* or field-scale.

In the following, two domain types are going to be distinguished: the model domain and subdomains. In order to process a simulation, a finite area or volume with clear boundary conditions has to be defined. This will be referred to as *model domain* and the associated boundaries are called *external boundaries*. In Figure 2.1, the external boundaries $\partial\Omega$ are situated on the solid rectangle while the model domain is sketched as the area Ω within this rectangle. In order to apply a multiphysics scheme with horizontal coupling, the model domain is divided into *subdomains* (as will be discussed in Section 2.8). In Figure 2.1, the subdomains are represented by the areas Ω_1 and Ω_2, while the boundary between the subdomains, the *internal boundary* is marked with $\partial\Omega_{12}$.

2.2 Representative elementary volume concept

The model concepts in this work are based on the consideration of the porous medium as a continuum consisting of a solid and one or more fluid phases being present at every point in space. This means that the fluid flow is not considered in individual pores but is averaged over a representative elementary volume (REV) and described by averaged velocities. The reason for this average is that the microscale modeling – i.e. the modeling of the complex velocity field inside every pore – is not practicable for the most interesting questions since already a model domain of one cubic meter may contain millions or billions of pores. Thus, neither the exploration of their topology nor the calculation of microscale flow through every single pore lies within today's capabilities.

As basis for a correct averaging, a size of the REV has to be specified. A minimum size is reached, when the average of the considered quantity stays constant, i.e. that slight extensions or reductions of the considered volume do not lead to significant changes of the averaged quantity. Figure 2.2 illustrates the relation between the size (radius r) of an averaging volume and the value of an averaged physical quantity on the example of the porosity ϕ. For a disappearing radius, the porosity is either zero or one as becomes clear from Figure 2.2, right. With increasing radius, the porosity fluctuates until it reaches a constant value at r_{min}. If a heterogeneous medium is considered, the porosity begins to change again when the volume is large enough to hit heterogeneities as, e.g., sand lenses in a loamy soil. The same considerations as for the porosity can be applied to other physical quantities giving the possibility to *replace the actual medium by a fictitious continuum in which we may assign values of any property to any point in space* (Bear [1979]). That is, all physical quantities are now described by functions continuous in space, where it has to be mentioned that many quantities which are of importance for the following derivations – such as porosity, permeability and saturations – only exist in this continuum approach, making the introduction of the REV concept indispensable. Finally it has to be mentioned that minimum and

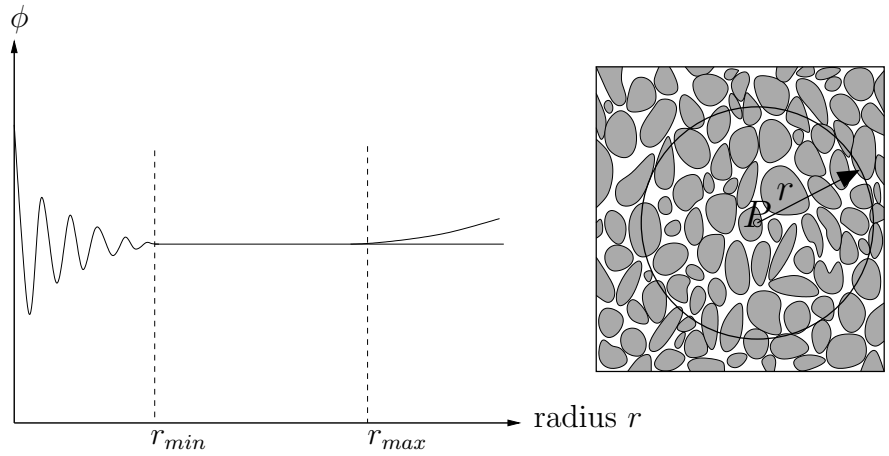

Figure 2.2: Relation between an averaged quantity and the size of the averaging volume (after Bear [1972]).

maximum REV sizes may differ between different parameters (such as porosity or permeability) or processes (such as fluid flow or heat conduction) as is pointed out, for instance in Buchter [1984].

2.3 Fluid properties

The fundamental step in the development of a model for porous media flow, is the distinction of the phases. A phase is defined as a continuous substance with homogeneous properties which is separated from other phases – with other properties – by a sharp interface. In the context of porous media flow, two types of phases are distinguished: the immobile solid phase, of which the matrix of the porous medium consists and one or several fluid phases – which are in turn distinguished in gaseous and liquid – flowing through the pore space of the matrix.

2.3.1 Phase composition

Each phase is made up of one or more components, where a component can be any chemical substance or group of substances such as air (which is then called pseudo-component). Although distinct phases may not be miscible, there is mass transfer between them at the interface. Mass transfer from a solid, liquid or gaseous phase to a liquid phase is usually called dissolution. Mass transfer from a liquid to a gaseous phase is called vaporization or, if a usually gaseous component is transferred, degassing. Finally, the mass transfer from a liquid or gaseous to a solid phase and vice versa is addressed by adsorption and desorption, respectively. If a usually solid component is transferred from a fluid to a solid phase, this is called precipitation. The composition of

a phase may have strong influences on its properties and physical and chemical behavior, making it necessary to introduce measures for the amount of contained components. Depending on the scientific disciplines, different measures are preferred. However, only those being of interest for this thesis are introduced. In general, the index α denotes the phase and the index κ the component.

- The mole fraction (dimensionless) relates the number of molecules n_α^κ of one component in a phase to the overall number of molecules in the phase n_α:

$$x_\alpha^\kappa = \frac{n_\alpha^\kappa}{n_\alpha}\,, \tag{2.1}$$

- The mass fraction (dimensionless) relates the mass of a single component κ to the total mass of the phase α and is related to the mole fraction via the molar masses M^κ by

$$X_\alpha^\kappa = \frac{x_\alpha^\kappa M^\kappa}{\sum_\kappa x_\alpha^\kappa M^\kappa}\,. \tag{2.2}$$

- Concentrations (in units of density) are defined as mass of a component per unit volume and are related to the mass fractions via the phase density ϱ_α (see below) by

$$C_\alpha^\kappa = X_\alpha^\kappa \varrho_\alpha\,. \tag{2.3}$$

By definition, mass fractions as well as mole fractions sum up to unity

$$\sum_\kappa X_\alpha^\kappa = \sum_\kappa x_\alpha^\kappa = 1\,. \tag{2.4}$$

2.3.2 Density

As physical quantity of each phase, the density is defined by mass per volume with SI-unit [kg/m^3]. In general, densities depend on temperature T, pressure p and composition of a phase:

$$\varrho_\alpha = \varrho_\alpha\left(p, T, X_\alpha^\kappa\right) \tag{2.5}$$

Liquids Due to the small distances between the molecules in liquids, pressure has only little influence on their density. In most applications of flow models in porous media, the pressure changes are relatively small compared to the immense forces that are needed to significantly compress liquids. Thus, the pressure dependence of these phases is usually neglected. As an example, the compressibility of water at normal conditions is $\kappa_{water} = 4.8 \cdot 10^{-10}$ Pa^{-1}, which means that a pressure increase of 208 bar would result in a volume decrease of one percent. Temperature, however, does affect

the density of liquids stronger and its influence may not be neglected in non-isothermal models. Depending on the solute and its interactions with the solvent, the composition of liquids may have a strong influence on density of a liquid phase. As an example, salt may raise the density of water by 20 percent, whereas it is hardly affected by dissolved oxygen.

Gases Both temperature and pressure have a strong influence on the density of gases, as is expressed by the ideal gas law, which is approximately valid for all gases at low pressures:

$$\varrho = \frac{R_s T}{p} \tag{2.6}$$

Here, R_s is the specific gas constant and T is the absolute temperature. According to Amagat's law, the volume of ideal gas mixtures equals the sum of the volume of the components. The composition of the gas phase can thus be incorporated easily by the calculation of a medium-specific gas constant

$$R_s = \frac{R}{\sum_\kappa M^\kappa x^\kappa} = R \cdot \sum_\kappa \frac{M^\kappa}{X^\kappa}\,, \tag{2.7}$$

with R, the universal gas constant.

2.3.3 Viscosity

Fluids may be defined as materials that continue to deform in presence of any shear stress (Bear [1972]). Viscosity is a measure that relates the velocity of this deformation to the applied shear stress. Consider an infinitesimal fluid volume as displayed in Figure 2.3. Shear stress τ_{yx} in horizontal direction applies to the top and bottom edge of the volume and thus it is deformed with an angular velocity $\partial\varphi/\partial t$. Newtonian fluids have

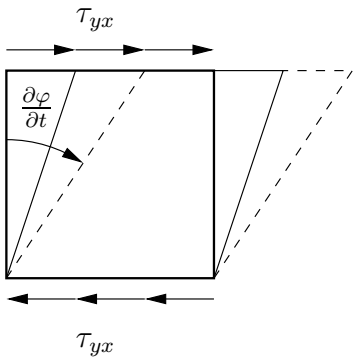

Figure 2.3: Fluid volume deformed with angular velocity $\partial\varphi/\partial t$ by shear stress τ_{yx}.

a linear relation between shear stress and deformation velocity which is expressed by the dynamic viscosity μ with the unit [Pa · s] (or in SI-units [kg/ (m · s)]):

$$\tau = \mu \frac{\partial \varphi}{\partial t} \tag{2.8}$$

Another common parameter in hydromechanics is the kinematic velocity with the unit [m^2/s], obtained through division of the dynamic viscosity by the fluids density

$$\nu = \frac{\mu}{\varrho} \,. \tag{2.9}$$

For liquids, viscosity does not change significantly with varying pressures, whereas it decreases with increasing temperatures. Gases, in contrary, have increasing viscosity with increasing temperature, where the proportionality $\mu \propto \sqrt{T}$ can be expressed for ideal gases (Atkins [1994]). The viscosity of ideal gases is independent of pressure and also in real gases, the viscosity is not affected by pressure over wide ranges (Atkins [1994]). For the calculation of the temperature dependence of real gases, Sutherland's formula (e.g. Böswirth [2005]) can be used:

$$\mu = \mu_0 \frac{T_0 + C}{T + C} \left(\frac{T}{T_0} \right)^{3/2} \tag{2.10}$$

Different approaches exist, to account for the composition of gases. The simplest is to weight the viscosities of the components with their mole fractions:

$$\mu = \sum_{\kappa} \mu^{\kappa} x^{\kappa} \,, \tag{2.11}$$

where the index κ denotes the components. In Herning and Zipperer [1936], it was found that the additional incorporation of the molar masses gives better matches to the viscosity of the mixture:

$$\mu = \frac{\sum_{\kappa} \mu^{\kappa} x^{\kappa} \sqrt{M^{\kappa}}}{\sum_{\kappa} x^{\kappa} \sqrt{M^{\kappa}}} \,. \tag{2.12}$$

2.3.4 Internal energy and enthalpy

To be able to describe the behavior of non-isothermal systems, the concept of internal energy U as caloric state variable has to be introduced. From the molecular point of view, internal energy is the amount of energy that is stored in the movement of molecules and atoms in terms of deviatoric translation, rotation, and vibration. From the continuum mechanic point of view, an infinitesimal change of internal energy is reached due to an amount of heat dQ brought into the system and due to mechanic

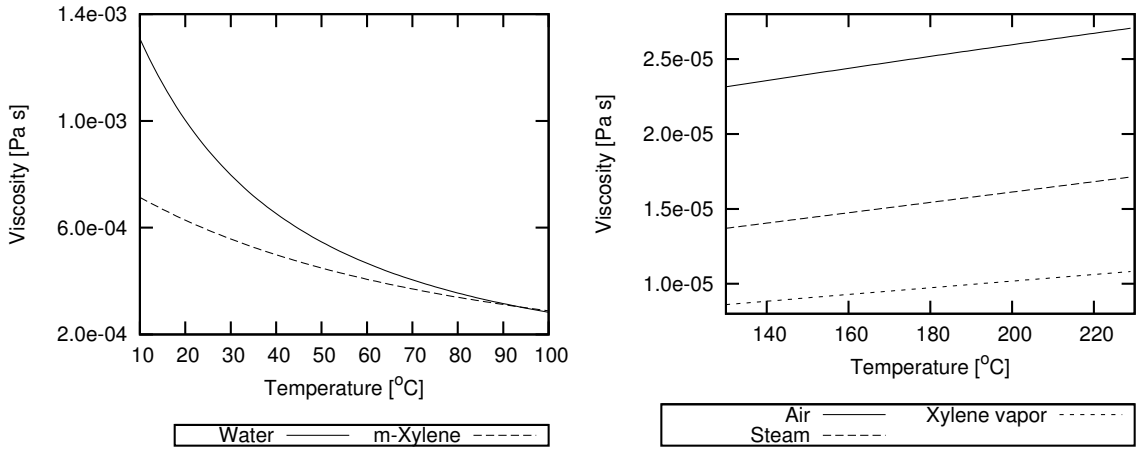

Figure 2.4: Selected viscosities at atmospheric pressure. Left: viscosity of liquid water and xylene. Right: viscosities of air, steam and xylene vapor.

work dW done on the system:

$$dU = dQ + dW \tag{2.13}$$

In the cases considered in this work, the mechanical work can be restricted to volume changing work done on the system. That is, the work which is necessary to change the volume of the system against a pressure. This gives

$$dU = dQ - p\,dV\,. \tag{2.14}$$

Since the internal energy of a system can not be measured directly, but only the mentioned amounts of heat or mechanic work, a reference point with defined temperature, pressure and volume is chosen and the internal energy of the system in other states is calculated by integrating equation 2.14. For continuum mechanic considerations it is more convenient to divide the internal energy by the mass of the associated phase to get the specific internal energy u denoting the energy stored in one unit mass

$$u = \frac{U}{m}\,, \tag{2.15}$$

with m, the mass of the considered system. The unit of the specific internal energy is [J/kg] or [m^2/s^2].

The internal energy of a phase changes with temperature. The changes in temperature and internal energy can be related to each other by a proportionality factor c_v, which is defined as the derivative of internal energy with respect to temperature at constant volume:

$$c_v = \left.\frac{\partial u}{\partial T}\right|_v \tag{2.16}$$

This proportional factor is called specific heat capacity and has the unit [J/ (kg · K)].

It denotes the amount of energy required to increase the temperature of one unit mass by one Kelvin. This relation, however, is only valid if the volume does not change. A second specific heat capacity is defined as the change of internal energy with respect to a change in temperature at constant pressure:

$$c_p = \left.\frac{\partial h}{\partial T}\right|_p \tag{2.17}$$

To increase the temperature of a phase at constant pressure, more energy is needed than in case of constant volume. That is because at constant pressure, the volume of matter increases with increasing temperature and thus volume changing work is done. If the volume is kept constant, the change of internal energy equals the heat added to a system. If the system can increase its volume against a constant pressure, a part of the added heat is emitted in form of mechanical work and the change of internal energy is not the same as the added heat. The added heat, however, equals the increase of another quantity, the *enthalpy*, which is defined as

$$H = U + pV\,. \tag{2.18}$$

As the internal energy, the enthalpy is related to the mass of the considered matter as well and thus the specific enthalpy is defined as the enthalpy per unit mass and denoted by the lower case letter h. The specific heat capacity at constant pressure can now be identified as the amount of heat required to increase the enthalpy by one Kelvin.

If a substance changes its state of matter, i.e. if a solid melts or if a liquid is vaporized, the molecules have to overcome the forces of attraction which hold them in the current state. For this, additional energy in the form of heat is needed. This is called *latent heat*, since an increase of energy does not change the temperature of the substance (as *sensible heat* does). The amount of energy which is needed to vaporize a unit mass of liquid is called *enthalpy of vaporization*.

2.3.5 Phase equilibria

A basic assumption in this work is that the compositions of phases are in thermodynamic equilibrium. That is, the phases have the same temperature, pressure and no more mass transfer between the phases takes place. Below, basic thermodynamic laws for the description of the phase equilibria are introduced. Related to modeling issues, this assumption is further discussed in Section 3.1.

Vapor pressure Consider a pure substance which is present as gas and liquid phase. The two phases are in contact and in equilibrium, i.e. there is no mass transfer of the substance between the phases. Then the pressure of the gas phase is called *vapor*

pressure. Its non-linear dependence on the temperature T can be described e.g., with Antoine's equation (e.g., Römpp et al. [1999])

$$p_{vap} = 10^{[a-b/(T-c)]}\,, \tag{2.19}$$

where the parameters a, b and c are fluid specific constants.

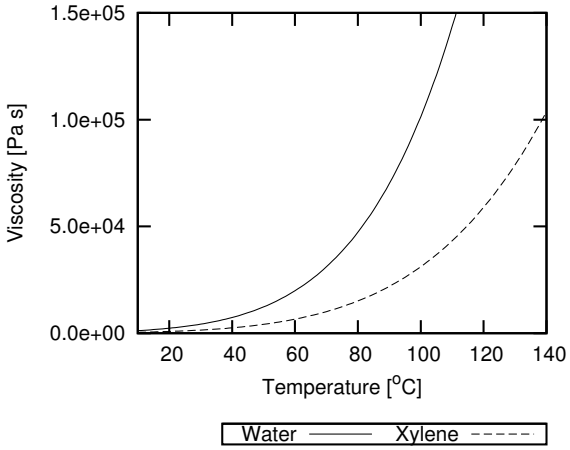

Figure 2.5: Vapor pressures of water and xylene

Dalton's Law Dalton's Law states that the pressure of a mixture of gases equals the sum of the pressures each component would have if it filled the whole volume alone

$$p_g = \sum_\kappa p_g^\kappa\,, \tag{2.20}$$

where p_g^κ is called *partial pressure* of component κ. This definition, however, is only valid for ideal gases where the pressure is a linear function of the molar density (Atkins [1994]). To make equation (2.20) valid for real gases, the partial pressure p_g^κ is defined to be proportional to the mole fraction of component κ in the gas

$$p_g^\kappa = x_g^\kappa p_g\,. \tag{2.21}$$

If this definition is combined with the vapor pressure, the mole fraction of a component κ inside a gas over a liquid can be evaluated as the ratio of the vapor pressure over the gas pressure.

Raoult's Law In a liquid which does not consist of only one component, the vapor pressure of each component is lowered. This lowering is described by Raoult's law to

be proportional to the mole fraction of the component in the liquid phase

$$p_g^\kappa = x_w^\kappa p_{vap}^\kappa \,, \tag{2.22}$$

where p_{vap}^κ is the vapor pressure of the pure liquid. Mixtures in which Raoult's law is valid for all mole fractions are called ideal. Although this behavior is seldom observed in reality, Raoult's law sufficiently describes the case of rather large mole fractions and is *true* for the vapor pressure of the solvent in an ideally diluted solution.

Henry's law Since Raoult's law is in reality only valid for solvents, another relation between partial gas pressure and liquid phase mole fraction is needed for the solute. This relation is given by Henry's law

$$p_g^\kappa = H_w^\kappa x_w^\kappa \,, \tag{2.23}$$

where H_w^κ is the *Henry coefficient*. The alternative name Henry *constant* is rather misleading since it has a strong temperature dependence which may be described according to Sander [1999]

$$H\left(T\right) = H^\Theta \cdot \exp\left(\frac{-\Delta h_{sol}}{R}\left(\frac{1}{T} - \frac{1}{T^\Theta}\right)\right) . \tag{2.24}$$

The superscript Θ denotes values at standard temperature 298.15 K and Δh_{sol} is the solution enthalpy.

Figure 2.6 shows the range of applicability of both Henry's law and Raoult's law for a binary system, where component 1 is a component forming a liquid phase, e.g. water, and component 2 is a component forming a gaseous phase, e.g. air. One can see that for low mole fractions of component 2 in the system (small amounts of dissolved air in the liquid phase), Henry's law can be applied whereas for mole fractions of component 1 close to 1 (small amounts of vapor in the gas phase), Raoult's law is the appropriate description. In general, the solvent follows Raoult's law as it is present in excess, whereas the dissolved substance follows Henry's law as it is highly diluted.

2.4 Permeability and Darcy's law

Fluid flow in porous media is driven by pressure differences. The relation between the pressure difference Δp and the discharge Q of a fluid through a one-dimensional column without gravity influences is given by the permeability of the porous medium and the viscosity of the fluid:

$$\frac{Q}{A} = \frac{1}{\mu} K \frac{\Delta p}{l} \,, \tag{2.25}$$

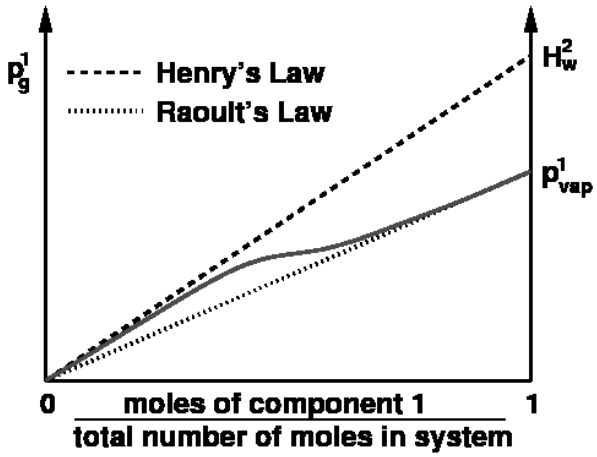

Figure 2.6: Applicability of Henry's law and Raoult's law for a binary gas–liquid system (after Lüdecke and Lüdecke [2000]).

where k denotes the permeability and A the cross-section area of the column and l its length. The ratio of discharge over area is the definition of the *Darcy velocity*. It is also often referred to as *filtration velocity* or *specific discharge* and is usually the quantity which is referred to when speaking of velocity of a fluid in this work. As all quantities presented in this section, it is only defined on a macroscopic scale reasonably larger than a single pore and is the result of averaging. Equation (2.25) is a definition of a scalar permeability in a one-dimensional fashion. In reality, however, the permeability may be anisotropic, which is the reason why it is commonly written as a tensor $\mathbf{K}$. Furthermore, not only the pressure gradient but also gravity has an effect on the fluid flow and thus Darcy's law for *single phase* flow is expressed in a vectorial notation as

$$\mathbf{v} = \frac{1}{\mu}\mathbf{K}\left(-\nabla p + \mathbf{g}\varrho\right) , \tag{2.26}$$

where the negative sign in front of the pressure gradient points out that flow is occurring in the direction of falling pressures. As stated above, the Darcy velocity is not the actual velocity of the fluid inside the porous medium, since it is an area average. To approximate the actual movement of the fluid in the flow direction, the Darcy velocity is divided by the effective porosity ϕ_e to get the *average velocity*

$$\mathbf{v}_a = \frac{\mathbf{v}}{\phi_e} .$$

The effective porosity considers the pore volume where flux actually takes place which means that dead-end pores are excluded. For the sake of simplicity, however, the effective porosity is usually approximated by the known porosity ϕ.

The validity of Darcy's law is limited to creeping flow conditions, which are in general defined by Reynolds numbers below one. The dimensionless Reynolds number is defined

as

$$Re = \frac{|\mathbf{v}_a| \cdot d}{\nu}\,, \tag{2.27}$$

with d a characteristic length and ν the kinematic viscosity. The characteristic length would in a porous medium be a pore diameter. Since this is not easily measured, for natural soils, the median grain diameter d_{50} is commonly used. Although creeping flow is limited to $Re < 1$, the influence of inertial and turbulent effects is negligible for Reynolds numbers up to 10 (Freeze and Cherry [1979], Bear [1979]).

2.5 Multi-phase flow in porous media

The laws and quantities describing the flow of fluids on the macroscale are presented in this section. These quantities are all based on the approach of averaging over a REV and are thus effective. They form the basis for the mathematical description of porous media flow on considerable scales.

2.5.1 Saturation

As the porosity, the saturation S is a dimensionless number describing a volume ratio. Consider the pore space volume V_p as introduced in section 2.2 and furthermore V_α, the volume occupied by a certain phase, e.g. water. Obviously, V_α must be included in V_p, since the rest of the REV volume is occupied by solids. The saturation of phase α is defined as the fraction of pore space, which is occupied by the phase: $S_\alpha = V_\alpha / V_p$. The pore space must always be filled by some fluid, i.e. that the volume of all phases must sum up to the pore space volume and thus all saturations must sum up to unity:

$$\sum_\alpha S_\alpha = 1\,. \tag{2.28}$$

If the saturation of one phase reaches unity, i.e., all the pore space is filled with this phase, the porous medium is commonly referred to as being *saturated* or *fully saturated* by this phase.

If in real system, one phase gets displaced by another, not all of the first phase is going to be removed. In contrary, there is a certain saturation which is held back inside the medium. This is due to capillary forces acting between the solid and the fluid phases. The saturation of a phase which can not be removed through displacement by another phase is called *residual saturation* $S_{r\alpha}$. It depends on the shape and size of the pores, the temperature and also on the displacement: If the medium was fully saturated before or if another phase was already present or if the saturation increased or decreased several times before, this generally has an influence on the residual saturation. This

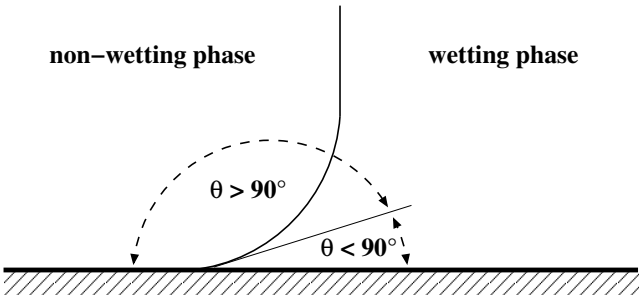

Figure 2.7: Contact angle between solid surface and fluid interface.

phenomenon is commonly referred to as *hysteresis*. However, the easiest approach, which is also used in this work, is to assign a residual saturation (which may also vary in space) to each phase. If a phase is present in residual saturation, or if the actual saturation is even lower, the phase is considered to be immobile and can only be removed by phase transition, i.e., vaporisation or dissolution.

2.5.2 Capillarity

Due to interfacial tension, forces occur at the interface of two phases. This effect is caused by interactions of the fluids on the molecular scale. Therefore, the interface between two fluid phases is curved and the equilibrium at the interface leads to a pressure difference between the phases called capillary pressure. It is commonly differentiated between wetting and non-wetting fluids. The difference is the contact angle which is measured between the solid surface and the interface of the phases as shown in Figure 2.7. The fluid with the accute contact angle has a higher affinity to the solid and tends to wet its surface. It is therefore called wetting. The non-wetting phase has correspondingly a lower affinity to the solid and is displaced by the wetting phase at the solid surface. The wetting and non-wetting behavior of fluids is caused by the already mentioned surface tension which is the energy needed to enlarge the surface between two phases by a unit area. In fact, the unit for the surface tension is [N/m], which reveals the term *tension* misleading, since it is better understood as a line load acting perpendicular to the contact line in the tangent direction of the interface. However, knowing the surface tensions between the non-wetting and wetting phase σ_{wn}, the non-wetting and solid phase σ_{sn}, and the wetting and solid phase σ_{sw}, the contact angle can be calculated using Young's equation

$$\cos(\Theta) = \frac{\sigma_{sn} - \sigma_{sw}}{\sigma_{wn}}. \tag{2.29}$$

Assuming that the interface between the two fluid phases lies inside a pore and no fluid movement can be observed, the capillary effect will lead to a pressure difference between the two fluids, which is called capillary pressure and is expressed by the Laplace

equation

$$p_c = p_n - p_w = \frac{2\sigma_{wn}\cos(\Theta)}{r}, \tag{2.30}$$

where r denotes the pore radius. From Equation (2.30), it can be seen that the capillary pressure is highest in pores of small diameters. That means if the non-wetting phase infiltrates a porous medium previously filled with the wetting phase, it will first penetrate the larger pores, whereas the wetting phase will stick to the smaller pores where the capillary pressure is high. To be able to calculate capillary pressures on an REV- or higher scale without explicitly resolving all pores, it is related to the ratio of amount of the phases (i.e. saturation, see Section 2.5.1). However, as discussed in Section 3.1, capillary pressures will not be further considered in the following.

2.5.3 Relative permeabilities and extended Darcy's law

In the case of multiphase flow, the different phases influence each other in their flow properties, which is accounted for by introducing a dimensionless factor k_r, the *relative permeability*. A basic consideration for the determination of this factor is that one phase will occupy parts of the flow paths which are therefore not passable for the second phase and vice versa. If the phases are assumed to be randomly distributed over the different flow paths, it appears reasonable to linearly scale the permeability of a phase with its saturation and thus set the relative permeability to $k_{r\alpha} = S_\alpha$. Due to capillary effects, however, the distribution of the phases in the pores will not be randomly but strongly specific. Capillary forces are low in wide pores which causes a non-wetting phase to penetrate these at first, while a wetting phase will stay inside narrow pores when its saturation drops. The narrower a pipe (or pore), the higher the occurring viscous friction. Thus, at low saturations of the wetting phase, its relative permeability rises slowly with increasing saturations because only narrow pores are occupied. For higher saturations, when the larger pores are penetrated, the relative permeability increases faster. The contrary holds for the non-wetting phase, which occupies large pores at low saturations making its relative permeability rise fast whereas it rises slower for high saturations when all large pores are already occupied and only small pores can be gained. As described, this behavior leads to a non-linear relation between relative permeability and saturation. The two most commonly used approaches for the mathematical description of the relative permeability are those after *Brooks and Corey* with

$$k_{rw} = S_e^{\frac{2+3\lambda}{\lambda}} \tag{2.31}$$

$$k_{rn} = (1 - S_e)^2 \left(1 - S_e^{\frac{2+\lambda}{\lambda}}\right) \tag{2.32}$$

and after *Van Genuchten* with

$$k_{rw} = S_e^{\epsilon}\left(1-\left(1-S_e^{\frac{1}{m}}\right)^{m}\right)^{2} \tag{2.33}$$

$$k_{rn} = (1-S_e)^{\gamma}\left(1-S_e^{\frac{1}{m}}\right)^{2m} . \tag{2.34}$$

The effective saturation S_e is determined by

$$S_e = \frac{S_w - S_{rw}}{1 - S_{rw} - S_{rn}} . \tag{2.35}$$

In the Brook-Corey model, the parameter λ is a measure for the uniformity of the pore-sizes and is, as well as the parameters ϵ, γ and m in the Van Genuchten approach, determined experimentally. Note that for non-linear relative permeability–saturation relations, the relative permeabilities of all phases do in general not sum up to unity, which emphasizes that the phases influence each other more than only blocking flow paths. As well as the residual saturation, the relative permeability shows hysteretic behavior which is, however, not further considered in the scope of this work.

The relative permeability concept is incorporated into Darcy's law by multiplication of the velocity of phase α by its relative permeability $k_{r\alpha}$ to get

$$\mathbf{v}_\alpha = \lambda_\alpha \mathbf{K}\left(-\nabla p_\alpha + \varrho_\alpha \mathbf{g}\right) , \tag{2.36}$$

where $\lambda_\alpha = k_{r\alpha}/\mu_\alpha$ denotes the mobility of phase α and p_α points out that the pressure of different phases may not be equal (caused by capillary effects).

2.6 Balance equations

In this section, the mass, momentum and energy balance equations for porous media flow are derived. In Hassanizadeh and Gray [1979], a general derivation of microscalic and macroscalic conservation equations can be found. In this work, however, only the macroscalic balance equations are considered. The basis for the balance will be the Reynolds transport theorem. It states that the total change of an extensive quantity $E = \int_G e\, dG$ inside a control volume G that is moved with the fluid is the sum of local changes of the intensive quantity$e$ in the control volume and the net flux of E over the control volume boundaries:

$$\frac{dE}{dt} = \int_G \frac{\partial e}{\partial t}\, dG + \int_\Gamma \mathbf{n}\cdot\mathbf{v}e\, d\Gamma , \tag{2.37}$$

where Γ denotes the control volume boundary. Using Gauß' theorem, the second term can also be expressed as a volume integral

$$\frac{dE}{dt} = \int_G \left[\frac{\partial e}{\partial t} + \nabla \cdot (\mathbf{v} e) \right] dG \,. \tag{2.38}$$

For the statement of a general balance equation, it is required that the physical property E is conserved and therefore does not change in time, i.e., $dE/dt = 0$. This requirement is extended by sources / sinks and a diffusive flux vector $\mathbf{w}$ of the property

$$\int_G \left[\frac{\partial e}{\partial t} + \nabla \cdot (\mathbf{v} e) \right] dG = \int_G \left(q^e - \nabla \cdot \mathbf{w} \right) dG \tag{2.39}$$

2.6.1 Multi-phase flow and transport

For the derivation of a multi-phase flow balance equation, the conservation of mass is required. That is, the mass of each phase has to be conserved which gives

$$e = \phi S_\alpha \varrho_\alpha \,. \tag{2.40}$$

On the REV-scale, diffusion and dispersion is not considered for multi-phase flow and the source term is expressed as a volumetric source q_α multiplied with the phase density. To account for the actual fluid movement, the borders of the control volume in Reynold's theorem are moved with the average velocity which is defined as $\mathbf{v}_{a\alpha} = \mathbf{v}_\alpha / (\phi S_\alpha)$. Applying these considerations to equation (2.39) yields

$$\int_G \left[\frac{\partial (\phi S_\alpha \varrho_\alpha)}{\partial t} + \nabla \cdot (\mathbf{v}_{a\alpha} \phi S_\alpha \varrho_\alpha) \right] dG = \int_G q_\alpha \varrho_\alpha \, dG \,, \tag{2.41}$$

Inserting the average velocity and rewriting equation (2.41) in differential form for each phase yields a system of n_α partial differential equations (with n_α, the number of phases):

$$\frac{\partial (\phi S_\alpha \varrho_\alpha)}{\partial t} = -\nabla \cdot (\varrho_\alpha \mathbf{v}_\alpha) + q_\alpha \varrho_\alpha \tag{2.42}$$

2.6.2 Compositional multi-phase flow and transport

The conserved quantity for the derivation of a compositional multi-phase flow equation is again mass. In the compositional case, however, it is required that the mass of each component is conserved. In general, each component may be present in each phase which means that the masses of the component in the different phases have to be summed up:

$$e = \phi \sum_\alpha \left(\varrho_\alpha S_\alpha X_\alpha^\kappa \right) = C^\kappa \,. \tag{2.43}$$

C^κ is called *total concentration* with the unit [kg/m^3] and denotes the total mass of component κ inside a unit volume. A component is spread by advection, diffusion and dispersion. Diffusion is the spreading of a component inside a phase due to molecular motion and causes a transport of the component in the direction of falling concentrations. It levels out spatial differences in concentrations and occurs in static and moving fluids. Dispersion is also called a diffusive flux, since it also reduces differences in concentration and transports a component in the direction of falling concentrations. It is, however, a hydrodynamic phenomenon and thus only occurs in moving fluids. The transport mechanism is not the movement of molecules but microscalic velocity fluctuations, swirls and differences of flow directions inside adjacent pores. These are caused by the pore geometries as well as by the presence of other fluid phases which block single pores and make the fluid flow around them inducing an accelerated or deflected flow. Both diffusion and dispersion are usually subsumed in a hydrodynamic dispersion tensor $\mathbf{D}_{pm}$ to write the diffusive/dispersive flux in the same fashion as the Fickian law

$$\mathbf{w} = -\sum_\alpha \left(\mathbf{D}_{pm,\alpha}\varrho_\alpha \nabla X_\alpha^\kappa\right) . \tag{2.44}$$

In equation (2.44), it is emphasized that diffusion takes place inside each phase, where each phase may also have an own dispersion tensor. The molecular diffusion in gas phases is higher than in liquids or in solids. It increases with increasing temperature and depends on the dissolved component and the solvent. The hydrodynamic diffusion tensor has the unit [m^2/s]. Inserting the total concentration, the diffusive flux and the mass source term q^κ into equation (2.39) yields

$$\int_G \left[\frac{\partial C^\kappa}{\partial t} + \nabla\cdot\left(\phi\sum_\alpha \mathbf{v}_{a\alpha} S_\alpha \varrho_\alpha X_\alpha^\kappa\right)\right] dG = \int_G \left[q^\kappa + \nabla\cdot\left(\sum_\alpha \mathbf{D}_{pm,\alpha}\varrho_\alpha\nabla X_\alpha^\kappa\right)\right] dG\,. \tag{2.45}$$

Inserting the average velocity rewriting the equation in differential form yields a system of n_κ partial differential equations (with n_κ, the number of components):

$$\frac{\partial C^\kappa}{\partial t} = -\nabla\cdot\sum_\alpha \left(\mathbf{v}_\alpha\varrho_\alpha X_\alpha^\kappa\right) + \sum_\alpha \left(\mathbf{D}_{pm,\alpha}\varrho_\alpha\nabla X_\alpha^\kappa\right) + q^\kappa \tag{2.46}$$

2.6.3 Non-isothermal Systems

In order to consider non-isothermal flow, energy has to be introduced as conserved quantity. In particular, only the internal energy is considered, since kinematic energy is of minor importance in light of the low flow velocities occurring in porous media. The internal energy per control volume is expressed as the sum of internal energies of

the fluids and the solid:

$$E = U = \int_G \left[\phi \sum_\alpha \left(u_\alpha S_\alpha \varrho_\alpha \right) + \left(1 - \phi \right) \varrho_s c_s T \right] \, dG \,, \tag{2.47}$$

where the subscript s denotes the solid and the internal energy in the solid is assumed to be a linear function of temperature with the heat capacity c_s. As mentioned in Section 2.3.4, changes in internal energy are caused by heat flux to, or by mechanical work done on a system,

$$\frac{dU}{dt} = \frac{dQ}{dt} + \frac{dW}{dt} \,. \tag{2.48}$$

The heat flux to the system occurs due to conduction, which is a transport of energy in the direction of falling temperatures. This transport is expressed in the same way as a diffusive flux by incorporating the heat conductivity of the porous medium with the unit $[\mathrm{W}/\left(\mathrm{m} \cdot \mathrm{K}\right)]$,

$$\mathbf{J} = -\lambda_{pm} \nabla T \,. \tag{2.49}$$

Note, that the heat conductivity in the porous medium λ_{pm} is subject to the saturation. That is because solid matrix and the different phases have different heat conductivities which contribute to the overall heat conductivities. Considerations on the determination of λ_{pm} subject to porosity and saturation can be found in Class [2001] and Hartmann et al. [2005]. In this work, the approach of Somerton as published in Somerton et al. [1974] is used. The heat conductivity is interpolated between the dry matrix conductivity $\lambda_{pm,d}$ and the conductivity of the fully liquid saturated porous medium $\lambda_{pm,w}$ by a root function of saturation:

$$\lambda_{pm} = \lambda_{pm,d} + \sqrt{S_w} \left(\lambda_{pm,w} - \lambda_{pm,d} \right) \,. \tag{2.50}$$

The heat flux to the system can be expressed as the net conduction rate across the control volume boundaries, or, after applying Gauß' theorem, as the divergence of conductive flux. Additionally a heat source q^u – which may be induced due to external heating – is part of the heat flux to the system.

$$\begin{aligned} \frac{dQ}{dt} &= -\oint_\Gamma \mathbf{n} \cdot \mathbf{J} \, d\Gamma + \int_G q^u \, dG = -\oint_\Gamma \mathbf{n} \cdot \left(-\lambda_{pm} \nabla T \right) \, d\Gamma + \int_G q^u \, dG \\ &= \int_G \left[\nabla \cdot \left(\lambda_{pm} \nabla T \right) + q^u \right] \, dG \,. \end{aligned} \tag{2.51}$$

The mechanical work done on the system is the flow of fluid phases across the control volume boundary against a pressure p,

$$\frac{dW}{dt} = -\oint_\Gamma \sum_\alpha p_\alpha \left(\mathbf{n} \cdot \mathbf{v}_\alpha \right) \, d\Gamma = -\int_G \nabla \cdot \left(p_\alpha \mathbf{v}_\alpha \right) \, dG \,. \tag{2.52}$$

The left hand side of equation (2.48) can be rewritten using Reynolds' transport theorem, where the velocity of the solid phase equals zero,

$$\frac{dU}{dt} = \int_G \frac{\partial}{\partial t}\left[\phi \sum_\alpha u_\alpha S_\alpha \varrho_\alpha + (1-\phi)\,\varrho_s c_s T\right] dG + \int_G \nabla \cdot \sum_\alpha \left(\mathbf{v}_\alpha \varrho_\alpha u_\alpha\right) dG \quad (2.53)$$

Inserting equations (2.51) through (2.53) into equation (2.48) and exploiting the definition of specific enthalpy $h_\alpha = u_\alpha + p_\alpha/\varrho_\alpha$ yields the energy balance equation for multi-phase flow,

$$\begin{aligned}&\int_G \frac{\partial}{\partial t}\left[\phi \sum_\alpha \left(u_\alpha S_\alpha \varrho_\alpha\right) + (1-\phi)\,\varrho_s c_s T\right] dG \\ &= -\int_G \left[\nabla \cdot \sum_\alpha \left(\mathbf{v}_\alpha \varrho_\alpha h_\alpha\right) + \nabla \cdot \left(\lambda_{pm} \nabla T\right) + q^u\right] dG\,. \end{aligned} \quad (2.54)$$

Abbreviating the internal energy per unit volume by

$$u_t = \phi \sum_\alpha \left(u_\alpha S_\alpha \varrho_\alpha\right) + (1-\phi)\,\varrho_s c_s T \quad (2.55)$$

and rewriting the equation in differential form yields

$$\frac{\partial u_t}{\partial t} = -\nabla \cdot \sum_\alpha \left(\mathbf{v}_\alpha \varrho_\alpha h_\alpha\right) + \nabla \cdot \left(\lambda_{pm} \nabla T\right) + q^u\,. \quad (2.56)$$

Due to the fact that internal energy cannot be measured, it is inconvenient for the use as a primary variable. Therefore, the right hand side of Equation 2.56 is commonly changed to a derivative of temperature with respect to time by inserting Equation 2.16. That way, temperature can be used as primary variable. The relation between temperature and internal energy, however, deviates considerably from this linear approximation. This has to be considered especially in gas/liquid systems where phase changes take place. Thus, the use of the internal energy – which is a quantity that can be balanced – is preferred in this work.

2.7 Model formulations

The methods for the solution of the equations for flow and transport in porous media as presented in Section 2.6, can basically be divided in two groups. If m is the number of phases or components considered, one way is to solve the m balance equations simultaneously. Since each equation influences the others, there exists a strong coupling between the variables and the solution of the equations which is why this method is

often referred to as *fully coupled.* The other possibility is to transform the system of equations into one pressure equation and $m-1$ transport equations to capture different processes: on the one hand, the motion of the fluids and on the other hand, the transport of mass or energy. Since in this case, the two processes are considered apart from each other, the method is often referred to as *decoupled*. In the further course, the decoupled methods are chosen to implement the derived equations. Thus, the focus will be set on their derivation. For the sake of completeness, however, the fully coupled methods will be addressed briefly.

2.7.1 Fully coupled formulations

In the derived balance equations, one can see an obvious coupling of the different variables. As an example, velocity is a function of pressure and therefore pressure affects the transport of mass and energy and thereby the actual saturation. Saturation, in turn, affects velocity and thereby the pressure distribution due to its impact on relative permeabilities and capillary pressures. Due to this relations, the balance equations for multiphase or compositional multiphase flow are commonly solved in a fully coupled way. That is, all primary variables are iterated simultaneously to match the criteria expressed by the balance equations. In order to use such an iterative scheme, several steps have to be done. First, primary variables have to be chosen. In case of a two-phase system, equation (2.42) gives two relations for two pressures and two saturations. This means, that two out of the four variables can be chosen as primary variables, while the other two have to be defined as secondary variables via closure relations. If, for example, one pressure and one saturation are chosen as primary variables, the secondary saturation is determined via the constraint that all saturations must sum up to unity. The secondary pressure is determined by the capillary pressure. The choice of primary variables may have a strong influence on the convergence of the algorithm and on the quality of the results, as discussed for example in Helmig [1998]. Furthermore, there may be situations, where one primary variable is not properly defined in the course of the simulation. The total displacement or dissolution of a phase in a three-phase or compositional model, respectively, can be mentioned as examples. In Class et al. [2002] and Huber [2000], the authors present primary variable switch methods to avoid numerical problems in such cases.

After having defined primary and secondary variables and the necessary closure relations, the balance equations are written in discrete form at each discretization point (nodes or cell centers, respectively, depending on the spatial discretization scheme). That is, the balance equations are transformed and expressed subject to the primary variables of the neighboring or all discretization points to get an expression of the form

$$\mathbf{A}(\mathbf{u})\,\mathbf{u} - \mathbf{r}(\mathbf{u}) = \mathbf{f}(\mathbf{u})\,. \tag{2.57}$$

	$\mathbf{A}(\mathbf{u})\,\mathbf{u}$	$\mathbf{r}(\mathbf{u})$	$\mathbf{f}(\mathbf{u})$
Phase mass	$\frac{\partial(\phi S_\alpha \varrho_\alpha)}{\partial t} + \nabla \cdot (\varrho_\alpha \mathbf{v}_\alpha)$	$+q_\alpha \varrho_\alpha$	$= 0$
Comp. mass	$\frac{\partial C^\kappa}{\partial t} + \nabla \cdot (\mathbf{v}_\alpha \varrho_\alpha X_\alpha^\kappa) + \sum_\alpha \mathbf{D}_{pm,\alpha} \nabla C_\alpha^\kappa$	$+q^\kappa$	$= 0$
Energy	$\frac{\partial u_t}{\partial t} + \nabla \cdot (\sum_\alpha \mathbf{v}_\alpha \varrho_\alpha h_\alpha) + \nabla \cdot (\lambda_{pm} \nabla T)$	$+q^u$	$= 0$

Table 2.1: Conservation equations for fluid flow in porous media.

In this equation, $\mathbf{u}$ represents the vector of unknown primary variables at all discretization points at the timestep $n+1$. The left hand side represents the discretized set of balance equations as summarized in Table 2.1. The vector of primary variables at time n is known from the last solution step or from the initial conditions. This expression is referred to as implicit time discretization. Since the whole set of equations is expressed in an implicit way (as $\mathbf{u}$ are the still unknown primary variables at time level $t + \Delta t$), the fully coupled method is also known as fully implicit. As can be seen in Table 2.1, the equations are expressed such that the right hand side vector $\mathbf{f}(\mathbf{u})$ equals zero. The task is now to find a set of primary variables $\mathbf{u}$ such that $\mathbf{f}(\mathbf{u})$ fulfills this constraint. The set of equations contains expressions which are non-linear functions of the primary variables such as relative permeabilities or spatial or temporal derivatives. Therefore, an iterative solution is sought which may be provided by the *Newton-Raphson* method. The result of the $r-th$ iteration step $\mathbf{f}(\mathbf{u}_r)$ is taken as defect and the next iteration step is calculated with

$$\mathbf{u}_{r+1} = \mathbf{u}_r - \left(\frac{\partial \mathbf{f}}{\partial \mathbf{u}}\right)_r^{-1} \cdot \mathbf{f}(\mathbf{u}_r) \; . \tag{2.58}$$

The Jacobian matrix $\partial\mathbf{f}/\partial\mathbf{u}$ contains the derivatives of defects of the balance equation at each discretization point subject to each primary variable. Since a rigorous evaluation of these derivatives is not possible or too costly, a numerical differentiation is carried out by

$$\left(\frac{\partial \mathbf{f}}{\partial \mathbf{u}}\right)_{ij} = \frac{\partial f_i}{\partial u_j} \approx \frac{f_i(..u_{j-1}, u_j + \Delta u_j, u_{j+1}..) - f_i(..u_{j-1}, u_j - \Delta u_j, u_{j+1}..)}{2\Delta u_j} \, , \tag{2.59}$$

where $\Delta u_j = \delta u_j$ is a very small increment (In Helmig [1998], $\delta = 10^{-8}$ is proposed). The advantages of the fully coupled method are the possibility of large time steps due to the time-implicit formulation. The disadvantage is that for each iteration step a system of equations of the size $n_e n_u$ (with n_e, the number of discretization points and n_u, the number of phases or components per point) has to be assembled and solved which involves rather high CPU time consumption.

2.7.2 Decoupled formulations

As the name implies, decoupled formulations split the balance equations in one pressure equation and one or more transport equations. The separation was originally intended to be able to mathematically classify the two equations as parabolic (pressure) and hyperbolic (transport) and was developed for a two-phase system neglecting capillarity in the classical paper Chavent [1976], where the author called its method *a new formulation*. Due to the introduction of the concept of fractional flows in the same paper, it is also often referred to as *fractional flow formulation*. In the following, the decoupled formulations for multiphase flow and transport and for isothermal and non-isothermal compositional multiphase flow and transport are introduced.

Multi-phase flow and transport In the case of immiscible phases, the transport of mass can be related directly to saturations. Therefore, the multi-phase balance equations are split into one pressure and one or more saturation equations.

Summation of the mass balance equation (2.42) over all phases yields

$$\sum_\alpha \frac{\partial \left(\phi S_\alpha \varrho_\alpha\right)}{\partial t} = -\sum_\alpha \nabla \cdot \left(\varrho_\alpha \mathbf{v}_\alpha\right) + \sum_\alpha q_\alpha \varrho_\alpha \,. \tag{2.60}$$

Applying the product rule to the left-hand side and to the first term on the right hand side of this equation and division by the density ϱ_α yields

$$\sum_\alpha S_\alpha \frac{\partial \phi}{\partial t} + \sum_\alpha \phi \frac{\partial S_\alpha}{\partial t} + \sum_\alpha \frac{\phi S_\alpha}{\varrho_\alpha} \frac{\partial \varrho_\alpha}{\partial t} = -\sum_\alpha \nabla \cdot \mathbf{v}_\alpha - \sum_\alpha \frac{\mathbf{v}_\alpha}{\varrho_\alpha} \cdot \nabla \varrho_\alpha + \sum_\alpha q_\alpha \,. \tag{2.61}$$

Since the saturations sum up to unity, the first term simplifies to $\partial\phi/\partial t$. The sum of derivatives of the saturations equals the derivative of the sum of saturations (which always equals unity). Hence, the derivative of the sum of saturations equals zero and the second term vanishes. Another reformulation yields the pressure equation for multiphase flow

$$\nabla \cdot \sum_\alpha \mathbf{v}_\alpha = -\frac{\partial \phi}{\partial t} - \sum_\alpha \frac{1}{\varrho_\alpha} \left(\phi S_\alpha \frac{\partial \varrho_\alpha}{\partial t} + \mathbf{v}_\alpha \cdot \nabla \varrho_\alpha \right) + \sum_\alpha q_\alpha \tag{2.62}$$

The phase velocities on the left hand side are commonly summed up to the total velocity

$$\mathbf{v} = \sum_\alpha \mathbf{v}_\alpha \,. \tag{2.63}$$

Introducing the total mobility $\lambda_t = \sum_\alpha \lambda_\alpha$ and the fractional flow function $f_\alpha = \lambda_\alpha / \lambda_t$

and insert extended Darcy's law from equation (2.36) to equation (2.63) yields

$$\mathbf{v} = \lambda_t \mathbf{K} \sum_\alpha \left(-f_\alpha \nabla p_\alpha + f_\alpha \varrho_\alpha \mathbf{g}\right) . \tag{2.64}$$

To make the presented equations mathematically and numerically convenient in the presence of capillary pressures, several formulations for the pressure in the definition of the total velocity have been developed. The most common global pressure formulations have been reviewed for two-phase flow in Helmig et al. [submitted]. In the same article, the authors present the phase pressure formulation for two-phase flow. A comparison of various three-phase flow formulations was published in Chen and Ewing [1997]. The idea of all these formulations is to rewrite equation (2.64) in terms of only one pressure, where different concepts of replacing one or all phase pressures are applied.

Since phase saturations sum up to unity, it is sufficient to formulate only one saturation equation for two-phase flow and two saturation equations for three-phase flow, respectively. It is derived by inserting the respective reformulation of equation (2.64) into the multiphase balance equation (2.42). Hence, the actual formulation of the saturation equation depends on the chosen pressure formulation.

Compositional multi-phase flow and transport A pressure equation similar to the multiphase decoupled formulation can be derived from equation (2.46). In Niessner [2006] and Huber [2000], the authors took the same steps as for the derivation of the multiphase decoupled formulation to get a pressure equation for the compositional multiphase system which is identical to equation (2.62) and derived transport equations in terms of a global pressure formulation. This formulation, however, does not consider significant changes in the volume of the fluid mixture and therefore estimates the overall density of the mixture wrongly. In fact, the pressure equation captures the spatial and temporal volume changes of the single phases due to compressibilities. However, volume changes of the whole mixture due to dissolution effects are not captured by the pressure equation. Consider for example a gas/liquid mixture with two components, where the component affine to the liquid may evaporate. An amount of the component will occupy a volume in the gas phase which may be magnitudes larger than its volume in the liquid phase. Since equation (2.62) assumes the velocity field to be divergence-free except of compressibilities, volume changes due to the described dissolution effect can not be captured.

An alternative pressure equation for compositional two-phase flow without capillary pressures was presented in Trangenstein and Bell [1989]. An expansion to three-phase compositional flow including capillary pressures – here, the authors used pressure formulation concepts as known from fractional flow formulations – was presented in Chen et al. [2000]. Inside an arbitrary control volume on REV-scale, the dimensionless specific phase volume v_α relates the volume occupied by phase α to the total cubature of

the control volume. It is emphasized, that v_α is not the specific fluid volume in the thermodynamic sense of volume per mass or mole. Since the pore space always has to be filled by some fluid, the sum of specific phase volume has to equal the porosity. Expressed for any time level $t + \Delta t$, this is

$$v_t\left(t + \Delta t\right) = \phi\left(t + \Delta t\right) , \tag{2.65}$$

where v_t is the total specific fluid volume defined as the sum of specific fluid volumina $v_t = \sum_\alpha v_\alpha$. This volume constraint is now expressed by a Taylor expansion of first order about time level t

$$v_t\left(t\right) + \Delta t \frac{\partial v_t}{\partial t} + \mathcal{O}\left(\Delta t^2\right) = \phi\left(t\right) + \Delta t \frac{\partial \phi}{\partial t} + \mathcal{O}\left(\Delta t^2\right) . \tag{2.66}$$

From the set of total concentrations C^κ and the pressure p, the splitting of components to the different phases can be evaluated as shown in Section 3.3. From this, in turn the specific fluid volumina are calculated easily with equation (3.11). Using the functional dependence $v_t = v_t\left(p, C^\kappa\right)$, the derivative of total specific volume over time in equation (2.66) can be expanded to

$$\frac{\partial v_t}{\partial t} = \frac{\partial v_t}{\partial p}\frac{\partial p}{\partial t} + \sum_\kappa \frac{\partial v_t}{\partial C^\kappa}\frac{\partial C^\kappa}{\partial t} \tag{2.67}$$

If furthermore the porosity is assumed to be a function of pressure, one can express its temporal derivative as

$$\frac{\partial \phi}{\partial t} = \frac{\partial \phi}{\partial p}\frac{\partial p}{\partial t} . \tag{2.68}$$

Inserting this to equation (2.66) yields after some reordering

$$\left(\frac{\partial v_t}{\partial p} - \frac{\partial \phi}{\partial p}\right)\frac{\partial p}{\partial t} + \sum_\kappa \frac{\partial v_t}{\partial C^\kappa}\frac{\partial C^\kappa}{\partial t} = \frac{\phi - v_t}{\Delta t} . \tag{2.69}$$

The derivative of total volume with respect to total concentration represents the increase of fluid volume if a unit mass of component κ is added to the mixture. In case of a single phase, it corresponds to the reciprocal of the fluid's mass density. The deivative $\partial v_t / \partial p$ is the compressibility of the fluid mixture. Inserting the compositional multi-phase balance equation (2.46) into Equation (2.69) yields the compositional multi-phase pressure equation

$$\begin{aligned} & c_t \frac{\partial p}{\partial t} + \sum_\kappa \frac{\partial v_t}{\partial C^\kappa} \sum_\alpha \nabla \cdot \left(\mathbf{v}_\alpha \varrho_\alpha X_\alpha^\kappa\right) \\ = \; & \sum_\kappa \frac{\partial v_t}{\partial C^\kappa}\left(q^\kappa + \nabla \cdot \left(\sum_\alpha \mathbf{D}_{pm,\alpha} \varrho_\alpha \nabla X_\alpha^\kappa\right)\right) + \varepsilon , \end{aligned} \tag{2.70}$$

where ε replaces the negative of the right hand side term in equation (2.69) and c_t expresses a total compressibility

$$\varepsilon = -\frac{\phi - v_t}{\Delta t} \tag{2.71}$$

$$c_t = -\frac{\partial v_t}{\partial p} + \frac{\partial \phi}{\partial p}\,. \tag{2.72}$$

As in equation (2.46), the phase velocity $\mathbf{v}_\alpha$ is expressed by extended Darcy's law. It is emphasized that at time level t the fluid volume does not necessarily match the pore volume. In fact, the pressure is to be chosen in such a way, that volume errors are corrected and equation (2.65) is fulfilled at time $t + \Delta t$ (Trangenstein and Bell [1989]). That is, if too much fluid is present in the control volume ($v_t > \phi$), the pressure has to increase in order to push fluid out and vice versa. Equation (2.70) predicts the changes in total specific volume due to changes in total concentrations and compensates potential volume mismatches by adjusting the pressure field accordingly. The equation is readily ordered by known parameters on the right hand side and unknowns on the left hand side.

Since the volume constraint is not always satisfied numerically, the saturations S_α are redefined to be the ratio of the volume of phase α to the volume of all phases or

$$S_\alpha = \frac{v_\alpha}{\sum_\alpha v_\alpha}\,, \tag{2.73}$$

which is the same as the previous definition in Section (2.5.1) in case the volume constraint is fulfilled.

After having solved the pressure equation, the phase velocities can be easily computed with extended Darcy's law and inserted to the multiphase component balance.

Non-isothermal compositional multi-phase flow and transport The derivation of the non-isothermal compositional pressure equation is basically identical to the isothermal pressure equation. Starting from the Taylor expansion of the volume constraint, the functional dependence of the total specific volume is extended to the internal energy per unit volume u_t to $v_t = v_t\,(p, C^\kappa, u_t)$. Instead of the internal energy, also the temperature could be used as variable of for v_t. At the boiling point of a liquid, however, the derivative $\partial v_t / \partial T$ gets infinite. Additionally to the argument outlined in Section 2.6.3, this motivates to prefer internal energy as primary variable. Now the derivative of the total specific volume is expanded to

$$\frac{\partial v_t}{\partial t} = \frac{\partial v_t}{\partial p}\frac{\partial p}{\partial t} + \sum_\kappa \frac{\partial v_t}{\partial C^\kappa}\frac{\partial C^\kappa}{\partial t} + \frac{\partial v_t}{\partial u_t}\frac{\partial u_t}{\partial t}\,. \tag{2.74}$$

Inserting this into the Taylor expansion of the volume constraint (Equation (2.66)) yields

$$\left(\frac{\partial v_t}{\partial p} - \frac{\partial \phi}{\partial p}\right)\frac{\partial p}{\partial t} + \sum_\kappa \frac{\partial v_t}{\partial C^\kappa}\frac{\partial C^\kappa}{\partial t} + \frac{\partial v_t}{\partial u_t}\frac{\partial u_t}{\partial t} = \frac{\phi - v_t}{\Delta t}\,. \tag{2.75}$$

As above, the compositional multiphase balance equation (2.46) and additionally the energy balance equation (2.56) is inserted to yield the pressure equation for non-isothermal compositional multiphase flow

$$\begin{aligned} & c_t\frac{\partial p}{\partial t} + \sum_\kappa \frac{\partial v_t}{\partial C^\kappa}\sum_\alpha \nabla\cdot(\mathbf{v}_\alpha \varrho_\alpha X_\alpha^\kappa) + \frac{\partial v_t}{\partial u_t}\sum_\alpha \nabla\cdot(\mathbf{v}_\alpha\varrho_\alpha h_\alpha) \\ = & \sum_\kappa \frac{\partial v_t}{\partial C^\kappa}\left(q^\kappa + \nabla\cdot\left(\sum_\alpha \mathbf{D}_{pm,\alpha}\varrho_\alpha \nabla X_\alpha^\kappa\right)\right) \\ & + \frac{\partial v_t}{\partial u_t}\left(q^u + \nabla\cdot(\lambda_{pm}\nabla T)\right) + \varepsilon\,. \end{aligned} \tag{2.76}$$

After solving this equation, the resulting pressures are used to evaluate the component mass balance and the energy balance equations. The derivative $\partial v_t/\partial u_t$ is a measure of thermal expansion of the fluid mixture. For a single phase – i.e. there are no phase changes due to an increase of internal energy – this derivative is

$$\frac{\partial v_t}{\partial u_t} = \phi\frac{1}{V_f}\frac{\partial V_f}{\partial T}\frac{\partial T}{\partial u_t} = \phi\frac{\alpha_T}{c_{v,t}}\,, \tag{2.77}$$

where α_T is the thermal expansion coefficient and $c_{v,t}$ is the combined isocoric heat capacity of the fluid and the solid matrix.

2.8 Multiphysics concepts

In this section, the concepts for horizontal coupling (see Figure 1.2) are presented. The main idea is to split up the model domain to use models of different complexity in the different parts of the domain. In a subdomain of special interest, a complex model of high physical accuracy is employed, whereas in the rest of the domain, a simpler model matching the simpler physics is sufficient. By that, only as much effort as necessary is spent in the particular domain parts, computational power can be saved and the informations provided by the model are not redundant. Such a horizontal coupling of models requires the formulation of coupling conditions or internal boundary conditions. These involve basically the preservation of physical quantities, such as velocity, mass flux and pressure at the internal boundary. In the following, the concepts and formulations of the isothermal multiphysics model are introduced. Based on that, the non-isothermal multiphysics model is derived.

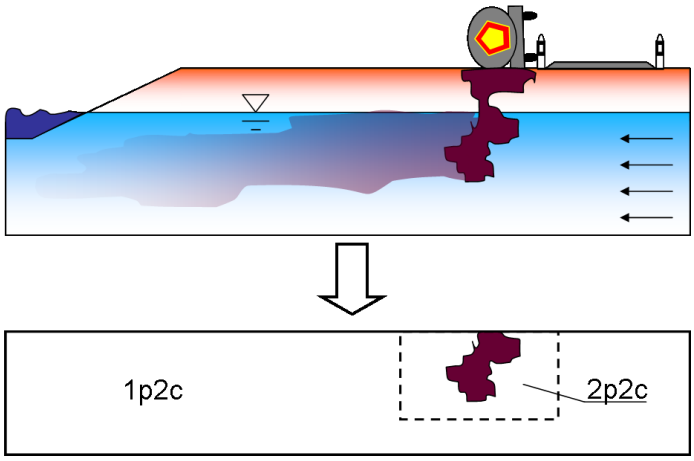

Figure 2.8: Example for a possible multiphysics application and decomposition of the model domain.

2.8.1 Multiphysics concept for isothermal systems

Consider, for example, a common application in the field of environmental engineering: a subsurface contamination as sketched in Figure 2.8, top. If the spreading of the contaminant in the groundwater is considered, the model domain would be chosen to begin at the water table. The model domain is then fully saturated with water except of a spill of NAPL. Inside this spill, contaminants of the NAPL are dissolved in water and transported away with the ambient water flow. To capture these effects, a two-phase two-component model would be necessary. However, two-phase flow is only taking place directly at the place where NAPL entered the soil, whereas the rest of the domain may be modeled with a single phase model. Furthermore, dissolution and mass exchange processes with effects on the flow and phase masses only take place where both phases are present, while the propagation of solutes can as well be simulated by a simple transport model. The concept is now to split the domain into two subdomains to apply different models: a two-phase two-component model and a single-phase transport model. The two subdomains are linked with each other at the internal boundary and so are the two models.

To realize this model, a formulation is needed which accounts for the physical processes happening in each part of the domain. The formulation has to allow for the distinct consideration of the different subdomains and also for their coupling via the internal boundaries. Therefore a decoupled formulation of a single-phase transport model is derived in the following.

Single phase pressure equation Reformulating the compositional multiphase pressure equation (2.70) for one phase (and therefore skipping the index α) yields

$$c_t \frac{\partial p}{\partial t} + \sum_\kappa \frac{\partial v_t}{\partial C^\kappa} \nabla \cdot (\mathbf{v} \varrho X^\kappa) = \sum_\kappa \frac{\partial v_t}{\partial C^\kappa} \left(q^\kappa + \nabla \cdot (\mathbf{D}_{pm} \nabla C^\kappa) \right) + \varepsilon \,. \tag{2.78}$$

Since phase changes do not take place, the volume derivative subject to total concentrations can be set to $1/\varrho$ for both components. In a binary mixture, the diffusive flux of one component equals the negative of the diffusive flux of the second component, which means that they cancel out on the right hand side. Together, this gives

$$c_t \frac{\partial p}{\partial t} + \nabla \cdot \mathbf{v} = -\frac{1}{\varrho} \mathbf{v} \cdot \nabla \varrho + \sum_\kappa \frac{1}{\varrho} q^\kappa + \varepsilon \,. \tag{2.79}$$

Since only one phase is present, the sum of the mass sources of components divided by the phase density is the same as the volumetric source of the phase q^α as used in Section 2.6.1. Again skipping the phase indices yields

$$\nabla \cdot \mathbf{v} = -c_t \frac{\partial p}{\partial t} - \frac{1}{\varrho} \mathbf{v} \cdot \nabla \varrho + q + \varepsilon \,. \tag{2.80}$$

Alternatively, a single phase pressure equation can be derived from the (immiscible) multiphase pressure equation (2.62) which is shown after introducing two transformations for single-phase flow. The mass of a single phase filling the pore space of a unit volume is $\phi\varrho$. The change of the volume of a unit mass of a fluid is $dv = d(1/\varrho)$. The change of volume of a fluid filling a unit volume is then obtained by multiplying the change of the volume of a unit mass with the mass filling a unit volume:

$$\frac{\partial v_t}{\partial p} = \phi \varrho \frac{\partial 1/\varrho}{\partial p} \,. \tag{2.81}$$

This corresponds to the common definition of compressibility as

$$c = \frac{1}{V} \frac{\partial V}{\partial p} \,. \tag{2.82}$$

The derivative of total volume with respect to pressure can be expanded to get

$$\frac{\partial v_t}{\partial p} = \phi \varrho \frac{\partial 1/\varrho}{\partial p} \frac{\partial \varrho}{\partial 1/\varrho} \frac{\partial 1/\varrho}{\partial \varrho} = \phi \varrho \frac{\partial \varrho}{\partial p} \left(-\frac{1}{\varrho^2} \right) = -\frac{1}{\varrho} \phi \frac{\partial \varrho}{\partial p} \,. \tag{2.83}$$

To derive the single-phase pressure equation from the decoupled immiscible multiphase formulation, Equation (2.62) is rewritten for one phase:

$$\nabla \cdot \mathbf{v} = -\frac{\partial \phi}{\partial t} - \frac{1}{\varrho} \left(\phi \frac{\partial \varrho}{\partial t} + \mathbf{v} \cdot \nabla \varrho \right) + q \,. \tag{2.84}$$

Now, equation 2.83 is used to replace the temporal derivative of the density by the derivative of the total volume. Then, the total compressibility c_t as defined in equation (2.72) can be introduced to get

$$\nabla \cdot \mathbf{v} = -c_t \frac{\partial p}{\partial t} - \frac{1}{\varrho} \mathbf{v} \cdot \nabla \varrho + q \,. \tag{2.85}$$

The pressure equations (2.80) and (2.85) differ in the error term, which can not be found in the multiphase pressure equation. By this comparison, however, it can be motivated to introduce a similar term to the multiphase pressure equation for the case of compressible flow. To be able to quantify the volume mismatch, the saturation equation must be reformulated to a mass transport equation and must be evaluated for each phase (as addressed in Coumou [2008]).

Single phase transport equation The transport equation is clearly found by rewriting the compositional transport equation (2.46) for only one phase:

$$\frac{\partial C^\kappa}{\partial t} = -\nabla \cdot (\mathbf{v} \varrho X^\kappa) + \mathbf{D}_{pm} \varrho_\alpha \nabla X^\kappa + q^\kappa \tag{2.86}$$

If, additionally, incompressible flow can be assumed, this equation can be simplified further. Inserting the definition of the total concentration (Equation (2.43)) and applying the product rule yields

$$S\varrho \frac{\partial X^\kappa}{\partial t} + SX^\kappa \frac{\partial \varrho}{\partial t} + \varrho X^\kappa \frac{\partial S}{\partial t} = -\nabla \cdot (\mathbf{v} \varrho X^\kappa) + \mathbf{D}_{pm} \varrho \nabla X^\kappa + q^\kappa \,. \tag{2.87}$$

Since only one phase is present, the saturation always equals unity. Hence, the third term on the left hand side equals zero. The same holds for the second term due to the assumed incompressibility. For the same reason, the density can be written in front of the derivative operators on the right hand side. Now introduce a volumetric source q as above with $q^\kappa = q \varrho X_q^\kappa$, where X_q^κ is the mass fraction of component κ in the source flow. Together this yields

$$\frac{\partial X^\kappa}{\partial t} = -\nabla \cdot (\mathbf{v} X^\kappa) + \mathbf{D}_{pm} \nabla X^\kappa + q X_q^\kappa \,. \tag{2.88}$$

Note that this equation is only valid for incompressible flow.

Coupling concept A comparison of the pressure equations for compositional multiphase flow (Equation (2.70)) and for single phase transport (Equation (2.85)) shows their resemblance. As the name implies, both equations have the pressure distribution as unknown. The terms of both equations have the same dimension (specific volume per

time). Furthermore, both equations have the same physical relevance: the local conservation of fluid volume. The same holds for the transport equations, which represent the conservation of mass.

For incompressible single-phase flow, the pressure equation (2.85) and the transport equation (2.88) of the solute is evaluated. If compressible flow is considered, the transport equation (2.86) of all components is evaluated and volumetric errors are calculated.

Figure 2.8 (bottom) shows a possible model domain for the example problem introduced above. Inside the subdomain, which is marked by the dashed rectangle, a two-phase two-component model is applied whereas the rest of the domain is represented by a single-phase transport model. The coupling conditions at the internal boundary are continuity of pressure and continuity of mass flux for each component. Furthermore, the subdomain has to be chosen in such a way that only one phase may flow across its boundaries. This is to guarantee that the assumption of single-phase flow outside the subdomain is not violated (see also Section 3.6.3).

2.8.2 Multiphysics concept for non-isothermal Systems

Consider again the example of subsurface contamination but now with a source of thermal energy. This could for example be a so-called *heat well* which is an enhanced subsurface remediation technique as displayed in Figure 2.9, top. At the spot where thermal energy is brought into the system, the soil and the fluid phases are heated and heat is also transported to the surrounding area by convection and conduction. In some cases, the source of thermal energy may even be that strong that a liquid phase reaches its boiling point. To capture these effects, a rather expensive, non-isothermal compositional multiphase flow model has to be set up. This is, however, not necessary in all parts of the model domain since a significant change in temperature only takes place near the heat source. It is therefore proposed to incorporate non-isothermal models in this subdomain of special interest. A possible model domain setup for this approach is sketched in Figure 2.9, bottom, where the subdomain for the non-isothermal models is marked by the dashed rectangle (green). Inside this subdomain, non-isothermal isoenergetic phase equilibrium calculations as presented in Section 3.3.4 and the non-isothermal pressure equation (2.76) are applied. For the case of non-isothermal one-phase flow, equation (2.76) can be simplified in a similar way as presented in Section 2.8.1, where the term containing the derivative of total specific volume subject to internal energy will remain to get

$$\frac{1}{\varrho}\nabla\cdot(\mathbf{v}\varrho)+\frac{\partial v_t}{\partial u_t}\nabla\cdot(\mathbf{v}\varrho h)=-c_t\frac{\partial p}{\partial t}+q+\varepsilon\,. \tag{2.89}$$

This pressure equation is applied to the subdomain which is labeled with 1pni. The full compositional, non-isothermal multiphase model will, however, only be applied in

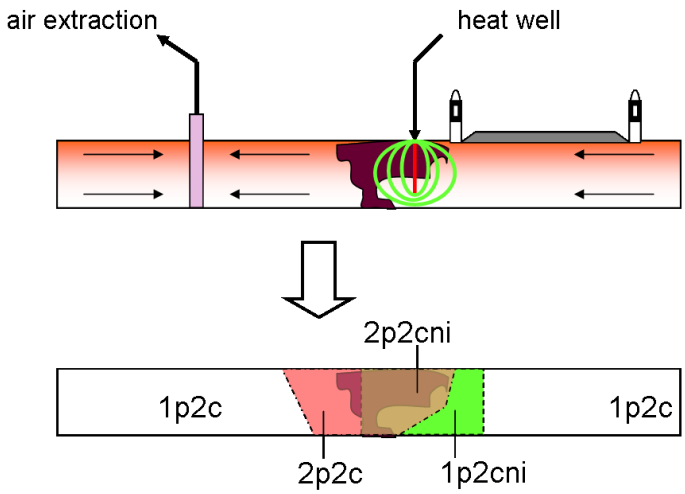

Figure 2.9: Multiphysics decomposition of the model domain for non-isothermal models.

the brown shaded subdomain where the non-isothermal and the 2p2c-subdomain overlap to the 2p2cni-subdomain. Inside the rest of the dash-dotted subdomain (red), the compositional multiphase pressure equation (2.70) is applied. The remaining part of the model domain is described by the single phase model as derived in Section 2.8.1. Analytic solutions of the heat conduction equation state that the whole system will change its temperature instantaneously if thermal energy is added at one place. However, considerable changes will only occur in the near field around the energy source, whereas temperature changes in farther away areas will stay very low. It is therefore proposed to define a threshold of temperature change ΔT_{thresh} as criterion for considerably low temperature changes. The dash-dotted "non-isothermal" subdomain in Figure 2.9 has to be chosen in such a way, that the difference between initial temperature and actual temperature in course of the simulation never exceeds the threshold. Outside the dash-dotted subdomain, the temperature is approximated linearly by

$$T = T_{init} + C_v \left(u_t - u_t \left(T_{init} \right) \right) , \tag{2.90}$$

where the overall isochoric heat capacity per unit volume C_v is evaluated by

$$C_v = \phi \varrho_s c_s + (1 - \phi) \sum_{\alpha} S_\alpha \varrho_\alpha c_{v,\alpha} , \tag{2.91}$$

with $c_{v,\alpha}$, the specific heat capacity of phase α.

Multiphase flow	Eq.
$\nabla \cdot \sum_\alpha \mathbf{v}_\alpha = -\frac{\partial \phi}{\partial t} - \sum_\alpha \frac{1}{\varrho_\alpha} \left[\phi S_\alpha \frac{\partial \varrho_\alpha}{\partial t} + \mathbf{v}_\alpha \cdot \nabla \varrho_\alpha \right] + \sum_\alpha q_\alpha$	2.62
Compositional multiphase flow $c_t \frac{\partial p}{\partial t} + \sum_\kappa \frac{\partial v_t}{\partial C^\kappa} \sum_\alpha \nabla \cdot (\mathbf{v}_\alpha \varrho_\alpha X_\alpha^\kappa) =$ $\sum_\kappa \frac{\partial v_t}{\partial C^\kappa} \left(q^\kappa + \nabla \cdot (\sum_\alpha \mathbf{D}_{pm,\alpha} \nabla C_\alpha^\kappa) \right) + \varepsilon$	2.70
Non-isothermal compositional multiphase flow $c_t \frac{\partial p}{\partial t} + \sum_\kappa \frac{\partial v_t}{\partial C^\kappa} \sum_\alpha \nabla \cdot (\mathbf{v}_\alpha \varrho_\alpha X_\alpha^\kappa) + \frac{\partial v_t}{\partial u_t} \sum_\alpha \nabla \cdot (\mathbf{v}_\alpha \varrho_\alpha h_\alpha) =$ $\sum_\kappa \frac{\partial v_t}{\partial C^\kappa} \left(q^\kappa + \nabla \cdot (\sum_\alpha \mathbf{D}_{pm,\alpha} \nabla C_\alpha^\kappa) \right) + \frac{\partial v_t}{\partial u_t} \left(q^u + \nabla \cdot (\lambda_{pm} \nabla T) \right) + \varepsilon$	2.76

Table 2.2: Pressure equations for flow and transport in porous media.

2.9 Summary

This section introduces the physical basis for the mathematical description of flow processes in porous media. After the definition of spatial scales and the introduction of the representative elementary volume concept, the physical properties of fluids and descriptions of their interactions were described. Using the REV concept, conceptual models for fluid-matrix interactions and fluid movement in single and multi-phase systems were introduced. Based on these flow equations and the physical properties, the balance equations for mass and energy in non-isothermal, compositional multiphase flow processes were derived as summarized in Table 2.1. To be able to properly decouple the occurring physical processes, decoupled mathematical formulations for the introduced conservation equations are derived. The pressure equations of the introduced decoupled models are summarized in Table 2.2. These are combined with the respective conservation equations from Table 2.1. Based on the decoupled models, multiphysics concepts for compositional isothermal and compositional non-isothermal flow processes were presented.

3 Numerical Implementation

The equations for flow and transport derived in the previous chapter can only be solved analytically under strong assumptions and in most cases only in one dimension in space. For higher dimensional calculations involving complex physical processes, numerical methods have to be used. The basis for the numerical solution is a discretization of the model domain in space and time to replace differential by discrete expressions. The discretization in space is done by a grid containing elements in shape of lines for a one-dimensional domain, triangles or squares or both for a two-dimensional domain (see Figure 3.1, left and middle), and tetrahedra or hexahedra or both for a three-dimensional domain. Each element spans between nodes which form its corners. It is usually assumed that the nodes and interfaces of adjacent cells match. If this is not the case, so-called hanging nodes result (see Figure 3.1, right). The spatial distribution of the variables between the discretization points is represented by discrete values at the discretization points and interpolation functions between them. The distance between the discretization points is in the following referred to as *discretization length*.

The temporal discretization is done by dividing the total time span of the simulation into a finite number of timesteps which may be of equal or different length. The change of a quantity e within one timestep can be calculated by a single step of the form $e_{t+\Delta t} = e_t + \partial e/\partial t \cdot \Delta t$. If the temporal derivative is calculated at the time level t, the timestep is called explicit Euler step. If, in contrary, the derivative is expressed subject to the variables at time level $t + \Delta t$, this is referred to as implicit Euler step. Other possibilities are multistep methods as Runge-Kutta or predictor-corrector schemes (see e.g., Deuflhard and Hohmann [2002]).

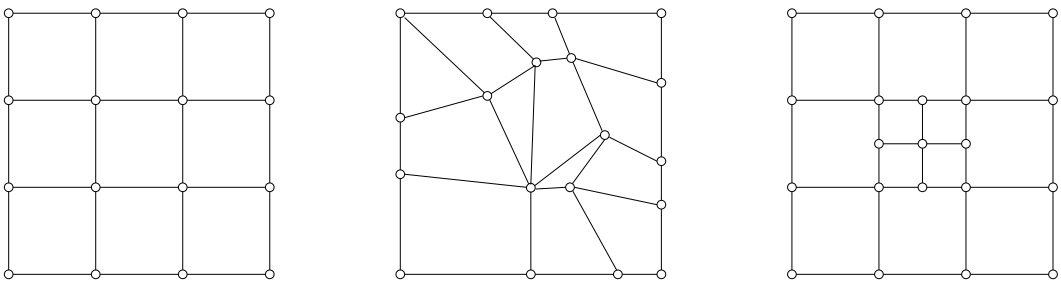

Figure 3.1: Example for a structured grid of quadrilaterals, an unstructured grid of quadrilaterals and triangles and hanging nodes in a quadrilateral grid due to local refinement.

In this work, a cell-centered finite volume method (FVM) spatial discretization is used, as this method is numerically robust and mass conservative (e.g., Huber and Helmig, 2000). This method considers the elements as control volumes and balances in- and outflow across the faces of the elements. The presented concepts are implemented to the toolbox DuMuX (Flemisch et al. [2007]), which is build on the numerical environment DUNE (Bastian et al. [2008a,b]).

3.1 General remarks

Before introducing the numerical methods in detail, some assumptions towards the involved physical processes are addressed. Some of these assumptions are inherent to the used model, i.e. only distinct processes can be described satisfactorily by the model. Other assumptions are made to reduce the model complexity for a first approach. In particular

- Capillary pressure is neglected ($p_\alpha = p$, $\forall \alpha$). This actually is a strong assumption which is made to be able to concentrate on other processes in a first step. Capillary pressure may strongly affect the flow behavior of different fluids especially when considering slow processes where they may introduce counter-current flow. The introduction of capillary pressure to the presented models should be possible with a proper implementation of the remarks related to gravity-induced counter-current flow which are addressed in Section 3.4.3.
- All processes are assumed to be advectionally dominated, i.e., the transport of quantities is mainly influenced by fluid movement and not by diffusive processes. This is an assumption for the meaningful application of the presented IMPES scheme. Particularly, molecular diffusion and hydrodynamic dispersion are neglected ($D_{pm} = 0$). For reasonable advective fluid fluxes, the influence of molecular diffusion is very low, whereas a sound representation of hydrodynamic dispersion introduces further sophisticated calculations which are not focus of this work.
- A maximum of three components is assumed, where certain mixtures, such as air or xylol, are combined to pseudo-components. The reason for this is that further components would introduce complex iteration schemes to phase stability calculations. It is emphasized that exactly these complex phase stability calculations and their time consumption are one of the motivations of the present work and the author is well aware of their relevance. However, the focus lies on their avoidance rather than on their elaborate implementation which, in turn, lies in the field of thermodynamics or chemical engineering.
- Thermodynamic equilibrium is assumed. That is, at the end of each timestep, no local kinetics are considered. In particular, this means that the soil and all fluid

phases have locally the same temperature and no heat exchange is taking place, and the mass exchange between the fluid phases is completed. These assumptions are justified by the fact that the considered flow velocities are sufficiently low and the contact areas between the phases are sufficiently large to obtain an instantaneous equilibrium.

Although, in general, advectional domination of transport processes is assumed, heat conduction – which is a diffusive process – will not be neglected. It has a very strong influence on energy transport and may in fact be dominant.

3.2 Time discretization

The particular advantage of the decoupled equations presented in Section 2.7.2 is their formal resemblance to single-phase flow and transport equations (Chen and Ewing [1997]) and the possibility to apply similar numerical methods. As shown in Trangenstein and Bell [1989] and Chen et al. [2000], the compositional pressure equation is of parabolic type and the saturation equation is of hyperbolic type. A solution approach for such a system of equations is the so-called IMPES (Implicit Pressure Explicit Saturation) method which was introduced for immiscible two-phase flow in Sheldon et al. [1959]. A more general formulation can be found in Aziz and Settari [1979]. An expansion of this concept to compositional multiphase systems was presented in Young and Stephenson [1983] and later on referred to as IMPESC or IMPEC (Implicit Pressure Explicit Saturation and / or Concentration) method (Sleep and Sykes [1993]). The core of these concepts is that the pressure equation is solved implicitly, and the transport equations are solved explicitly. The (unknown) pressure at each node or cell center at the current time level depends on the (also unknown) pressures at the neighboring nodes or cell centers at the *same* time level, which means that an *implicit* formulation is necessary. This will lead to a system of equations with as many unknowns as discretization points (as will be shown in Section 3.4). After the solution of the pressure equation, the fluid phase velocities can be calculated by extended Darcy's law and used as input to the saturation or concentration equations (here called *transport equations*), which are then solved *explicitly*. That is, the coefficients are assumed to stay constant throughout one timestep. Due to its hyperbolic property, the transport equation can then be solved for the current time level by using the known distribution and temporal derivatives of the conserved quantity from the last time level. Both, implicit and explicit solutions are schematically displayed in Figure 3.2. The transport equation could also be solved implicitly, which leads to better approximations of diffusive processes but yields bad solutions of advective processes due to large numerical diffusion. After the solution of the transport equations, the total concentrations and the total internal energy per unit volume are known. However, the coefficients needed for the calculations of the next time step depend on the still unknown saturation and mass fractions inside

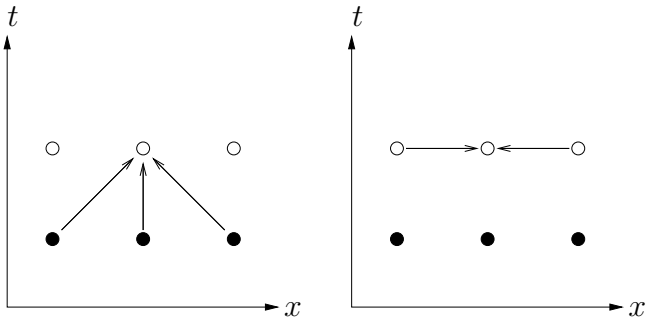

Figure 3.2: IMPES / IMPESC solution technique. Left: Explicit solution. Right: Implicit solution. Filled circles represent nodes with known primary variables, empty circles represent unknowns.

the phases. These secondary variables are determined by *phase equilibrium calculations* (also called *flash calculations*) as described in the following sections. All together, one timestep of the IMPEC method can be summarized as follows

1. Use the primary and secondary variables for time level t from the last time step solution to calculate the needed coefficients such as λ_α, ϱ_α, λ_{pm}, etc.
2. Solve the pressure equation for time level t using the coefficients evaluated in step 1.
3. Use the gained pressure and the coefficients from step 1. to calculate phase velocities and solve the transport equation to get the temporal derivatives of total concentrations and internal energy.
4. Determine a timestep Δt according to the velocities (as discussed below) and multiply it with the derivatives from step 3. to get the concentrations and internal energies at time level $t + \Delta t$.
5. Perform a phase equilibrium calculation to get the saturations and mass fractions at time level $t + \Delta t$ from the total concentrations calculated in step 4.

To guarantee stability of the explicit solution of the transport equations, the timestep has to be limited subject to discretization lengths and velocities. For one-dimensional propagation, this was already analyzed in Courant et al. [1928], leading to the stability criterion

$$\Delta t \leq \frac{\Delta x}{v_x}\,, \tag{3.1}$$

which is – according to the names of the authors – commonly referred to as the *Courant-Friedrich-Lewy- or CFL-criterion*. For more than one dimension and multiphase flow, this criterion has to be extended. For a FVM discretization, the following timestep

restriction is proposed (Helmig et al. [submitted]):

$$\begin{aligned} \Delta t_{in} &= \frac{V}{\left| \int_\Gamma \sum_\alpha \left(\mathbf{v}_{\alpha,in} \cdot \mathbf{n} \right) d\Gamma \right|} \\ \Delta t_{out} &= \frac{V}{\left| \int_\Gamma \sum_\alpha \left(\mathbf{v}_{\alpha,out} \cdot \mathbf{n} \right) d\Gamma \right|} \\ \Delta t &\leq a \, \min \left(\Delta t_{in}, \Delta t_{out} \right) , \end{aligned} \tag{3.2}$$

where V is the cubature of the current control volume and the denominators represent the total volumetric inflow and outflow over the control volume boundaries. This local criterion has to be evaluated for every cell and the minimum local Δt determines the timestep. Due to the non-linear behavior of multiphase flow, it is necessary to strengthen the timestep condition by adjusting the parameter a to a value smaller than unity. This can either be done heuristically or by a calculation taking into account some more detailed analysis of the non-linear behavior as presented in Aziz and Settari [1979]. Writing equation (3.2) for one dimension, a constant velocity in x-direction v_x and a equal to unity will lead to the CFL criterion again. In Sleep and Sykes [1993], a local stability criterion considering diffusive fluxes is expressed as

$$\Delta t \leq \left[2 D_{pm} \left(\frac{1}{\Delta x^2} + \frac{1}{\Delta y^2} \right) + \frac{v_x}{\Delta x} + \frac{v_y}{\Delta y} \right]^{-1} , \tag{3.3}$$

where Δx and Δy denote the discretization lengths and v_x and v_y the velocity components in x and y direction, respectively. As mentioned above, diffusive mass transport is assumed to be negligible. However, heat conduction is still considered to take place, as it has a high influence on energy transport. By comparison of dimensions, the diffusion coefficient can be replaced by the thermal conductivity and the overall heat capacity per unit volume as introduced in Section 2.8.2 to get a local stability criterion including thermal conduction

$$\Delta t \leq \left[2 \frac{\lambda_{pm}}{C_p} \left(\frac{1}{\Delta x^2} + \frac{1}{\Delta y^2} \right) + \frac{v_x}{\Delta x} + \frac{v_y}{\Delta y} \right]^{-1} . \tag{3.4}$$

Equation (3.3) is obviously defined for a regular axis-parallel grid in two dimensions. To get a more general criterion for finite volume methods and arbitrary dimensions, the first term is reformulated and combined with (3.2) to

$$\Delta t \leq a \left[2 \frac{\lambda_{pm}}{C_p} \frac{n_{dim}}{\bar{l}^2} + \frac{1}{\min \left(\Delta t_{in}, \Delta t_{out} \right)} \right]^{-1} . \tag{3.5}$$

Here, the sum of square reciprocals of discretization lengths was replaced by the number of dimensions n_{dim} over the square of a mean discretization length $\bar{l}$.

From the stability criteria considering diffusive effects, it becomes obvious that an explicit discretization of the transport equations is only meaningful for advection-dominated processes, as diffusion considerably lowers the maximum timestep size. For diffusion-dominated processes, an implicit discretization is more advantageous since it is stable for all time-step sizes. Transport processes which are significantly influenced by both, advection and diffusion, may be represented best by operator splitting schemes, which combine the advantages of explicit and implicit time-stepping by solving an advective and a diffusive transport equation separately (see e.g., Espedal and Karlsen, 1998).

3.3 Isobaric flash calculation

At the end of each transport step, the total concentration of each component is known. However, the saturation and the phase compositions are not regarded during the evaluation of the transport equation since only the total concentrations are balanced. To determine saturations and phase compositions from the known data, a flash-calculation has to be performed. The extend of such flash calculations varies depending on the number of phases and components. To get a clear understanding of the involved concepts, this section is structured as follows: First, some basic definitions are introduced, the equations for phase equilibrium calculations are derived and the assessment of equilibrium ratios (see below) is discussed. Afterwards, the practical implementation of isothermal two- and three-phase flash calculations is discussed to eventually introduce a method for a non-isothermal two-phase flash.

3.3.1 Rachford-Rice equation

Instead of the total concentrations, their relations to each other, expressed by the feed mass fractions Z^κ, are used. These are defined as the ratio of the mass of component κ to the total mass of the feed (the mixture of all components)

$$Z^\kappa = \frac{C^\kappa}{\sum_\kappa C^\kappa}\,. \tag{3.6}$$

Note that the total concentrations, which are of the unit $\left[\mathrm{kg/m^3}\right]$ are replaced by a dimensionless variable. It is assumed that the phases are in equilibrium, i.e., the phase compositions are stable. For this case, *equilibrium ratios* or *K-factors* are defined as the ratio of the mass fractions of one component inside phase α over the mass fraction of the same component inside a reference phase r,

$$K_\alpha^\kappa = \frac{X_\alpha^\kappa}{X_r^\kappa}\,, \tag{3.7}$$

where K_r^κ obviously always equals unity:

$$K_r^\kappa = \frac{X_r^\kappa}{X_r^\kappa} \equiv 1\,. \tag{3.8}$$

As stated in Aziz and Wong [1989], the dominant phase of a component is often selected as reference phase, so r can be different for each component. As well as the masses of the components, the masses of the phases are related to each other by the phase mass fractions ν_α. These are defined as the mass of phase α over the mass of all phases. The phase mass fractions can be evaluated from the saturations and vice versa by

$$\nu_\alpha = \frac{S_\alpha \varrho_\alpha}{\sum_\alpha S_\alpha \varrho_\alpha} \tag{3.9}$$

$$S_\alpha = \frac{\nu_\alpha / \varrho_\alpha}{\sum_\alpha (\nu_\alpha / \varrho_\alpha)}\,. \tag{3.10}$$

Note that these relations also hold if the volume constrain in Equation (2.65) is not fulfilled. The specific phase volumes can only be expressed by inclusion of the total concentrations and the phase densities with

$$v_\alpha = \frac{\nu_\alpha}{\varrho_\alpha} \sum_\kappa C^\kappa\,. \tag{3.11}$$

As any mass fraction introduced before, the phase mass fractions sum up to unity

$$\sum_\alpha \nu_\alpha = 1\,. \tag{3.12}$$

To relate the phase mass fractions to the feed mass fractions, the total concentrations from equation (2.43) are inserted to equation (3.6):

$$Z^\kappa = \frac{\sum_\alpha (S_\alpha \varrho_\alpha X_\alpha^\kappa)}{\sum_\kappa (\sum_\alpha S_\alpha \varrho_\alpha X_\alpha^\kappa)}\,. \tag{3.13}$$

The denominator can be rewritten as $\sum_\alpha (S_\alpha \varrho_\alpha \sum_\kappa X_\alpha^\kappa)$, where the mass fractions of each phase sum up to unity (see Section 2.3.1). Thus, equation (3.13) can be rewritten as

$$Z^\kappa = \sum_\alpha \left(X_\alpha^\kappa \frac{S_\alpha \varrho_\alpha}{\sum_\alpha S_\alpha \varrho_\alpha} \right) = \sum_\alpha X_\alpha^\kappa \nu_\alpha\,. \tag{3.14}$$

Inserting the definition of the equilibrium ratios (Equation (3.7)) for X_α^κ to equation (3.14) and rearranging for X_r^κ yields

$$X_r^\kappa = \frac{Z^\kappa}{\sum_\alpha K_\alpha^\kappa \nu_\alpha}\,. \tag{3.15}$$

Since, by definition, the phase mass fractions sum up to unity, one phase mass fraction can be eliminated by $\nu_e = 1 - \sum_{\alpha \neq e} \nu_\alpha$ to get

$$X_r^\kappa = \frac{Z^\kappa}{\sum_{\alpha \neq e} \left(K_\alpha^\kappa - K_e^\kappa\right) \nu_\alpha + K_e^\kappa}\,, \tag{3.16}$$

where the phase e may be chosen arbitrarily. The component mass fractions of any phase sum up to unity and thus the difference of the sum of component mass fractions of any phase and the phase e equals zero, which can be written as $(n_\alpha - 1)$ equations for all phases except of the eliminated one. To avoid mistakes, the phases in this equation are denoted by the subscript β, where the equation is written for all $\beta \neq e$

$$\sum_\kappa X_\beta^\kappa - \sum_\kappa X_e^\kappa = \sum_\kappa \left(X_\beta^\kappa - X_e^\kappa\right) = 0\,. \tag{3.17}$$

Substituting X_β^κ with the equilibrium ratio according to Equation (3.7) and X_e^κ according to Equation (3.16) yields another set of $(n_\alpha - 1)$ equations, which are again written for all $\beta \neq e$:

$$\sum_\kappa \frac{Z^\kappa \left(K_\beta^\kappa - K_e^\kappa\right)}{K_e^\kappa + \sum_{\alpha \neq e} \left(K_\alpha^\kappa - K_e^\kappa\right) \nu_\alpha} = 0 \tag{3.18}$$

If *one* phase is chosen as reference phase for all components and the same phase is also chosen to be eliminated ($e = r$), then $K_e^\kappa = 1$ holds for all κ and the set of equations (3.18) simplifies to

$$\sum_\kappa \frac{Z^\kappa \left(K_\beta^\kappa - 1\right)}{1 + \sum_{\alpha \neq e} \left(K_\alpha^\kappa - 1\right) \nu_\alpha} = 0\,, \tag{3.19}$$

which is known as the *Rachford-Rice equation*. Equations (3.18) or (3.19) together with the constraint (3.12) give n_α relations for the n_α unknowns ν_α. In case of three or more phases, the set of Rachford-Rice equations in general has to be solved simultaneously using an iterative procedure (e.g., Newton-Raphson as explained in Section 2.7.1).

Note that the same equations can be derived considering mole fractions. In this case, all variables have to be replaced by the corresponding mole-fraction based ones. The equilibrium ratios for mole fractions be denoted by

$$k_\alpha^\kappa = \frac{x_\alpha^\kappa}{x_r^\kappa}\,, \tag{3.20}$$

the feed mole fractions by

$$z^\kappa = \frac{Z^\kappa / M^\kappa}{\sum_\kappa Z^\kappa / M^\kappa}\,, \tag{3.21}$$

and the phase mole fraction by $\nu_{\alpha,mole}$. To compute the phase mass fraction from the

phase mole fraction, one can use

$$\nu_\alpha = \frac{\nu_{\alpha,mole}\bar{M}_\alpha}{\sum_\alpha \nu_{\alpha,mole}\bar{M}_\alpha}\,, \tag{3.22}$$

where $\bar{M}_\alpha$ is the mean molar mass of phase α with

$$\bar{M}_\alpha = \sum_\kappa x_\alpha^\kappa M^\kappa\,. \tag{3.23}$$

For two phases, only one equation remains, which may be solved analytically for two or three components or iteratively for more than three components. For three phases and three components, phase equilibria can be calculated analytically as well, whereas in the general case, the Rachford-Rice equation has to be solved iteratively. It is emphasized that the equilibrium ratios are not necessarily constant but may depend on the phase composition. In this case, the flash calculation is done by successive substitution. That is, after each solution of the Rachford-Rice equation and calculation of the compositions, new equilibrium ratios are evaluated to be put into the Rachford-Rice equation again. In the following, equations to obtain equilibrium ratios as well as some analytical solutions of equations (3.18) and (3.19) are presented.

3.3.2 Equilibrium ratios

Obtaining the equilibrium ratios for the phase distribution is one of the cruxes of matter in performing a flash calculation. For the applications in petroleum and reservoir engineering, pressure and temperature dependent K-factors can be found in the literature (e.g., Wiesepape et al. [1977], McCain [1990]). However, the formally most accurate way to derive equilibrium ratios is to start from the thermodynamic requirement of equality of fugacities. The fugacity f is originally used to describe the deviations of chemical potentials from those of an ideal gas and can be regarded as an adjusted pressure, since it has the same unit as pressure. It describes the tendency of a component to exit a phase which is also the meaning of the name (lat. fugere = to flee). It is formally defined as (Michelsen and Mollerup [2007])

$$RT\,\ln\frac{f^\kappa\left(T,p,x\right)}{p_0} = \mu^\kappa\left(T,p,x\right) - \mu^{\kappa\circ}\left(T,p,x\right)\,, \tag{3.24}$$

where R is the universal gas constant, p_0 is a reference pressure, μ is the chemical potential and the superscript $\circ$ denotes an ideal substances. The temperature T, pressure p and compositions x in parenthesis emphasize the dependencies on these variables. The fugacity of a component in a mixture is commonly defined using the fugacity coefficient

$$f^\kappa = \varphi^\kappa p x^\kappa\,. \tag{3.25}$$

If the equality of fugacity is stated as equilibrium condition, the fugacity of a component κ inside each phase has to equal the fugacity of the component in its reference phase $f_\alpha^\kappa = f_r^\kappa$ .Inserting equation (3.25) for both phases yields

$$\varphi_\alpha^\kappa p x_\alpha^\kappa = \varphi_r^\kappa p x_r^\kappa \,. \tag{3.26}$$

The pressure p cancels out and one can easily derive an equilibrium ratio for mole-fractions

$$k_\alpha^\kappa = \frac{x_\alpha^\kappa}{x_r^\kappa} = \frac{\varphi_r^\kappa}{\varphi_\alpha^\kappa} \,. \tag{3.27}$$

The crucial point is to find the fugacity coefficients of mixtures, which is commonly done by integrations of real gas factors gained from thermodynamic equations of state (see e.g. Michelsen and Mollerup [2007]) and involves rather complex thermodynamics. Since the fugacities depend on the phase compositions, the flash calculation has to be carried out iteratively in *any* case. However, highly exact flash calculations lie beyond the scope of this work. Hence, this approach is not further considered in this work, but it is emphasized that determining equilibrium ratios via fugacity coefficients is common practice especially in petroleum and chemical engineering and may involve massive consumptions of computational power.

Equilibrium ratios for a two-phase two-component mixture In this work, the considerations from Niessner and Helmig [2007] are used for a fast and easy evaluation of equilibrium ratios. First, a two-phase two-component system of one gaseous phase g and one liquid phase w is considered, where component A is affine to the liquid phase and component B is a gas. This could be, as an example a system of air and water at standard conditions, where air as a pseudo-component would be tagged as component B and water as component A. Using Raoult's law, the mole fraction of component 1 in the liquid phase can be expressed by its partial pressure in the gas phase by rearrangement of equation (2.22)

$$x_w^A = \frac{p_g^A}{p_{vap}^A} \,. \tag{3.28}$$

The partial pressure, in turn, can be replaced by inserting equation (2.21) to get

$$x_w^A = \frac{x_g^A p_g}{p_{vap}^A} \,. \tag{3.29}$$

Taking the liquid phase as reference for component A, the equilibrium ratio can be defined by rearranging equation (3.29) to

$$k_g^A = \frac{x_g^A}{x_w^A} = \frac{p_{vap}^A}{p_g} \,. \tag{3.30}$$

	component κ	A	B	
phase	ref. phase r	w	w	g
liquid	$k_w^\kappa = x_w^\kappa / x_r^\kappa$	1	1	p_g / H_w^B
gas	$k_g^\kappa = x_g^\kappa / x_r^\kappa$	p_{vap}^A / p_g	H_w^B / p_g	1

Table 3.1: Equilibrium ratios for a two-component gas / liquid system.

Using the Henry coefficient H_w^B of component B in the liquid phase, the mole fraction x_w^B can be expressed by rearranging equation (2.23)

$$x_w^B = \frac{p_g^B}{H_w^B}\,. \tag{3.31}$$

The partial pressure is again replaced by equation (2.21). If the liquid phase is defined as reference phase for component B, the equilibrium ratio is

$$k_g^B = \frac{x_g^B}{x_w^B} = \frac{H_w^B}{p_g}\,. \tag{3.32}$$

If, however, the gas phase is selected as reference phase since it is dominant for component B, the equilibrium ratio will be

$$k_w^B = \frac{x_w^B}{x_g^B} = \frac{p_g}{H_w^B}, \tag{3.33}$$

whereas in this case, k_g^B would equal unity. In the latter case – with the gas phase being the reference phase for component B – equation (3.18) would apply. The Rachford-Rice equation (3.19) could be used, if the liquid phase is selected as reference for both components. Table 3.1 shows the K-factors for the two-component gas / liquid system in dependence of the choice of the reference phase.

Equilibrium ratios for a three-phase three-component mixture Now, a three-phase, three-component system with two liquid phases w, n and a gas phase g is considered. The components A through C are associated to the phases w through g, so component C is a gas component now. As an example, this might be a system of an aqueous phase, a NAPL (non-aqueous phase liquid), and air, where component A would be water, component B a hydrocarbon as xylene and component C a pseudo-component air. Now a set of nine equilibrium ratios is required (three phases times three components), where the ratios for the respective reference phases are known to be unity (see Equation (3.8)).

Phase w: Consider the water phase to be the reference phase for all components, then $k_w^\kappa \equiv k_r^\kappa \equiv 1$ holds.

Phase g: For components A and C in the phases w and g, the relations from above can be used:

$$k_g^A = \frac{p_{vap}^A}{p_g} \tag{3.34}$$

$$k_g^C = \frac{H_w^C}{p_g}\,. \tag{3.35}$$

For low concentrations of component B in the water phase, its partial pressure in the gas phase is computed using Henry's law

$$p_g^B = x_w^B H_w^B\,. \tag{3.36}$$

Inserting Equation (2.21) for the partial pressure and rearranging yields

$$k_g^B = \frac{x_g^B}{x_w^B} = \frac{H_w^B}{p_g}\,. \tag{3.37}$$

Phase n: Component B is the solvent in n and thus its gas phase partial pressure is calculated using Raoult's law

$$p_g^B = x_n^B p_{vap}^B\,, \tag{3.38}$$

which must be equal to the partial pressure of component B over phase w, so equations (3.36) and (3.38) can be combined to get

$$k_n^B = \frac{x_n^B}{x_w^B} = \frac{H_w^B}{p_{vap}^B}\,. \tag{3.39}$$

Combining the vapor pressure of component A over phase w

$$p_g^A = x_w^A p_{vap}^A\,, \tag{3.40}$$

and Henry's law for component A in phase n

$$p_g^A = x_n^A H_n^A\,, \tag{3.41}$$

the equilibrium ratio k_n^A is

$$k_n^A = \frac{x_n^A}{x_w^A} = \frac{p_{vap}^A}{H_n^A}\,. \tag{3.42}$$

What remains, is the equilibrium ratio of the gaseous components between the two liquid phases. Over both phases w and n, the partial pressure of component C is

	component κ	A	B		C	
phase	ref. phase r	w	w	n	w	g
water	$k_w^\kappa = x_w^\kappa / x_r^\kappa$	1	1	p_{vap}^B / H_w^B	1	p_g / H_w^C
napl	$k_n^\kappa = x_n^\kappa / x_r^\kappa$	p_{vap}^A / H_n^A	H_w^B / p_{vap}^B	1	H_w^C / H_n^C	p_g / H_n^C
gas	$k_g^\kappa = x_g^\kappa / x_r^\kappa$	p_{vap}^A / p_g	H_w^C / p_g	p_{vap}^B / p_g	H_w^C / p_g	1

Table 3.2: Equilibrium ratios for a three-component gas / liquid / liquid system.

determined using Henry's law with

$$p_g^C = x_w^C H_w^C \tag{3.43}$$

$$p_g^C = x_n^C H_n^C \,. \tag{3.44}$$

These two equations can again be combined to get

$$k_n^C = \frac{x_n^C}{x_w^C} = \frac{H_w^C}{H_n^C} \,. \tag{3.45}$$

The equilibrium ratios for the three-phase system with phase w as reference for all components as derived here are summarized in Table 3.2 in the columns headed by w. If all K-values are derived using the same reference phase, the Rachford-Rice equation (3.19) can be used for the phase equilibrium calculation. For the case of each component's dominant phase being chosen as reference phase, the equilibrium ratios for component B and C are listed in the columns headed by n and g, respectively. In the latter case, equation (3.18) has to be chosen for the phase equilibrium calculation. The advantage of defining the dominant phase of a component as reference is that the assumption of one component being not soluble in a certain phase can be made. If one phase is chosen as reference phase for all components and any of the components is not soluble in the reference phase then the K-values for this component were not defined or infinite.

3.3.3 Isothermal isobaric flash

After having introduced the Rachford-Rice equation and the equilibrium ratios, simple methods to implement isothermal two- and three-phase flash calculations are presented.

Two-phase, two-component flash To determine the phase distribution for two phases and two components with phases w and g (this is just an exemplary choice which can be replaced arbitrarily) where phase w is chosen as phase to eliminate,

equation (3.18) is rewritten as

$$\frac{Z^A\left(K_g^A - K_w^A\right)}{K_w^A + \left(K_g^A - K_w^A\right)\nu_g} + \frac{Z^B\left(K_g^B - K_w^B\right)}{K_w^B + \left(K_g^B - K_w^B\right)\nu_g} = 0\,. \tag{3.46}$$

The analytical solution to this equation is

$$\nu_g = -\frac{Z^A\left(K_g^A - K_w^A\right)K_w^B + Z^B\left(K_g^B - K_w^B\right)K_w^A}{\left(K_g^A - K_w^A\right)\left(K_g^B - K_w^B\right)}\,. \tag{3.47}$$

The solution of the flash calculation for a given feed composition can be gained in two ways.

a) First, by calculating the K-values related to mass fractions by solving the system of equations

$$\begin{aligned} k_w^A x_r^A + k_w^B x_r^B &= 1 \\ k_g^A x_r^A + k_g^B x_r^B &= 1 \end{aligned} \tag{3.48}$$

for the reference mole fractions x_r^A, x_r^B. The mole fractions in the other phases are calculated using the definition of K-values (Equation (3.20)) which also holds . The mole fractions are transformed to mass fractions using equation (2.2) and then the mass fraction equilibrium ratios are computed by (3.7). Assume that the dominant phase of component A is phase w and that component A is a solute in phase g and vice versa for component B. A physical solution to Equation (3.47) – that is, $0 < \nu_g < 1$ – exists if $Z^A > X_g^A$ and $Z^B > X_w^B$. Otherwise, if $Z^A < X_g^A$, component A is completely dissolved in phase g and only that phase is present. Then, ν_g is set to unity and X_g^A is corrected to match Z^A. The same holds analogously for phase w if $Z^B < X_w^B$.

b) The second way is to rewrite equation (3.47) using the corresponding mole fraction quantities

$$\nu_{g,mole} = -\frac{z^A\left(k_g^A - k_w^A\right)k_w^B + z^B\left(k_g^B - k_w^B\right)k_w^A}{\left(k_g^A - k_w^A\right)\left(k_g^B - k_w^B\right)}\,. \tag{3.49}$$

To compute the feed mole fractions z^κ from the feed mass fractions, the following equation is used

$$z^\kappa = \frac{Z^\kappa M^\kappa}{\sum_\kappa Z^\kappa M^\kappa}\,.$$

If all K-values are computed using phase w as reference, Equation (3.19) can be used to evaluate the phase equilibrium. Rewritten for two phases, it is one equation

$$F(\nu_g) = \sum_\kappa \frac{Z^\kappa \left(K_g^\kappa - 1\right)}{1 + \left(K_g^\kappa - 1\right)\nu_g} = 0\,. \tag{3.50}$$

Equation (3.50) is monotonically decreasing with ν_g. If a physical solution $0 < \nu_g < 1$ exists, then $F(0) \geq 0$ and $F(1) \leq 0$ holds. Inserting this to equation (3.50) yields two stability criteria

$$\sum_\kappa Z^\kappa K_g^\kappa \;\geq\; 1\,, \tag{3.51}$$

$$\sum_\kappa \frac{Z^\kappa}{K_g^\kappa} \;\geq\; 1\,. \tag{3.52}$$

If the former is violated, only phase w is present, if the latter is violated, only phase g is present. The same criteria can be expressed analogously for mole fractions. Note that these criteria can be applied for an arbitrary number of components.

Three-phase, three-component flash For three phases and three components, equation (3.14) is a system of three equations. Combined with equation (3.7) it can be written for each component as

$$X_r^\kappa K_w^\kappa \nu_w + X_r^\kappa K_n^\kappa \nu_n + X_r^\kappa K_g^\kappa \nu_g \;=\; Z^\kappa \tag{3.53}$$

This can also be expressed in terms of mole fractions by replacing the variables with the corresponding mole fraction related quantities, which yields three equations for the three unknowns $\nu_{\alpha,mole}$:

$$\begin{aligned}
x_r^A k_w^A \nu_{w,mole} + x_r^A k_n^A \nu_{n,mole} + x_r^A k_g^A \nu_{g,mole} &= z^A \\
x_r^B k_w^B \nu_{w,mole} + x_r^B k_n^B \nu_{n,mole} + x_r^B k_g^B \nu_{g,mole} &= z^B \\
x_r^C k_w^C \nu_{w,mole} + x_r^C k_n^C \nu_{n,mole} + x_r^C k_g^C \nu_{g,mole} &= z^C\,.
\end{aligned} \tag{3.54}$$

As coefficients in equation (3.54), the mole fractions inside the reference phase are needed. These can be obtained in an analogous way as for the two-phase two-component flash by solving the system of equations

$$\begin{aligned}
x_r^A k_w^A + x_r^B k_w^B + x_r^C k_w^C &= 1 \\
x_r^A k_n^A + x_r^B k_n^B + x_r^C k_n^C &= 1 \\
x_r^A k_g^A + x_r^B k_g^B + x_r^C k_g^C &= 1\,.
\end{aligned} \tag{3.55}$$

The phase mole fractions from the solution of equation (3.54) can be transformed to mass fractions using equation (3.22). If the solution yields any phase mass fraction $\nu_\alpha < 0$, this means that the corresponding phase is not present and a two-phase three-component flash with the two remaining phases has to be evaluated instead.

Two-phase, three-component flash To confirm the presence of two phases, the stability criteria (3.51) and (3.52) have to be checked. Since these criteria only hold if K-values are determined using the same reference phase for all components, the equilibrium ratios may as well be transformed. Assume two phases w, g and K-values K_w^κ, K_n^κ, where each component may have a different reference phase. If the K-values $K_\alpha^\kappa|_w$ with phase w as reference phase are sought, they can be gained with

$$K_\alpha^\kappa|_w = \frac{X_\alpha^\kappa}{X_w^\kappa} = \frac{X_\alpha^\kappa / X_r^\kappa}{X_w^\kappa / X_r^\kappa} = \frac{K_\alpha^\kappa}{K_w^\kappa}\,. \tag{3.56}$$

If we assume phase w to be eliminated, equation (3.18) can be written for two phases and three components as

$$\begin{aligned} \frac{Z^A\left(K_g^A - K_w^A\right)}{K_w^A + \left(K_g^A - K_w^A\right)\nu_g} + \frac{Z^B\left(K_g^B - K_w^B\right)}{K_w^B + \left(K_g^B - K_w^B\right)\nu_g} \\ + \frac{Z^C\left(K_g^C - K_w^C\right)}{K_w^C + \left(K_g^C - K_w^C\right)\nu_g} \;=\; 0\,. \end{aligned} \tag{3.57}$$

Multiplying by the denominators of all three terms and rearranging yields a quadratic equation of the form

$$a\left(\nu_g\right)^2 + b\nu_g + c = 0 \tag{3.58}$$

with the coefficients

$$\begin{aligned} a &= \left(K_g^A - K_w^A\right)\left(K_g^B - K_w^B\right)\left(K_g^C - K_w^C\right) \\ b &= Z^A\left(K_g^A - K_w^A\right)\left(\left(K_g^B - K_w^B\right)K_w^C + \left(K_g^C - K_w^C\right)K_w^B\right) \\ &\quad + Z^B\left(K_g^B - K_w^B\right)\left(\left(K_g^A - K_w^A\right)K_w^C + \left(K_g^C - K_w^C\right)K_w^A\right) \\ &\quad + Z^C\left(K_g^C - K_w^C\right)\left(\left(K_g^A - K_w^A\right)K_w^B + \left(K_g^B - K_w^B\right)K_w^A\right) \\ c &= Z^A\left(K_g^A - K_w^A\right)K_w^B K_w^C + Z^B\left(K_g^B - K_w^B\right)K_w^A K_w^C \\ &\quad + Z^C\left(K_g^C - K_w^C\right)K_w^A K_w^B \end{aligned}$$

After solving equation (3.58) with the quadratic formula, the mass fractions in the phases can be evaluated with equation (3.15).

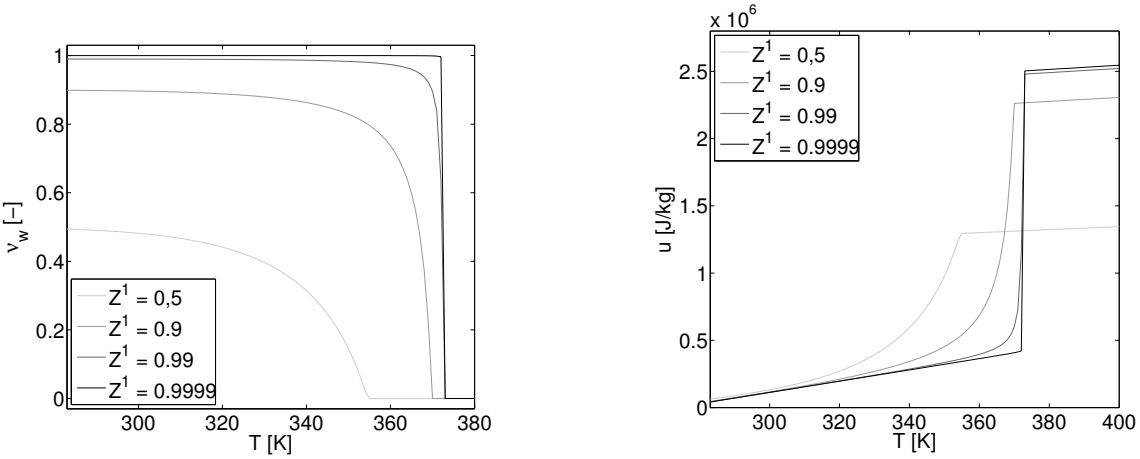

Figure 3.3: Phase mass fractions and internal energy per unit mass of a water air mixture.

3.3.4 Isoenergetic isobaric flash

In case of a non-isothermal compositional model, the total concentrations and the internal energies per unit volume are known at the end of each transport step. Now, the temperature is not fixed as in the isothermal flash calculation but is dependent on the internal energy and the phase state of the mixture. The left hand side of Figure 3.3 shows the phase mass fraction ν_w of the liquid phase of an air-water mixture over temperature for a pressure of 1 bar and different feed compositions (Z^1 denotes the feed mass fraction of water). The right hand side of Figure 3.3 shows the internal energy per unit mass u_t of the same mixtures. An isoenergetic flash calculation has to find a temperature T and a corresponding phase distribution such that the internal energy per unit volume u_t matches the *actual* internal energy u_{spec}. That is, the system of equations (3.18) or (3.19) is extended by the constraint

$$u_t = \left(\sum_\kappa C^\kappa\right)\left(\sum_\alpha u_\alpha \nu_\alpha\right) + (1-\phi)\,\varrho_s c_s T \stackrel{!}{=} u_{spec}\,. \tag{3.59}$$

Due to the strong non-linear behavior of the internal energy, this task can only be solved iteratively. One possibility for a solution is the use of a Newton-Raphson iteration to solve for the set of phase mass fractions ν_α and the temperature T at the same time. This, however, involves numerical evaluations of derivatives and an appropriate starting point for the iteration. Finding suitable starting values is in fact an aspect which may require much effort, as described for example in Saha and Caroll [1997]. Another solution method is to perform an outer loop iterating temperature around an isothermal flash as presented in Agarwal et al. [1991].

Depending on the temperature of a two-component mixture of a gas and a liquid,

different phase states exist: for temperatures below the boiling point, a single- or two-phase mixture; at the boiling point, a boiling liquid and a gas phase; for temperatures above the boiling point, a single gas phase. The flash calculation has to be carried out according to these states. Therefore, as a first step, the boiling point temperature of the liquid, i.e. the temperature where $p_{vap} = p$, is determined. At this point, a pure substance transforms from the liquid to the gaseous state. For the specified set of total concentrations, the internal energy per unit volume $u_t \big|_{T_{vap},\nu_g=1}$ is determined for the case, that the whole mixture is in the gaseous state. Now this internal energy is compared to the internal energy u_{spec} specified as input. If $u_t \big|_{T_{vap},\nu_g=1} < u_{spec}$, the whole mixture is in gaseous state and the temperature inside the control volume must be higher than the boiling point temperature. In this case, no phase equilibrium calculations must be performed, since the mixture is definitely in the gaseous state. If $u_t \big|_{T_{vap},\nu_g=1} > u_{spec}$, the mixture may be in a single- or two-phase state (see Figure 3.3, left hand side). In this case, an isothermal two-phase flash is performed for each considered temperature.

After the determination of the possible phase state, the temperature is iterated. As starting point, the boiling point temperature T_{vap} is used. A stable iterative scheme for the task of matching the specified internal energy is the tangent method which needs a second starting point. The temperature of the last time step or the initial temperature is used for this. The temperature of the next iteration step is determined by

$$T_{new} = T_i - \frac{u_j - u_i}{T_j - T_i} \left(u_i - u_{spec}\right) , \tag{3.60}$$

where the indices i, j refer to the last two iteration steps. This procedure is depicted in Figure 3.4, left hand side, where the arrow points to the temperature T_{new}. In Agarwal et al. [1991], the authors propose to define bounding temperatures T_{up}, T_{lo} with corresponding levels of internal energy $u_{up} > u_{spec} > u_{low}$. These temperature / energy pairs are updated whenever T_{new} lies between them according to

$$\begin{aligned} T_{up} &= T_{new} \quad if \quad u\left(T_{new}\right) > u_{spec} \\ T_{lo} &= T_{new} \quad if \quad u\left(T_{new}\right) < u_{spec} . \end{aligned}$$

If T_{new} is outside of these boundaries, equation (3.60) is evaluated using the bounding temperatures instead of the temperatures of the last iteration steps.

In case of a pure or nearly pure substance, the iteration scheme as proposed above will not work if the specified internal energy lies between the internal energies of the completely liquid and completely gaseous state due to the infinite inclination of the internal energy function at the boiling point (see Figure 3.4, right hand side). In this case, however, the internal energy is a linear function of the phase mass fraction. Therefore the phase mass fraction can be determined according to the *Lever rule* (see

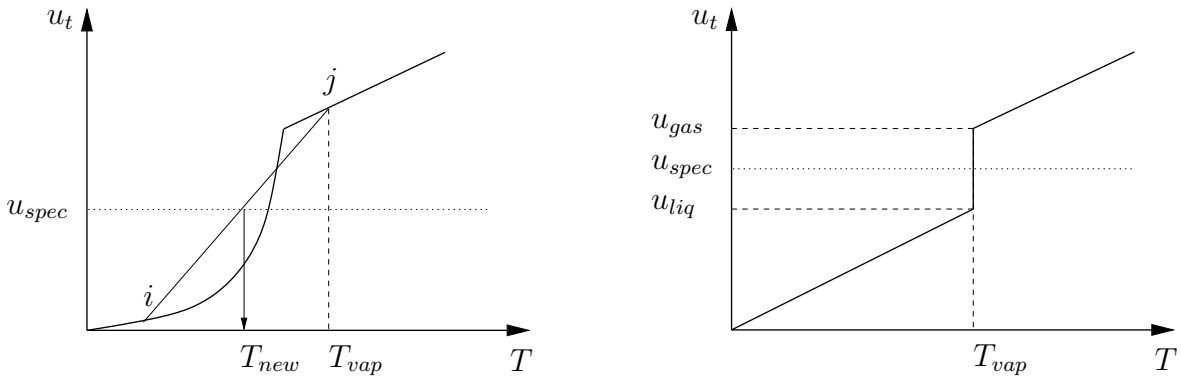

Figure 3.4: Two-phase isoenergetic flash calculations for moderate (left) and very low concentrations (right) of gas component.

e.g., Atkins [1994]) to

$$\nu_l = u_l + \frac{u_{spec} - u_l}{u_g - u_l}\,. \tag{3.61}$$

3.4 Spatial discretization: Finite Volumes

As already mentioned in the introduction of this chapter, the cell centered finite volume method is used for the spacial discretization due to its robustness and mass conservativity. It discretizes the model domain with control volumes which balance the fluxes of mass or energy across their faces. Cell centered finite volumes use the elements of the grid as control volumes and the discretization points are the element- or cell centers. The partial differential equations are then integrated over each control volume.

3.4.1 Pressure equation

For the sake of readability, the discretization is shown on the example of the isothermal compositional pressure equation. The extension of the presented considerations to the non-isothermal pressure equation is straightforward.

Integration of equation (2.70) over the control volume G yields

$$\begin{aligned} &\int_G c_t \frac{\partial p}{\partial t} dG + \int_G \sum_\kappa \frac{\partial v_t}{\partial C^\kappa} \nabla \cdot \sum_\alpha \left(\mathbf{v}_\alpha \varrho_\alpha X_\alpha^\kappa\right) dG \\ = \; &\int_G \sum_\kappa \frac{\partial v_t}{\partial C^\kappa} q^\kappa dG + \int_G \varepsilon dG\,, \end{aligned} \tag{3.62}$$

where the diffusion term is neglected according to the assumptions made in Section 3.1. Total compressibility, sources and the volumetric error term are considered to be

piecewise constant and thus the corresponding integrals can be replaced by a multiplication with the control volume cubature $|V|$. The Gauss-Green formula allows to replace the volume integral of the divergence by an integral over the control volume surface Γ:

$$\begin{aligned} & |V|\, c_t \frac{\partial p}{\partial t} + \oint_\Gamma \sum_\kappa \frac{\partial v_t}{\partial C^\kappa} \mathbf{n} \cdot \sum_\alpha \left(\mathbf{v}_\alpha \varrho_\alpha X_\alpha^\kappa\right) d\Gamma \\ & - \int_G \sum_\kappa \nabla \frac{\partial v_t}{\partial C^\kappa} \cdot \sum_\alpha \left(\mathbf{v}_\alpha \varrho_\alpha X_\alpha^\kappa\right) dG \\ = \; & + |V| \sum_\kappa \frac{\partial v_t}{\partial C^\kappa} q^\kappa + |V|\, \varepsilon \,, \end{aligned} \tag{3.63}$$

where $\mathbf{n}$ denotes the outward pointing normal on the surface. Inserting extended Darcy's law from Equation (2.36) yields

$$\begin{aligned} & |V|\, c_t \frac{\partial p}{\partial t} + \oint_\Gamma \sum_\kappa \frac{\partial v_t}{\partial C^\kappa} \mathbf{n} \cdot \sum_\alpha \left[\lambda_\alpha \mathbf{K} \left(-\nabla p_\alpha + \varrho_\alpha \mathbf{g}\right) \varrho_\alpha X_\alpha^\kappa\right] d\Gamma \\ & - \int_G \sum_\kappa \nabla \frac{\partial v_t}{\partial C^\kappa} \cdot \sum_\alpha \left[\lambda_\alpha \mathbf{K} \left(-\nabla p_\alpha + \varrho_\alpha \mathbf{g}\right) \varrho_\alpha X_\alpha^\kappa\right] dG \\ = \; & + |V| \sum_\kappa \frac{\partial v_t}{\partial C^\kappa} q^\kappa + |V|\, \varepsilon \,. \end{aligned} \tag{3.64}$$

As discussed in Section 3.1, capillarity is being neglected. Hence, all phase pressures are equal: $p_\alpha = p$. Some reordering and separation of the pressure gradients and gravity vectors further leads to

$$\begin{aligned} & |V|\, c_t \frac{\partial p}{\partial t} - \oint_\Gamma \mathbf{n} \cdot (\mathbf{K} \nabla p) \sum_\alpha \left[\lambda_\alpha \varrho_\alpha \sum_\kappa \left(\frac{\partial v_t}{\partial C^\kappa} X_\alpha^\kappa\right)\right] d\Gamma \\ & + \int_G (\mathbf{K} \nabla p) \cdot \sum_\alpha \left[\lambda_\alpha \varrho_\alpha \sum_\kappa \left(\nabla \frac{\partial v_t}{\partial C^\kappa} X_\alpha^\kappa\right)\right] dG \\ = \; & - \oint_\Gamma \mathbf{n} \cdot (\mathbf{K} \mathbf{g}) \sum_\alpha \left[\lambda_\alpha \varrho_\alpha \varrho_\alpha \sum_\kappa \left(\frac{\partial v_t}{\partial C^\kappa} X_\alpha^\kappa\right)\right] d\Gamma \\ & + \int_G (\mathbf{K} \mathbf{g}) \cdot \sum_\alpha \left[\lambda_\alpha \varrho_\alpha \varrho_\alpha \sum_\kappa \left(\nabla \frac{\partial v_t}{\partial C^\kappa} X_\alpha^\kappa\right)\right] dG \\ & + |V| \sum_\kappa \frac{\partial v_t}{\partial C^\kappa} q^\kappa + |V|\, \varepsilon \,. \end{aligned} \tag{3.65}$$

All pressure-dependent terms are now aligned at the left hand side, while the gravitational terms are shown on the right. This structure is already in accordance with the structure of the linear system of equations which will be introduced below. The right hand side only consists of known coefficients and can be evaluated at each time level. The left hand side contains the sought pressures and will be transformed into a stiffness matrix and a vector of unknowns.

The differential and integral operators in this equation now have to be transferred to discrete forms to be able to calculate them numerically. Figure 3.5 schematically shows a cell in the grid and its k-th neighboring cell. At each control volume, the pressure equation is discretized in the following way:

- At each cell interface, the integrands are approximated to be constant . Then the integral over the k-th interface can be replaced by the product with the area $|A_k|$ of the surface. The integral over the whole surface, $\oint_\Gamma \mathbf{n} \cdot (.)\, d\Gamma$, is thus replaced by a sum over all interfaces $\sum_k |A_k|\, \mathbf{n}_k \cdot (.)$, where $\mathbf{n}_k$ is the outward pointing normal on the k-th interface.

- The volume integrals are evaluated by a decomposition of the cell volume as shown in Figure 3.5, right hand side. Each cell interface k is assigned a weighting factor w_k and the subvolume $w_k\,|V|$. The sum over all weighting factors of a cell obviously has to equal unity. The integrand is evaluated at the interface and approximated to be constant inside the subvolume. Thus, the volume integral $\int_G (.)\, dG$ can be replaced by $\sum_k w_k\,|V|\,(.)$.

- The pressure gradient is approximated to be constant between two discretization points. Thus, the pressure gradient ∇p at the k-th interface is replaced by $-\frac{p-p_k}{|\mathbf{u}_k|}\frac{\mathbf{u}_k}{|\mathbf{u}_k|}$, with p and p_k being the pressures at the current cell center and the k-th neighboring cell center, respectively, while $\mathbf{u}_k$ is the vector connecting the two cell centers.

- The gradient of the volume derivatives, $\nabla\left(\partial v_t/\partial C^\kappa\right)$, can be interpreted in two ways: either the volume derivative is approximated as piecewise constant, resulting in a zero gradient; or the volume derivative is approximated by linear interpolation between two cell centers and its gradient is determined in the same way as the pressure gradient (as presented below).

- The time derivative of the pressure, $\partial p/\partial t$, is approximated by $\left(p^t - p^{t-\Delta t}\right)/\Delta t$, where p^t is the sought pressure at the current cell center and $p^{t-\Delta t}$ is the pressure known from the last timestep.

Inserting these approximations into Equation (3.67) yields

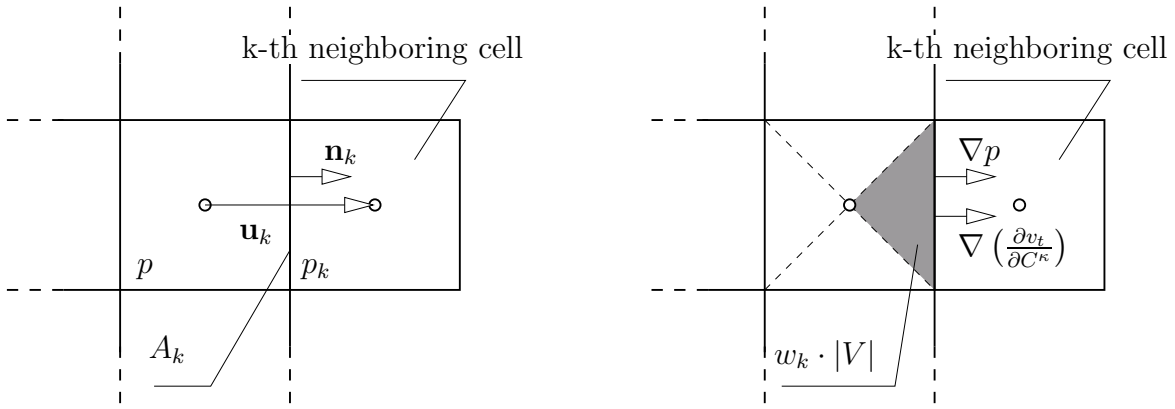

Figure 3.5: Vector and interface notation in FVM scheme.

$$
\begin{aligned}
& |V|\, c_t \frac{p^t}{\Delta t} \\
& + \sum_k |A_k|\, \mathbf{n}_k \cdot \left(\mathbf{K} \frac{p^t - p_k^t}{|\mathbf{u}_k|} \frac{\mathbf{u}_k}{|\mathbf{u}_k|} \right) \sum_\alpha \left[\lambda_\alpha \varrho_\alpha \sum_\kappa \left(\frac{\partial v_t}{\partial C^\kappa} X_\alpha^\kappa \right) \right] \\
& - |V| \sum_k w_k \left(\mathbf{K} \frac{p^t - p_k^t}{|\mathbf{u}_k|} \frac{\mathbf{u}_k}{|\mathbf{u}_k|} \right) \cdot \sum_\alpha \left[\lambda_\alpha \varrho_\alpha \sum_\kappa \left(\frac{\frac{\partial v_t}{\partial C^\kappa} - \left(\frac{\partial v_t}{\partial C^\kappa}\right)_k}{|\mathbf{u}_k|} \frac{\mathbf{u}_k}{|\mathbf{u}_k|} X_\alpha^\kappa \right) \right] \\
= & - \sum_k |A_k|\, \mathbf{n}_k \cdot (\mathbf{Kg}) \sum_\alpha \left[\lambda_\alpha \varrho_\alpha \varrho_\alpha \sum_\kappa \left(\frac{\partial v_t}{\partial C^\kappa} X_\alpha^\kappa \right) \right] \\
& + |V| \sum_k w_k\, (\mathbf{Kg}) \cdot \sum_\alpha \left[\lambda_\alpha \varrho_\alpha \varrho_\alpha \sum_\kappa \left(\frac{\frac{\partial v_t}{\partial C^\kappa} - \left(\frac{\partial v_t}{\partial C^\kappa}\right)_k}{|\mathbf{u}_k|} \frac{\mathbf{u}_k}{|\mathbf{u}_k|} X_\alpha^\kappa \right) \right] \\
& + |V| \sum_\kappa \frac{\partial v_t}{\partial C^\kappa} q^\kappa + |V|\, c_t \frac{p^{t-\Delta t}}{\Delta t} + |V|\, \varepsilon\,, \qquad (3.66)
\end{aligned}
$$

where the known pressure $p^{t-\Delta t}$ is already written on the right hand side. The determination of the volume derivatives in Equation (3.66) depends on the choice of their approximation. In the case of a piecewise constant approximation, the volume derivative is always chosen from the current cell. In case of a linear approximation, it is evaluated at the interface by linear interpolation. For each neighboring cell k, the permeability is determined by the harmonic mean of the permeabilities at the current and at the k-th cell center. All other coefficients are determined by fully upwind as discussed in Section 3.4.3.

Although this derivation is mathematically consistent, it turned out that it does not represent gravitational effects properly for all grids. As an example, take the grid

sketched in Figure 3.6. It has a constant inclination at which the top and bottom cell interfaces are oriented, whereas the interfaces in the horizontal direction are vertical. For convenience, consider the gradient of volume derivatives to vanish and incompressible flow, so all terms but the interface integrating ones vanish in Equation (3.66). Now, consider the zoomed-out cells in Figure 3.6. At the (vertical) interface between two horizontally adjacent cells, the normal vector points in a horizontal direction. Thus, the scalar product of the normal and the gravity vector vanishes. Consequently, the right hand side of Equation (3.66) equals zero which means that gravity is not regarded here. If no flow occurs (i.e. under hydrostatic conditions) one expects a higher pressure in the left cell due to the elevation difference Δz. The solution of Equation (3.66), however, does only show a variation in pressure in the vertical direction and constant pressure throughout the horizontal layers. To overcome this weakness, it is proposed to replace the normal vector $\mathbf{n}$ by the vector connecting the cell centers normalized to unit length $\mathbf{u}/|\mathbf{u}|$. This would in turn overestimate the cross section of flow which is smaller orthogonal to $\mathbf{u}$ than orthogonal to $\mathbf{n}$. Therefore, the proposed vector is furthermore scaled by the scalar product $(\mathbf{u}/|\mathbf{u}|)\cdot\mathbf{n}$. The normal vector $\mathbf{n}$ is hence replaced by

$$\mathbf{s} = \mathbf{u}\,(\mathbf{u}\cdot\mathbf{n})\,/\,|\mathbf{u}|^{\mathbf{2}}\,.$$

This yields the final form of the discretized pressure equation:

$$\begin{aligned}
& |V|\, c_t \frac{p^t}{\Delta t} \\
& + \sum_k |A_k|\, \mathbf{s}_k \cdot \left(\mathbf{K} \frac{p^t - p_k^t}{|\mathbf{u}_k|} \frac{\mathbf{u}_k}{|\mathbf{u}_k|} \right) \sum_\alpha \left[\lambda_\alpha \varrho_\alpha \sum_\kappa \left(\frac{\partial v_t}{\partial C^\kappa} X_\alpha^\kappa \right) \right] \\
& - |V| \sum_k w_k \left(\mathbf{K} \frac{p^t - p_k^t}{|\mathbf{u}_k|} \frac{\mathbf{u}_k}{|\mathbf{u}_k|} \right) \cdot \sum_\alpha \left[\lambda_\alpha \varrho_\alpha \sum_\kappa \left(\frac{\frac{\partial v_t}{\partial C^\kappa} - \left(\frac{\partial v_t}{\partial C^\kappa}\right)_k}{|\mathbf{u}_k|} \frac{\mathbf{u}_k}{|\mathbf{u}_k|} X_\alpha^\kappa \right) \right] \\
= & - \sum_k |A_k|\, \mathbf{s}_k \cdot (\mathbf{K}\mathbf{g}) \sum_\alpha \left[\lambda_\alpha \varrho_\alpha \varrho_\alpha \sum_\kappa \left(\frac{\partial v_t}{\partial C^\kappa} X_\alpha^\kappa \right) \right] \\
& + |V| \sum_k w_k\, (\mathbf{K}\mathbf{g}) \cdot \sum_\alpha \left[\lambda_\alpha \varrho_\alpha \varrho_\alpha \sum_\kappa \left(\frac{\frac{\partial v_t}{\partial C^\kappa} - \left(\frac{\partial v_t}{\partial C^\kappa}\right)_k}{|\mathbf{u}_k|} \frac{\mathbf{u}_k}{|\mathbf{u}_k|} X_\alpha^\kappa \right) \right] \\
& + |V| \sum_\kappa \frac{\partial v_t}{\partial C^\kappa} q^\kappa + |V|\, c_t \frac{p^{t-\Delta t}}{\Delta t} + |V|\, \varepsilon\,, \qquad (3.67)
\end{aligned}$$

Equation (3.67) is readily ordered by terms containing unknowns on the left hand side and terms containing only known coefficients on the right hand side. It is evaluated at

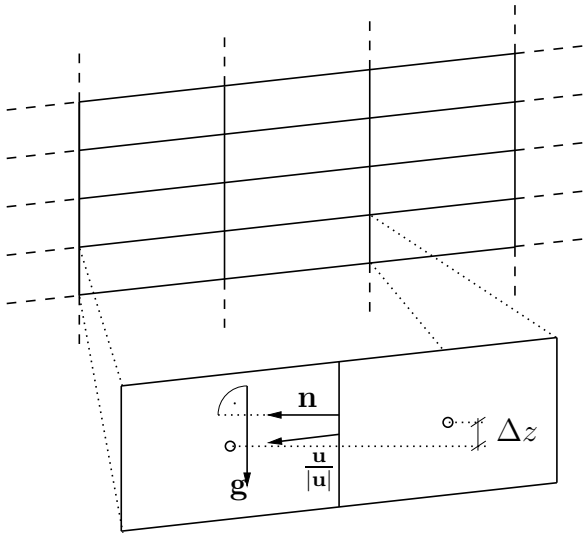

Figure 3.6: Non-Cartesian, regular grid with constant inclination.

each cell and written into a linear system of equations of the form

$$\mathbf{A}\mathbf{p} = \mathbf{r}\,, \tag{3.68}$$

where $\mathbf{A}$ is the stiffness matrix, $\mathbf{p}$ contains the unknown pressures at each cell center and $\mathbf{r}$ contains the right hand side of Equation (3.67) evaluated for each cell. This system is solved using an iterative solver provided by the DUNE Iterative Solver Template Library (see Bastian et al. [2008a]).

Treatment of the volume mismatch term In practical application of the described model, it turned out that an unconditional incorporation of the volume mismatch term ε causes a rather unstable behavior of the model. Since the pressure equation is based only on a first order Taylor approximation, very low volume mismatches with $|\phi - v_t| \ll \phi$ occur quite randomly throughout the whole domain. Incorporating these low mismatches into the pressure equation rather builds them up over several timesteps than balancing them. If they are neglected, in contrary, they cancel out automatically in subsequent timesteps. It therefore proved to be practical to define a threshold value τ_ε and only consider volume mismatches if $|\phi - v_t| \geq \tau_\varepsilon$ is fulfilled. A value of $\tau_\varepsilon = \phi \cdot 10^{-5}$ proved to work well. For very low timesteps Δt, however it has to be decreased. Since the denominator of ε contains Δt, the error term may jump from zero to considerably high values when the threshold is exceeded.

Additionally to the negligence of very low volume mismatches, it may be necessary to dampen the error term ε by a factor $f_\varepsilon < 1$. In case of occurrence of larger volume mismatches, this prevents abrupt local pressure changes and smoothly corrects the errors. A factor of $f_\varepsilon = 0.5...0.9$ was found heuristically and proofed to be suitable in

most applications.

3.4.2 Transport equations

As with the pressure equation, the concentration equation (2.46) is integrated over a control volume to get

$$\int_G \frac{\partial C^\kappa}{\partial t} dG = -\int_G \nabla \cdot \sum_\alpha \left(\mathbf{v}_\alpha \varrho_\alpha X_\alpha^\kappa\right) dG + \int_G q^\kappa dG\,, \tag{3.69}$$

where the hydrodynamic dispersion is again neglected. Application of the Gauss-Green formula and insertion of extended Darcy's law (2.36) yields

$$\int_G \frac{\partial C^\kappa}{\partial t} dG = -\oint_\Gamma \mathbf{n} \cdot \sum_\alpha \left(\lambda_\alpha \mathbf{K} \left(-\nabla p + \varrho_\alpha \mathbf{g}\right) \varrho_\alpha X_\alpha^\kappa\right) dG + \int_G q^\kappa dG\,. \tag{3.70}$$

The total concentration and its temporal derivative are approximated as piecewise constants as well as the source term. Hence, the volume integrals are replaced by a multiplication with the cell volume $|V|$. The pressure gradient and the surface integral are approximated in the same way as discussed for the pressure equation in the preceding section. The time derivative is approximated in by rearranging the first order Taylor series expansion $C^\kappa\left(t+\Delta t\right) = C^\kappa\left(t\right) + \left(\partial C^\kappa / \partial t\right) \Delta t$:

$$\begin{aligned} &\frac{C^\kappa\left(t+\Delta t\right) - C^\kappa(t)}{\Delta t} \\ = \; & -\sum_k \frac{|A_k|}{|V|} \mathbf{s}_k \cdot \sum_\alpha \left[\lambda_\alpha \mathbf{K} \left(\frac{p - p_k}{|\mathbf{u}_k|} \frac{\mathbf{u}_k}{|\mathbf{u}_k|} + \varrho_\alpha \mathbf{g}\right) \varrho_\alpha X_\alpha^\kappa\right] + q^\kappa\,. \end{aligned} \tag{3.71}$$

The discretization of the energy balance equation (2.56) is straightforward from the concentration equation. Integration over the control volume and application of the Gauß-Green formula yields

$$\int_G \frac{\partial u_t}{\partial t} dG = -\oint_\Gamma \mathbf{n} \cdot \left[\sum_\alpha \left(\mathbf{v}_\alpha \varrho_\alpha h_\alpha\right) + \lambda_{pm} \nabla T\right] d\Gamma\,. \tag{3.72}$$

The temperature gradient in the conduction term is discretized in the same way as the pressure gradient. The derivative of the internal energy with respect to time is again

approximated in first order. The discretized form of the energy balance is then

$$\frac{\partial u_t}{\partial t} = -\sum_k \frac{|A_k|}{|V|}\mathbf{s}_k \cdot \left[\sum_\alpha \left(\lambda_\alpha \mathbf{K}\left(\frac{p-p_k}{|\mathbf{u}_k|}\frac{\mathbf{u}_k}{|\mathbf{u}_k|} + \varrho_\alpha \mathbf{g}\right)\varrho_\alpha h_\alpha\right) - \lambda_{pm}\frac{T-T_k}{|\mathbf{u}_k|}\frac{\mathbf{u}_k}{|\mathbf{u}_k|}\right]. \tag{3.73}$$

As the permeability, the heat conductivity is determined by the harmonic mean of the current and k-th cell center's conductivity.

After the solution of the pressure equation, all coefficients on the right hand side of Equations (3.71) and (3.73) are known. Both transport equations are then evaluated for each cell.

3.4.3 Determination of coefficients by full upwinding

In Aziz and Settari [1979], the authors point out that a central weighting of coefficients – although of second order – leads to erroneous numerical results which is due to the hyperbolic nature of the transport equation. As solution, the evaluation of coefficients at the cell interfaces is done by upstream weighting or *full upwinding*. The upstream cell is determined by evaluating the potential gradient of each phase

$$\mathbf{\Phi}_\alpha = -\nabla p + \varrho_\alpha \mathbf{g}\,. \tag{3.74}$$

Discretized for each interface, this is

$$\mathbf{\Phi}_{\alpha,k} = \frac{p-p_k}{|\mathbf{u}_k|}\frac{\mathbf{u}_k}{|\mathbf{u}_k|} + \varrho_\alpha \mathbf{g}\,. \tag{3.75}$$

If the product of the potential gradient and the outward pointing normal at the k-th interface, $\mathbf{n}_k \cdot \mathbf{\Phi}_{\alpha,k}$, is positive, the coefficients are chosen from the current cell. If the product is negative, the coefficients are chosen from the k-th neighboring cell. At this point, special care must be taken for gravity-influenced systems where counter-current flow may occur. Here, upwind directions can be different for different phases. To obtain a unique potential gradient, the density ϱ_α in Equation (3.75) is determined by central weighting. If either of the densities were chosen for this equation, the direction of the potential gradient might differ dependent on the choice of the "upwind" cell.

The pressures at the current time level are not yet known during the setup of the pressure equation. Therefore, the pressures from the last timestep have to be used. If boundary conditions change rapidly this might naturally lead to a false approximation of the upwind direction. In this case, the pressure equation should thus be evaluated a second time.

3.4.4 Evaluation of derivatives of total specific volume

The volume derivatives are calculated numerically in the same way as introduced in Section 2.7.1. To calculate the volume derivative with respect to component ι, the following steps are carried out. (For notational convenience, ι denotes the component respect to which the derivative has to be determined and $\omega \neq \iota$ denotes the set of remaining components)

- The current phase mass fractions $\nu_\alpha\left(C^\omega, C^\iota\right)$ are known from the last flash calculation. The current total fluid volume is then determined by Equation (3.11):

$$v_t\left(C^\omega, C^\iota\right) = \sum_\alpha v_\alpha = \sum_\alpha \frac{\nu_\alpha}{\varrho_\alpha} \left(\sum_\kappa C^\omega + C^\iota \right) . \tag{3.76}$$

- The total concentration of component ι is increased by the increment ΔC^ι, while the total concentrations of the other components and the internal energy stay constant. With the increased total concentration, a flash calculation is performed to determine the phase mass fractions $\nu_\alpha\left(C^\omega, C^\iota + \Delta C^\iota\right)$ and the total volume $v_t\left(C^\omega, C^\iota + \Delta C^\iota\right)$.
- The derivative $\partial v_t / \partial C^\iota$ is then evaluated by

$$\frac{\partial v_t}{\partial C^\iota} = \frac{v_t\left(C^\omega, C^\iota + \Delta C^\iota\right) - v_t\left(C^\iota\right)}{\Delta C^\iota} . \tag{3.77}$$

The derivative of total specific volume with respect to internal energy is determined accordingly.

It turned out that best results were obtained when the increment of the conserved quantity (i.e., total concentration or energy) is chosen as large as its estimated change during the following timestep. As an example, consider a nonlinear relation between total specific volume and total concentration as sketched in Figure 3.7. Choosing $\Delta C^\iota = \delta C^\iota$ with δ being very small (e.g., $\delta = 10^{-8}$) approximates a tangent (the exact derivative) to the function. Consider now, the concentration C^ι to change by $\Delta_t C^\iota$ during the timestep. The change in total volume expected by this tangent, $\Delta v_{t,T}$ is higher than the actual change $\Delta v_{t,S}$ (see 3.7). A better approximation is therefore found if the increment ΔC^ι is chosen as what is expected to be $\Delta_t C^\iota$. To determine such an expected value, an additional step has to be included in the time discretization as discussed in the following section.

For the determination of the derivative of total specific volume with respect to pressure at temperatures below the boiling point, the execution of a flash calculation is not necessary. It is sufficient to consider only the influence the effect on the phase densities. If the temperature is at the boiling point, an increase in pressure results in condensation of vapor. This, in turn, leads to large changes in volume, since the differences in

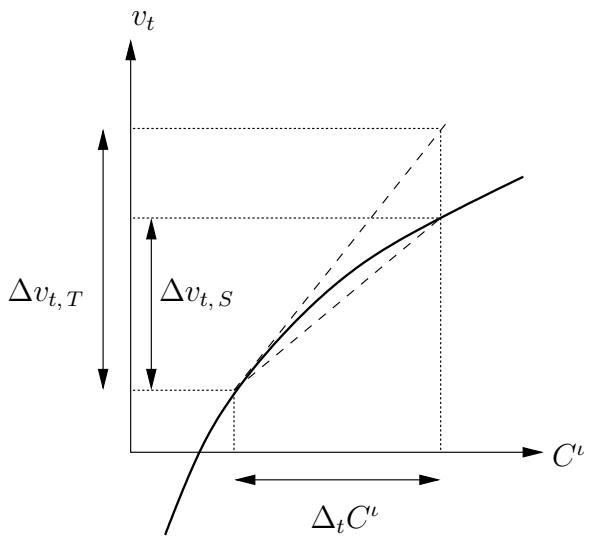

Figure 3.7: Tangent and secant method for numerical derivatives.

densities of a liquid and a gas may be several orders of magnitude. In Grant and Sorey [1979], the authors derive the compressibility of a gas-liquid mixture at boiling point. Consider one phase to be at the boiling point, i.e. $p = p_{vap}$. Consider further the pressure to increase by an infinitesimally small amount δp. Since the system must stay in a two-phase state, the temperature must rise by δT to ensure that the pressure equals the vapor pressure:

$$\delta T = \frac{\delta p}{\partial p_{vap}/\partial T} \,. \tag{3.78}$$

To increase the temperature of the solid matrix and the fluid phases, the enthalpy per unit volume must be increased by an amount $\delta h_{s,l}$. This amount can be found from the specific heat capacities of the fluids, $c_{p,\alpha}$, and solid phase, c_s,

$$\delta h_{s,l} = \left((1-\phi)\, \varrho_s c_s + \phi \sum_\alpha \varrho_\alpha c_{p,\alpha} \right) \delta T \,. \tag{3.79}$$

This energy must be supplied by latent heat, i.e. by the condensation of vapor. The mass of vapor that condenses within a unit volume is

$$\delta m = \delta h_{s,l} / \Delta H_{vap} \,, \tag{3.80}$$

where ΔH_{vap} is the enthalpy of vaporization. Due to the already mentioned difference of the densities of the boiling liquid, ϱ_l, and the gas phase,ϱ_g ,the total specific volume changes by

$$\delta v_t = \delta m \left(\frac{1}{\varrho_g} - \frac{1}{\varrho_l} \right) \,. \tag{3.81}$$

The derivative of volume with respect to pressure can now easily be found as

$$\frac{\partial v_t}{\partial p} = \frac{\left((1-\phi)\,\varrho_s c_s + \phi \sum_\alpha \varrho_\alpha c_{p,\alpha}\right)}{\left(\partial p_{vap}/\partial T\right)\Delta h_{vap}} \left(\frac{1}{\varrho_g} - \frac{1}{\varrho_l}\right) . \tag{3.82}$$

This derivative does not consider the compressibilities of the phases. However, in the case of a boiling liquid, the volume changes due to compressibilities are several orders of magnitude smaller than those due to the phase change.

3.5 Adapted time discretization

For upwinding of coefficients during the setup of the pressure equation, the pressures of the last time level are used (see Section 3.4.3). During the calculation of the initial pressure, however, this time level is not available. A similar problem arises when consistent initial conditions have to be found by a flash calculation. Thus, an initial guess of the pressure field is necessary for the first timestep. It is found by a standard fractional flow pressure equation with centrally weighted total mobilities (e.g., Cao et al. [2007] or Helmig [1998]).

As discussed in Section 3.4.4, the change of total concentrations during the timestep has to be estimated before solving the pressure equation. This is done in a pre-step by evaluating the transport equations using the pressures of the old time level.

The whole program cycle of a simulation run is displayed by Figure 3.8.

3.6 Multiphysics Implementation

As discussed in Section 2.8, the basis for the multiphysics concept is to locally adapt the model complexity to the occurring physical processes. The implementation of these concepts requires

- the decomposition of the model domain into subdomains and assigning models of the respective complexity to each of them
- discretization and application of the respective model inside the associated subdomain
- coupling the models at the subdomain boundaries.

The decomposition of the model domain to subdomains can be done statically, i.e. with fixed internal boundaries. In this case, the subdomains have to be chosen such that it is assured that complex processes never happen outside the associated subdomain. However, the place where certain processes happen is hardly predicted in advance of

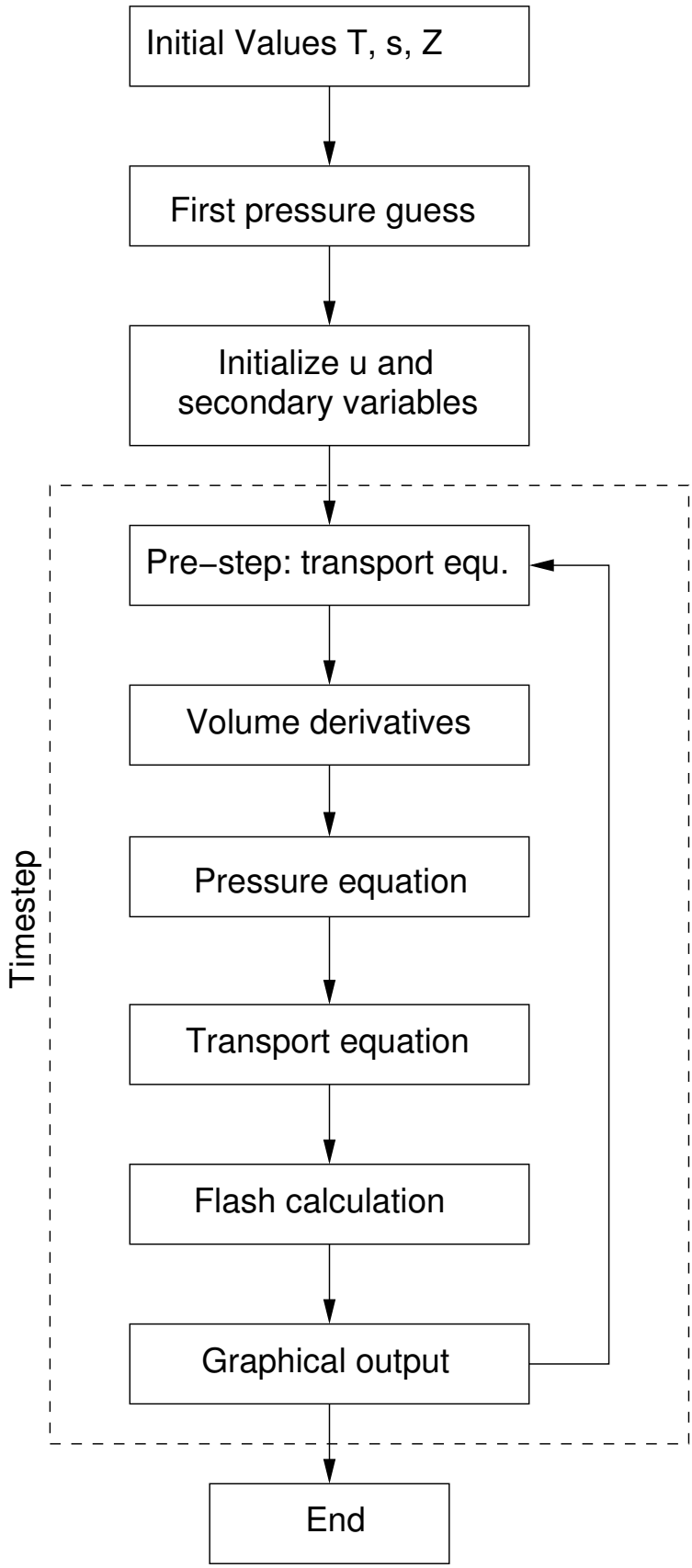

Figure 3.8: Program cycle of the decoupled compositional model.

the simulation. Therefore, a subdomain adaptivity scheme will be discussed in Section 3.6.3 after having introduced the implementation of the other tasks. For now, consider subdomains which are limited by internal boundaries which follow element edges, i.e. each cell lies definitely inside a single subdomain.

3.6.1 Multiphysics implementation for isothermal two-phase two-component systems

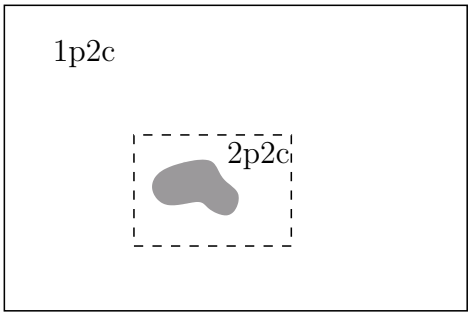

For this scheme, the model domain is divided into a single-phase two-component (1p2c) and a two-phase two-component (2p2c) subdomain. The discretization of the compositional multiphase pressure and transport equations was discussed elaborately in Section 3.4. Based on these considerations, the discretization of the single-phase pressure and transport equations is straightforward.

As mentioned in Section 2.8.1, the single-phase pressure equation and the compositional multiphase pressure equation have the same physical relevance, the same unknowns and the same dimensions. This motivates the use of both equations in the same global system of linear equations to evaluate the pressure distribution in the whole domain in a single step. The methods described in Wheeler et al. [1999] and Peszynska [2002], in contrary, solve the global problem by an iteration at the interface between the subdomains. This involves an evaluation of the pressure and/or transport equation for each subdomain for each iteration step, which obviously demands a manifold of the efforts of a single step solution. In this work, a single system of equations is assembled in order to solve the pressure equation. The assembly of this global system of linear equations is done by evaluating the entries in each row of the stiffness matrix either by the single-phase or the compositional multiphase pressure equation, depending on the position of the considered cell. Internally, however, the subdomain is not represented by a spatial function but only by a vector of Boolean variables which assigns the 1p2c/2p2c-state to each element index. If the cell lies inside the 2p-subdomain, the compositional multiphase pressure equation is used. If the cell lies inside the 1p-subdomain the single-phase pressure equation is used. This can also be applied to cells adjacent to the subdomain boundary, since all necessary coefficients can be determined: All coefficients of the phase not being present in the 1p-subdomain have to be set to zero. Then, all terms considering this phase in the compositional multiphase pressure equation vanish. Hence, the compositional multiphase pressure equation simplifies to the single-phase pressure equation at the subdomain boundary. The single-phase pressure equation, however, is only correct if no other phase flows across the boundary.

The same considerations are made for the transport equations. Depending on the flow conditions assumed in the single-phase domain (compressible or incompressible), the discretized transport equation (3.71) is solved for all components, or a discretized form of the simplified concentration equation (2.88) is solved for chosen components.

The coupling conditions – continuity of volumetric flux and mass flux across the boundary – are expressed by

$$\mathbf{n}_{\partial\Omega ij} \cdot \sum_{\alpha} \mathbf{v}_{\alpha} = \mathbf{n}_{\partial\Omega ij} \cdot \mathbf{v}_{\beta} \tag{3.83}$$

$$\mathbf{n}_{\partial\Omega ij} \cdot \sum_{\alpha} \mathbf{v}_{\alpha} \varrho_{\alpha} = \mathbf{n}_{\partial\Omega ij} \cdot (\mathbf{v}_{\beta} \varrho_{\beta}) \ , \tag{3.84}$$

where the left hand side represents the compositional multiphase subdomain and the right hand side the single-phase subdomain. The vector $\mathbf{n}_{\partial\Omega ij}$ be a normal to the internal boundary $\partial\Omega_{ij}$, and β denotes the phase being present in the 1p-subdomain. These conditions are fulfilled if the velocities and the densities at the boundary are the same on both sides. The densities are determined by full upwinding and the velocities by two-point flux approximation on both sides. Thus, the coupling conditions boil down to the requirement that only phase β flows across the boundary, since the other phase is not represented in the 1p-subdomain.

The benefit of this implementation is that in the single-phase subdomain, several computations can be avoided:

- The evaluation of the transport equation in the pre-step only has to be performed for the cells in the multiphase subdomain. Due to the explicit time discretization of the transport equation, it is evaluated cell-wise and does not depend on the results of other cells. Thus it can be computed only locally.
- The volume derivatives are only determined inside the multiphase subdomain. Evaluation of these derivatives requires one flash-calculation per component.
- The flash-calculation at the end of each time-step is only performed inside the multiphase subdomain.

3.6.2 Multiphysics implementation for non-isothermal two-phase two-component systems

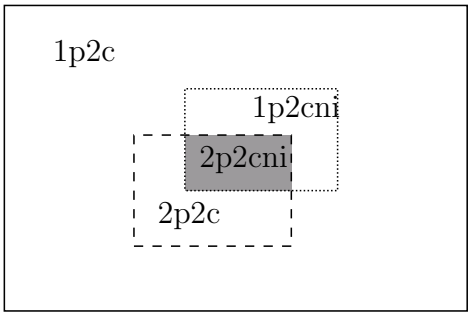

For this scheme, the model domain is divided into four subdomains: a two-phase subdomain with considerable temperature changes (2p2cni), a two-phase subdomain with low temperature changes (2p2c), a single-phase subdomain with considerable (1p2cni) and low (1p2c) temperature changes. The 1p2c and 2p2c subdomains are treated as before, whereas in the 1p2cni and 2p2cni subdomains the discretized form of the non-isothermal pressure equations (2.89) and (2.76), respectively, are used. Hence, the temperature dependent changes in density are explicitly regarded in the pressure equations of the 1p2cni and 2p2cni subdomains by an own term. In the 1p2c and 2p2c subdomain, this term is not included in the pressure equation. Since temperature changes are very low in these domains, however, the density changes are very low too and can be leveled out by the error terms of the pressure equations. It is emphasized that the 2p2c and 1p2c subdomain are not isothermal. In fact, the temperature may change but these changes are not explicitly considered in the pressure equations.

Since temperature influences density, incompressible flow can not be assumed in a non-isothermal system. To be able to consider compressibilities and temperature dependent changes in density, the total fluid mass and the total internal energy per unit volume have to be known throughout the whole domain. Hence, the concentration equations of both components as well as the energy equation have to be evaluated also in the single phase subdomains. Additionally to the coupling conditions of the preceding multiphysics scheme, the continuity of energy flux has to be assured. As well as the mass flux constraint, this is fulfilled as long as only one phase flows across the boundaries between single-phase and two-phase subdomains.

The benefit here is that

- The evaluation of the mass transport equation in the pre-step only has to be performed in the 2p2c and 2p2cni subdomains.
- The evaluation of the energy transport equation in the pre-step only has to be performed in the 2p2cni and 1pni subdomains.
- Volume derivatives with respect to mass are only computed in the 2p2c and 2p2cni subdomains.
- Volume derivatives with respect to internal energy are only computed in the 1pni and 2p2cni subdomains.

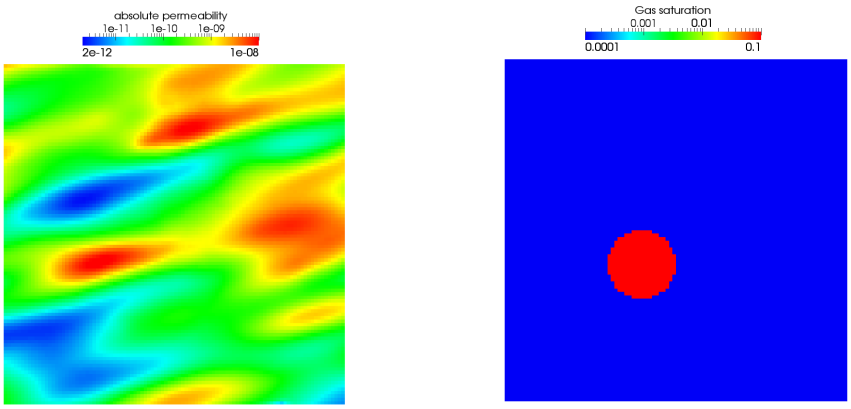

Figure 3.9: Example setup for isothermal 2p2c multiphysics model. Left: permeability field. Right: initial condition.

- The iterative isoenergetic isobaric flash calculation is only calculated in the 2p2cni subdomain.
- In the 1pni subdomain only the temperature is iterated to match the internal energy.
- In the 1p subdomain no flash calculation is performed.

3.6.3 Subdomain adaptivity

From the coupling conditions of the presented multiphysics implementations it becomes clear that the appropriate choice of the subdomain boundaries is crucial for the model quality. This can be demonstrated by comparing the multiphysics model with the standard compositional two-phase model on the following example: Consider a domain of ten by ten meter fully saturated with water except for a bubble of residual air and a permeability field as displayed in Figure 3.9. On top and bottom, it is confined by no-flow boundaries, while the pressure boundaries to the sides cause a flux from left to right. In the two-phase zone, air is dissolved in water and transported further to the right hand side boundary.

To show the necessity of an adaptive subdomain, the multiphysics model is first employed with a fixed, rectangular 2p2c-subdomain which is considerably larger than the two-phase zone(see Figure 3.11, bottom line). This choice fulfills the coupling condition that only one phase may flow across the subdomain boundary since the gas phase is immobile anyway. However, when looking at the breakthrough curves of dissolved gas at the right hand side boundary in Figure 3.10, differences between the full compositional model and the multiphysics model can be discovered: the outflow of the multiphysics model has a slightly higher peak, while it is more retarded in the full compositional model. The reason for this behavior can be discovered when comparing the satura-

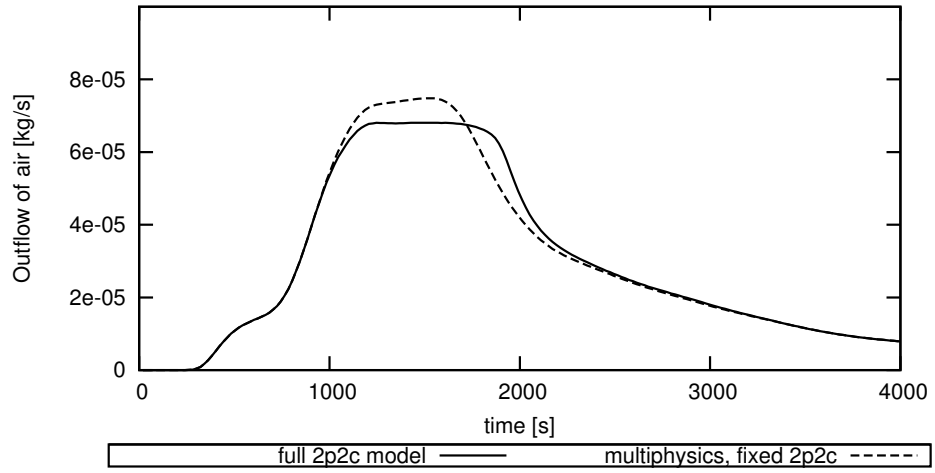

Figure 3.10: Breakthrough curves of 2p2c model and multiphysics model.

tions of the models in Figure 3.11. The solubility of air in water is proportional to the pressure (see Henry's law in Section 2.3.5). When water flows by the bubble, air is dissolved in it according to the local pressure. Since downstream of the bubble the pressure decreases, the solubility decreases too. Therefore, degassing takes place and the gas phase appears (see Figure 3.11, top row). In the multiphysics model, this process can only be represented in the 2p2c-subdomain. Thus, the degassing in the upper part of the domain is not represented as can be seen from Figure 3.11, middle row.

To avoid this problem, an adaptive subdomain was implemented. Demixing is most likely to occur in the cell downstream of a cell where two phases are present since here, the solubility is slightly decreased as compared to the upstream cell. The most logical choice of the subdomain therefore contains all cells where two phases are present and all cells downstream adjacent to them. Determining which cells are downstream of the two-phase zone would require an additional step where velocities are calculated. To avoid this superfluous calculations, *all* cells adjacent to the two-phase zone are included in the 2p2c-subdomain. During the flash calculation at the end of each time step, the two-phase state is controlled in each cell of the 2p2c-subdomain and, if necessary, the subdomain is adapted. This guarantees that the subdomains are chosen such that the coupling condition is fulfilled, demixing effects are represented and the 2p2c-subdomain is as small as possible. The application of this subdomain to the considered problem is shown in Figure 3.11, bottom row, where it can be seen that the demixing effects of the full compositional model are completely represented. Note that this minimalist choice of the 2p2c-subdomain is only possible due to the explicit solution scheme and the Courant-Friedrich-Levy-criterion (see Section 3.2) which ensures that mass may only be transported one cell further per time step.

The choice of the "non-isothermal" subdomains is controlled via the threshold temperature. As described in Section 2.8.2, a threshold temperature difference ΔT_{thresh}

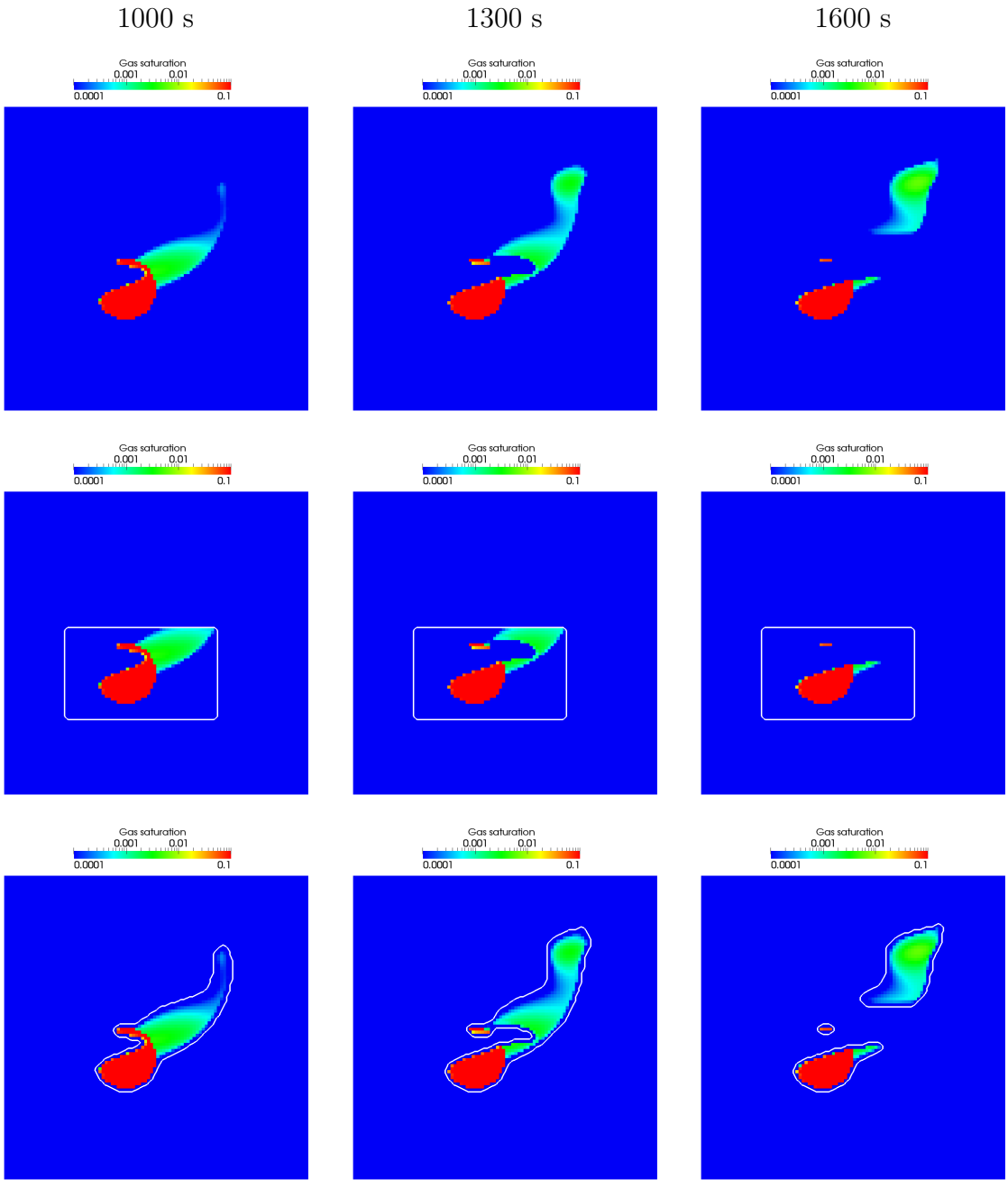

Figure 3.11: Saturations in full compositional 2p2c model (top) and in the multiphysics model with fixed (middle) and adaptive (bottom) 2p2c-subdomain. The white lines mark the subdomain boundary.

is defined. For temperature changes below this threshold, internal energy is assumed to be a linear function of temperature and the changes in total specific volume are considered to be low. The non-isothermal subdomain is then determined such that outside its boundaries, the temperature changes stay below this threshold difference:$|T - T_{init}| < \Delta T_{thresh}$. Naturally, the choice of this threshold difference is a crucial decision which influences the quality of the model. Therefore, this choice should be made according to the specific simulation problem. It must be guaranteed that within the threshold, no discontinuities in internal energy (such as at the boiling point of a liquid) may be reached. Furthermore, the threshold difference should be considerably lower than the expected highest temperature difference during the simulation run. Solubilities of any components in any phases have a considerable dependence on temperature. That is, in the 1p2cni-subdomain an increased probability of demixing exists. Therefore, mass fractions and solubilities are compared after each timestep in this subdomain.

4 Test cases

In this section, several test cases are presented to validate the introduced models. First, the non-isothermal model is compared to experimental data and results of other models. Then the accordance of the presented multiphysics approaches with the globally complex models is shown.

4.1 Non-isothermal single-phase flow

The non-isothermal compositional model is compared to a two-dimensional experiment which was set up by Li Yang at Institute of Hydraulic Engineering, University of Stuttgart. Detailed descriptions of the setup and further experiments can be found in Zhao [2006]. A heater element is placed in vertical direction inside a porous medium made up of glass beads. Figure 4.1 shows the whole flume which consists of a steel frame with vertical reinforcement bars, a glass plate on the front side and a steel and plywood compound at the back side. Glass beads of uniform size are packed between the glass plate and the steel plate with a thickness of 7 cm. The steel frame on top and bottom and the distributors to the sides confine the packing which has a planar size of $1\,\mathrm{m} \times 1.2\,\mathrm{m}$. Furthermore, the heater which is run with an input of 200 Watts is shown in Figure 4.1.

Since the model is set up two-dimensionally, the heat conductivity of the glass and steel plates have to be incorporated by increasing the conductivity of the matrix. This is done using the thickness d of the various layers by

$$\bar{\lambda}_{pm} = \frac{d_{pm}\lambda_{pm} + d_g\lambda_g + d_{st}\lambda_{st}}{d_{pm}}\,, \tag{4.1}$$

where the indices pm, g and st stand for the matrix, the glass plate and the steel plate, respectively. The steel bars which are mounted for reinforcement of the glass plate additionally increase the heat conductivity. However, since their extent orthogonally to the glass plate is higher than the glass bead packing itself, it is unlikely, that the bars contribute to the heat conduction inside the matrix with the whole cross-sectional area. The increase of heat conduction at the bars is therefore set heuristically. The glass and steel plates also have to be respected for the determination of the heat capacity of the

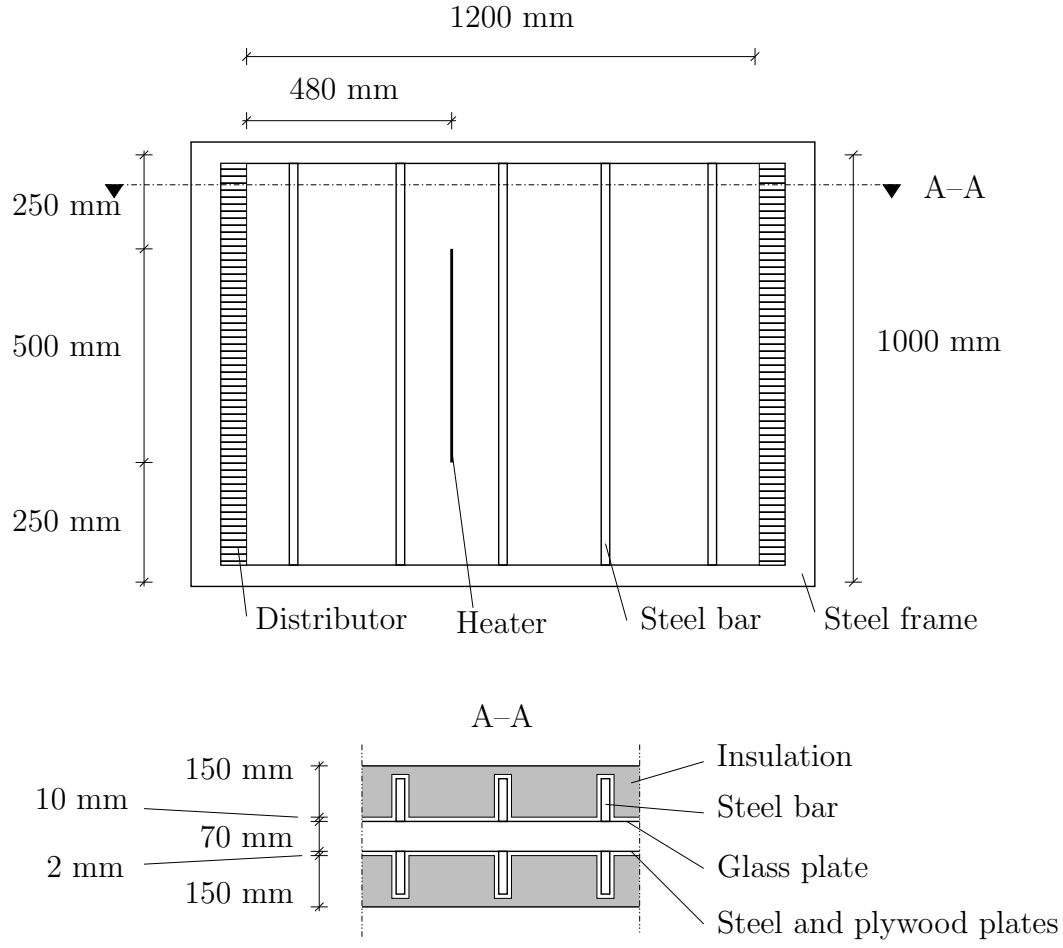

Figure 4.1: Setup of single-phase non-isothermal flow flume experiment.

Porosity ϕ	0.4
Permeability $\mathbf{K}$	$10^{-9}\,\mathrm{m}^2$
Heat conductivity $\bar{\lambda}_{pm}$	$1.53\,\frac{\mathrm{W}}{\mathrm{m\,K}}$
Heat conductivity at steel bar $\bar{\lambda}_{pm}$	$2.0\,\frac{\mathrm{W}}{\mathrm{m\,K}}$
Heat capacity $\bar{C}_p$	$3.22 \cdot 10^6\,\frac{\mathrm{J}}{\mathrm{m^3K}}$
Heat capacity at steel bar $\bar{C}_p$	$3.5 \cdot 10^6\,\frac{\mathrm{J}}{\mathrm{m^3K}}$
Ambient air temperature T_{amb}	$19\,^{\circ}\mathrm{C}$
Heat loss, front q^u	$-0.214\,\frac{\mathrm{W}}{\mathrm{m^2K}} \cdot (T - T_{amb})$
Heat loss, front at steel bar q^u	$-0.98\,\frac{\mathrm{W}}{\mathrm{m^2K}} \cdot (T - T_{amb})$
Heat loss, back q^u	$-0.203\,\frac{\mathrm{W}}{\mathrm{m^2K}} \cdot (T - T_{amb})$
Initial temperature T_{init}	$17.5\,^{\circ}\mathrm{C}$
Heat input	$200\,\mathrm{W}$

Table 4.1: Model parameters for 2-D single-phase non-isothermal setup.

2-D model. A mean heat capacity $\bar{C}_p$ of the solid per unit volume is calculated by

$$\bar{C}_p = \frac{d_{pm}\,(1-\phi)\,\varrho_g c_{p,g} + d_g \varrho_g c_{p,g} + d_{st}\varrho_{st} c_{p,st}}{d_{pm}}\,, \tag{4.2}$$

with the same indices as above. The influence of the steel bars is again estimated heuristically. Although the flume is isolated with styrofoam, heat losses have to be considered. They are incorporated using Fourier's law:

$$q^u = -\frac{1}{\sum d_i/\lambda_i}\,(T - T_{amb})\,, \tag{4.3}$$

where T_{amb} is the ambient air temperature. The layers considered for the heat conductivity in this equation are the glass plate and the styrofoam or steel bar on the front and the steel and plywood plates and the insulation or steel bar at the back. At the front, the heat losses are considered to be higher at the steel bars, whereas it is assumed that the steel and plywood plates homogeneously distribute the heat losses at the back. All model parameters are listed Table 4.1.

During the experiment run, the temperature was measured by thermography. For the visualization of the flow field, two stripes of tracer were brought into the flume

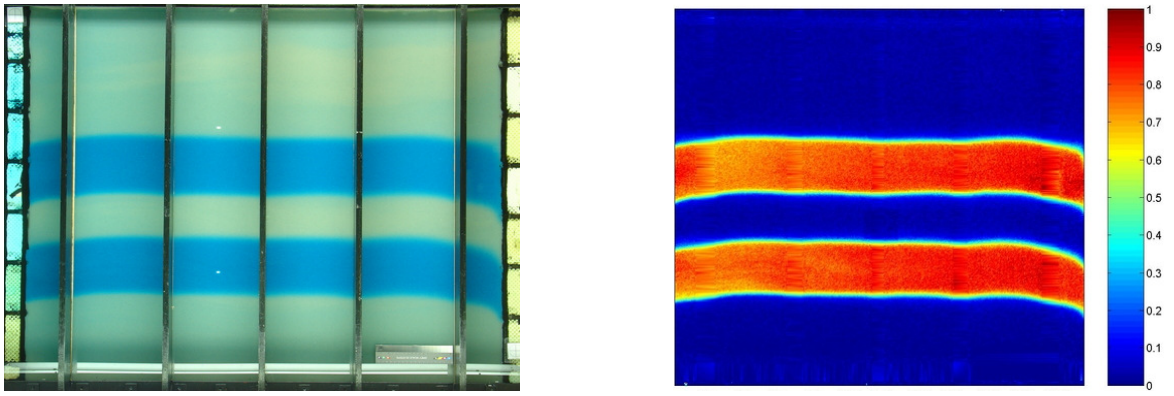

Figure 4.2: Initial concentration distribution of the non-isothermal single-phase experiment. Left: photography of the flume at initial state, Right: concentrations calculated from the photography.

before starting the experiments. In further course, photographs of the flume were taken. The tracer concentrations were calculated from the pictures by linking the color of the porous medium to concentrations. The initial concentration distribution is displayed in Figure 4.2. For the simulation, the domain was discretized by square elements of 1 cm length in x and y direction, yielding a grid of 120 times 100 elements. The temperatures from experimental measurements and simulation of the vertical heat well are displayed in Figure 4.3. It can be seen that the simulated temperatures in the direct vicinity of the heater are higher than the measured ones. This may have different reasons. In the experiment, the heating element is placed in the middle of the flume which explains a slight temperature decrease to the outside. Furthermore, the temperature measurements using spectroscopy are dependent on the right assumption of an emissivity of the surface being measured and the heat radiation may also be distorted by absorptions of the glass front. From the pictures taken at advanced times, however, it can be seen that the energy content of the simulated flume is significantly higher than in the experiment. It is assumed that these deviations are due to heat losses in the experiment which could not be captured in the simulation. Very good accordance between measurement and simulations could be achieved in tracer transport as displayed in Figure 4.4. Although the topmost front of very low concentrations as observed in the experiment after 60 minutes could not be reproduced with the simulation, the main front reached the same height. The vertical tracer stripes of the experiment can only be reproduced rudimentary with the simulation, which could, however be done by a higher grid resolution. For the time levels 300 and 500 minutes, the tracer concentrations in the horizontal stripes of the simulation are rather low as compared to the experimental data. This is due to the slow transport downwards. The timestep size in the simulation is determined by the high velocities at the heater element. The distance, the tracer is transported downwards per timestep is significantly lower than the discretization length at the sides. This causes high numerical diffusion

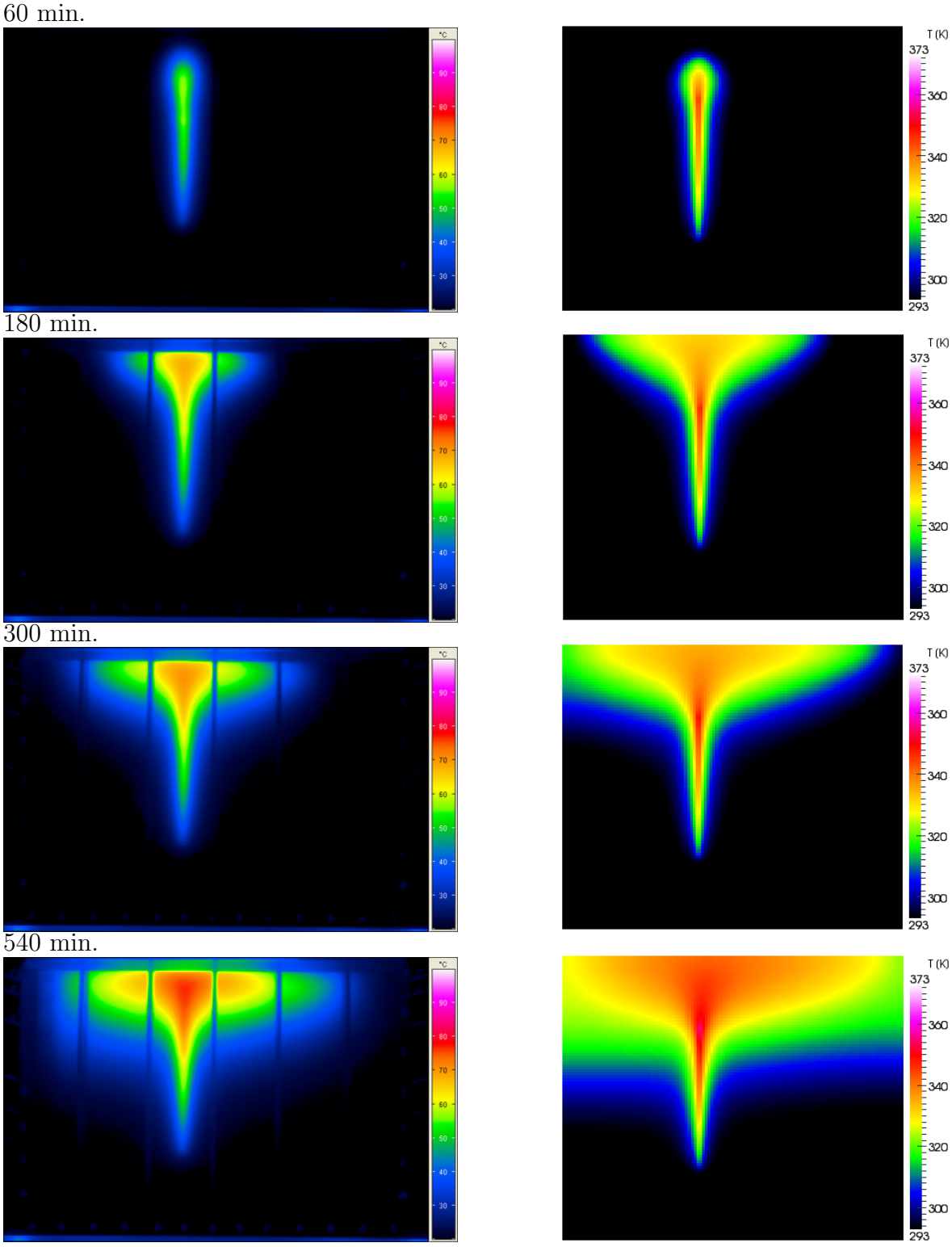

Figure 4.3: Comparison of measured and simulated temperatures for 2-D heat well experiment. Left: measurements. Right: simulation.

which smears out the concentration peaks. To decrease this effect, a finer grid could be used. Since this causes considerable computational efforts and the principal effect of buoyancy induced flow is also shown by the presented calculations, a recalculation with a finer grid is not considered further.

4.2 Single-component two-phase flow

To verify the results of the implemented non-isothermal model for boiling point conditions, it is compared with the model HYDROTHERM from US Geological Survey (Kipp et al. [2008]). HYDROTHERM is developed to model the flow of pure water through geological formations, where the water can be in the states liquid, gaseous and supercritical. Since constitutive relations for supercritical water are not yet implemented in DuMuX, the presented tests are performed for subcritical conditions near the boiling point. As first test, steam is injected into a water-saturated one-dimensional domain of 2000 m length. The boundaries are defined by constant pressure and temperature. Table 4.2 lists all model parameters. Note that HYDROTHERM implements the heat conductivity independent of saturation, i.e. as a constant value. For the two simulations presented in this section, this assumption was also used in the DuMuX code. The domain is discretized by 50 elements in the DuMuX code. HYDROTHERM realizes Dirichlet-type boundary conditions by fixing the temperature and pressure values at the boundary cells. To get comparable results of both codes, the domain in the HYDROTHERM simulation was chosen one discretization length larger in the horizontal direction (40 meters) and discretized by 51 elements. Figure 4.5 shows the results of both models after $1.2 \cdot 10^9$ s simulation time. In the top left picture, it can be seen that the saturation calculated by the DuMuX code does not exactly match the residual liquid water saturation. This is basically caused by pressure fluctuation which occur during the model run. As will be discussed in Section 4.5, the determination of the derivative of volume with respect to internal energy near boiling conditions is hardly ever accurate. This leads to rather high volume errors at the condensation front (in Figure 4.5, approximately at 1800 m) which have to be balanced by the pressure equation in the next timestep. Each time, the pressure is at a low level, a higher amount of water is flashed into the gas phase. Since the evaporated water is transported away with the gas phase in the next time step, the saturations fall below the residual saturation. Although the saturations are underestimated by the DuMuX code, the position of the saturation front is predicted very well and also the match between temperature and pressure is satisfying. As a second test of single-component two-phase flow, a two-dimensional setup is considered. The domain is 100 m long and 20 m high. The bottom and top boundaries are assigned no-flow conditions, while the left and right boundaries have Dirichlet type conditions: on the left, the pressure is constant at 10 MPa while on the right, the pressure is hydrostatic with 1.7 MPa at the bottom of the domain. All parameters are again listed in Table 4.2. The domain was discretized by a regular grid

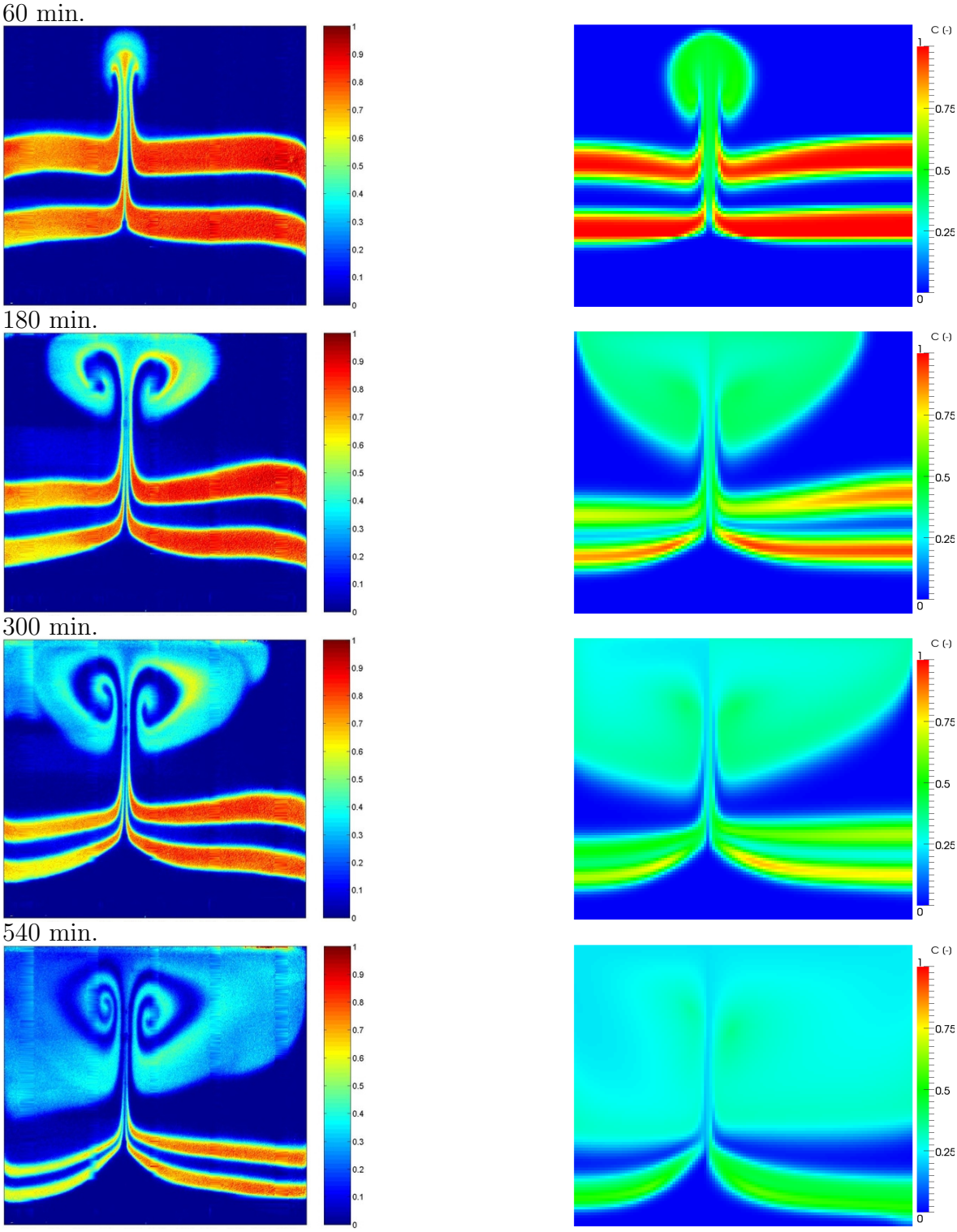

Figure 4.4: Comparison of measured and simulated tracer concentrations for 2-D heat well experiment. Left: measurements. Right: simulation.

Parameter	1 - D	2 - D
Porosity ϕ	0.3	0.4
Permeability $\mathbf{K}$	$10^{-14}\,\mathrm{m}^2$	$10^{-11}\,\mathrm{m}^2$
Heat conductivity $\bar{\lambda}_{pm}$	$1.54\,\frac{\mathrm{W}}{\mathrm{m\,K}}$	$2.8\,\frac{\mathrm{W}}{\mathrm{m\,K}}$
Soil heat capacity $c_{p,s}$	$880\,\frac{\mathrm{J}}{\mathrm{kg\,K}}$	$880\,\frac{\mathrm{J}}{\mathrm{kg\,K}}$
Soil density	$2750\,\frac{\mathrm{kg}}{\mathrm{m}^3}$	$2750\,\frac{\mathrm{kg}}{\mathrm{m}^3}$
Residual saturation liquid water S_{rw}	0.3	0.1
Residual saturation steam S_{rn}	0.0	0.0
Left hand side boundary pressure	$10^7\,\mathrm{Pa}$	$10^7\,\mathrm{Pa}$
Right hand side boundary pressure	$10^6\,\mathrm{Pa}$	hydrostatic
Initial temperature T_{init}	$170\,^{\circ}\mathrm{C}$	$20\,^{\circ}\mathrm{C}$
Injection temperature T_{steam}	$350\,^{\circ}\mathrm{C}$	$370\,^{\circ}\mathrm{C}$

Table 4.2: Model parameters for steam injection in one-dimensional domain.

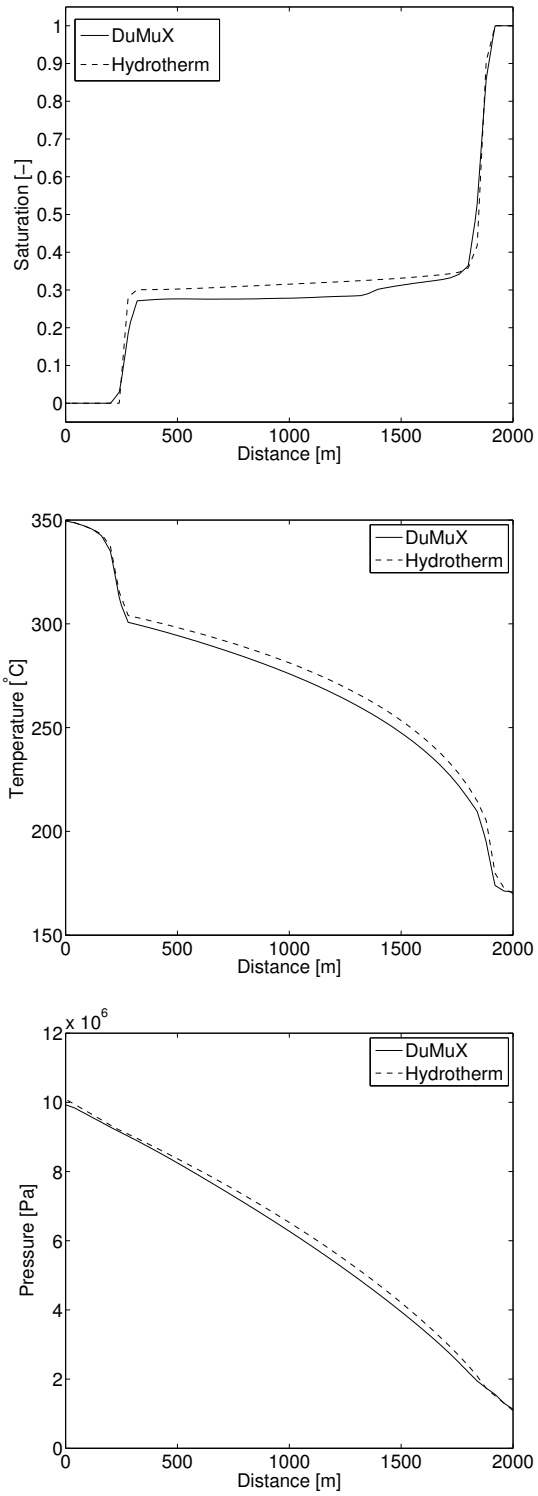

Figure 4.5: Comparison of simulation results for steam injection into a water-saturated 1-D domain. Results of DuMuX and HYDROTHERM after $1.2 \cdot 10^9$ seconds.

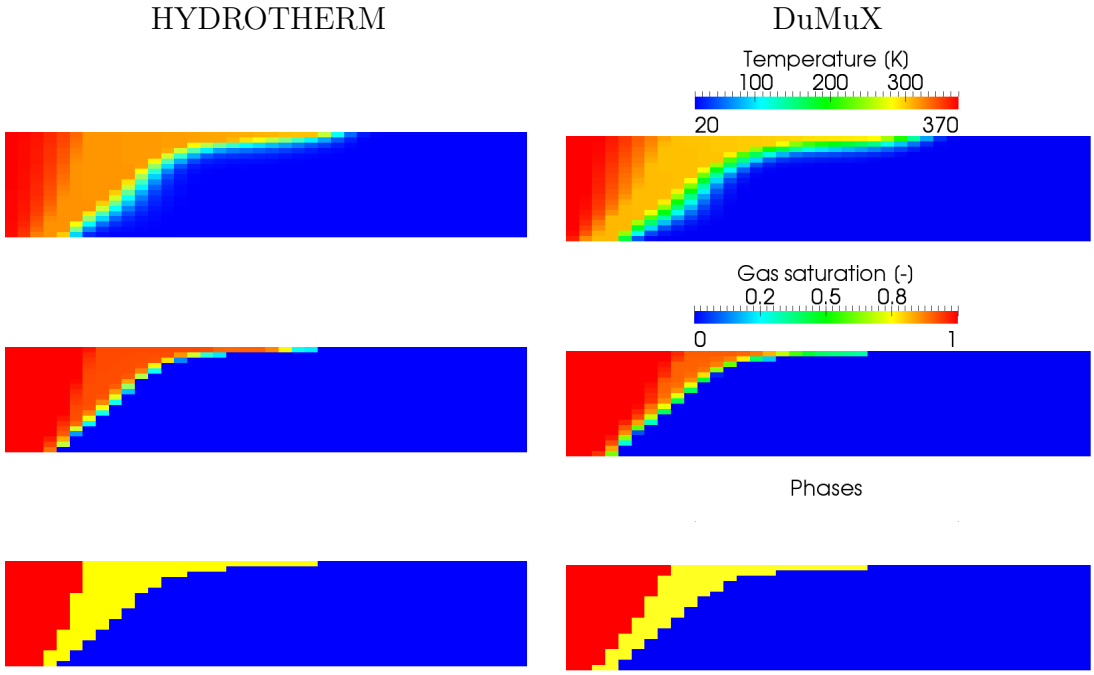

Figure 4.6: Comparison of simulation results for steam injection in a water-saturated 2-D domain. Results of DuMuX and HYDROTHERM after 14500 seconds. Bottom row: phase state. Red: steam, blue: liquid water, yellow: two-phase region.

with rectangular elements of 2.5 m by 1 m in x and y direction, respectively. Again, the different realization of Dirichlet boundary conditions has to be regarded. Hence, the HYDROTHERM grid contains 41×20 cells as opposed to the DuMuX grid which consists of 40×20 cells. Figure 4.6 displays the results of both models after 14500 seconds of simulation time. The additional cell of the HYDROTHERM results is already cut off. As in the one-dimensional model, the condensation front is predicted similarly by both models. As can be seen particularly from the bottom row pictures, the two-phase zone is predicted more narrow by the DuMuX code. However, the liquid water saturation in this zone is also higher than in the HYDROTHERM results. Thus, the injected energy is comparable. A reason for this difference may be the slightly different left hand side boundary conditions or the possibly occurring pressure fluctuations as discussed for the one-dimensional example.

4.3 Non-isothermal two-phase two-component flow

The validation of the DuMuX model for non-isothermal two-phase two-component flow is done by comparison with two one-dimensional experiments. The data is taken from Färber [1997], where the author describes several experiments to investigate flow and

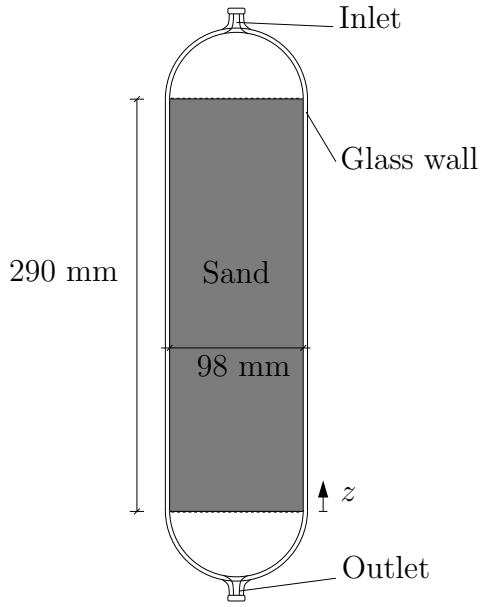

Figure 4.7: Sketch of the setup of the 1-D column experiment.

transport during in-situ soil remediation measures. Both experiments were carried out using a glass column filled with coarse sand as sketched in Figure 4.7. The sand filling has diameter of 98 mm and a length of 290 mm, whereas the glass walls have a thickness of 3 mm. As described for the flume experiments in Section 4.1, increased values for the heat capacity and heat conductivity of the soil were used in the model to take into account the influence of the glass walls. The further model parameters are summarized in Table 4.3.

In the first experiment, saturated steam (i.e., boiling point temperature, no liquid particles in the gas phase) is injected into a modified setup with a horizontal column of one meter length. At the start, the column is completely dry and has a temperature of 20 °C. The further model parameters are summarized in Table 4.3. Steam is injected from the left at a constant rate of 1.15 kg/h which was realized by a flow-controlled pump. Considering the left hand side boundary as origin, the pressures were measured during the experiment at the positions $x = 0$, $x = 200\,mm$ and $x = 800\,mm$. The temperatures were measured at the same positions and additionally at $x = 350\,mm$, $x = 500\,mm$, $x = 650\,mm$. Figure 4.8, top plots a selection of the measured values, where the pressures are displayed as the difference to the surrounding air pressure. The ordinate is scaled with the dimensionless enthalpy H^*. It is the enthalpy of the injected steam over the amount of energy needed to heat the whole column from the initial temperature to the boiling point where $H^* = 1$ corresponds to approximately 1000 seconds. As the steam enters the cold soil, it condenses and forms a liquid water phase. The released enthalpy of vaporization heats the soil until the boiling point is reached. The injected steam can then pass the heated area and displace the condensed water. This way, a front evolves which gradually moves through the column. Since

Parameter for injection of...	steam	hot air
Column length	1 m	0.29 m
Column orientation	horizontal	vertical
Porosity ϕ	0.37	
Permeability $\mathbf{K}$	$3 \cdot 10^{-10}\,\mathrm{m}^2$	
Heat conductivity $\bar{\lambda}_{pm}$	$0.35...1.7\,\frac{\mathrm{W}}{\mathrm{m\,K}}$	
Soil heat capacity $c_{p,s}$	$840\,\frac{\mathrm{J}}{\mathrm{kg\,K}}$	
Soil density	$2750\,\frac{\mathrm{kg}}{\mathrm{m}^3}$	$2750\,\frac{\mathrm{kg}}{\mathrm{m}^3}$
Residual saturation liquid water S_{rw}	0.1	0.1...0.2
Residual saturation gas S_{rn}	0.0	0.0
Inflow boundary pressure	-	$10^5\,\mathrm{Pa}$
Injection rate	$1.15\,\frac{\mathrm{kg}}{\mathrm{h}}$	-
Outflow boundary pressure	$10^5\,\mathrm{Pa}$	$9.9 \cdot 10^4\,\mathrm{Pa}$
Initial temperature T_{init}	$20\,^\circ\mathrm{C}$	$20\,^\circ\mathrm{C}$
Injection temperature T_{inj}	$100\,^\circ\mathrm{C}$	$155\,^\circ\mathrm{C}$

Table 4.3: Model parameters for injection of steam and hot air into the glass column.

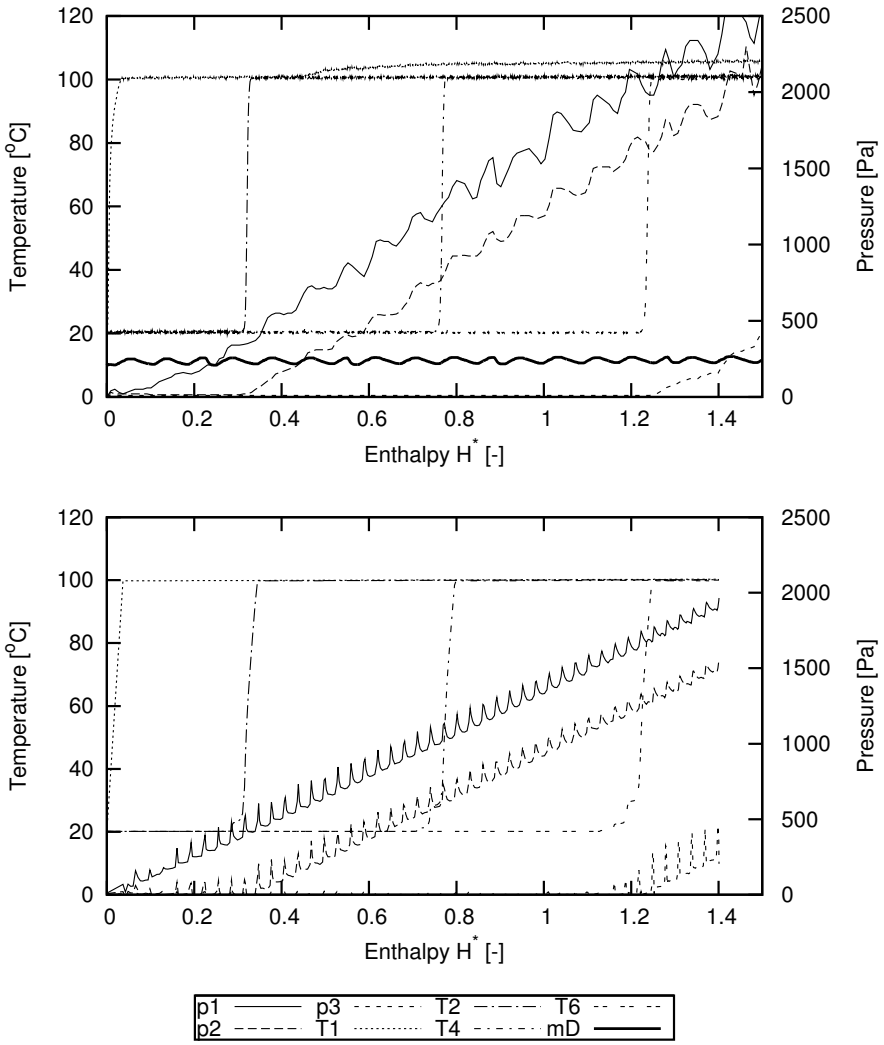

Figure 4.8: Measurements and simulation results for steam injection into dry horizontal column. Top: experimental results after Färber [1997]. Bottom: simulation results

both, liquid water and the hot steam have a higher viscosity than air, the pressure at the inlet increases. From the abrupt rise of the measured temperatures, it can be seen that the condensation front is very sharp. After the front has passed $x = 200\,\text{mm}$ and $x = 800\,\text{mm}$, the pressures at these positions rise analogously to the pressure at the inlet. Figure 4.8, bottom displays the simulation results for this setup with the same scaling of the ordinate. Only the temperatures at the same positions as the pressure sensors are plotted. As approximation to the pressure and temperature sensor at the inlet, the values inside the first cell are displayed. By comparison with Figure 4.8, top, it can be seen that the velocity of the condensation front as well as the sharp shape are perfectly reproduced by the model. The pressure oscillations which were already mentioned in the preceding section, can also be seen from this graph. Although oscillations of the pressure are also observed in the experiment the oscillations in the model are a purely numerical artefact which will be discussed in Section 4.5. The oscillations which were observed during the experiment are caused by the regulation of the injection pump and the resulting small oscillations of the injection rate which is represented by the thick solid line in Figure 4.8, top (denoted by mD). The absolute values of the pressures predicted by the experiment are lower than the measured pressures. Since the Reynolds number is at $Re_{50} \approx 8$, a significant deviation from Darcy's law can be excluded. However, the permeability of the coarse sand is given as a general value for all experiments in Färber [1997] and is furthermore subject to the conditions of the packing procedure. The differences of the measured and simulated pressure are therefore likely to arise from deviations of the soil's permeability.

In the second experiment, hot air was injected into a vertical column of 29 cm height as sketched in Figure 4.7. Initially, the column is again at a temperature of $20\,°C$ and the saturation increases from $S_w \approx 0.09$ at the top to $S_w \approx 0.21$ at the bottom. Although the residual saturation is at $S_{rw} = 0.1$, the water at the bottom of the column is held in place by capillary suction and is quasi immobile. To regard this in the model, the residual saturation is linearly increased from $S_{rw} = 0.09$ at the top to $S_{rw} = 0.21$ at the bottom. As well as the residual saturation, the initial saturation is set to increase from top to bottom with the same values. The spatial mean of the initial saturation – and therefore also the total amount of water in the column – is the same for model and experiment. All model parameters are again summarized in Table 4.3. The hot air heats the soil and the water as it enters the porous medium. Due to the heating, the vapor pressure of the water is increased and a higher amount of water can evaporate. A part of the evaporated water condenses in the cooler areas downstream such that the saturation increases minimally and water can flow out of the column in phase. The part of the water which is still dissolved in air is carried away with the gas phase. Considering the lower boundary of the soil probe as $z = 0$ (see Figure 4.7), temperatures are measured at $z = 0\,\text{mm}$ (T4), $z = 90\,\text{mm}$ (T3) and $z = 200\,\text{mm}$ (T2). Figure 4.9, top plots the measured temperatures and the saturations at $z = 30\,\text{mm}$, $z = 90\,\text{mm}$, $z = 190\,\text{mm}$ and $z = 250\,\text{mm}$ over time. The timescale on the ordinate is chosen as the

number of injected pore volumes. The heat losses to the surrounding air are estimated from the stationary state at the end of the experiment and included into the model by a sink term of $q^u = \Delta T \cdot 9\,\mathrm{W}/(\mathrm{m}^3 \cdot \mathrm{K})$. The results of the simulation using the parameters of Table 4.3 are plotted in Figure 4.9, middle. It can be seen, that the arrival times of the drying front as well as of the temperature increase are comparable in model and experiment. The considerable delay of the temperature increase at T3 can be explained by differences in the initial saturation distribution. The sensitivity of the results to initial saturations was also emphasized in Färber [1997]. However, the locally slower increase in temperature at all three measurement points stays peculiar. The first suspicion which imposes itself is obviously a wrong consideration of the matrix heat capacity. A significant lowering of the heat capacity, however, only resulted in a faster progress of the drying front whereas the local increase of temperature did not occur to be considerably faster. A good fit could be achieved by restricting the heat *conductivity* to $0.35\,\mathrm{W}/(\mathrm{m}\cdot\mathrm{K})$ – i.e. the conductivity of the dry soil – for all saturations. The results of this simulation run are plotted in Figure 4.9, bottom. A reason for this behavior is not easily found. In Färber [1997], the author describes the evolution of a wet layer at the walls of the column. This is especially observed for slow processes as in the current experiment (the total duration was approximately 9 hours). Due to the heat losses, the temperatures at the walls are lower and water can condense here. Consequently, three-dimensional flow and transport processes take place which can not be fully represented by the one-dimensional model setup.

4.4 Isothermal three-phase three-component flow

In this section, a simple example for the application of a three-phase three-component model is presented. It is not meant as quantitative nor as qualitative validation but only represents a short study for the applicability of the model. Following the two-dimensional example for a soil vapor extraction in Class [2001], a domain of $1\,\mathrm{m} \times 0.74\,\mathrm{m}$ of coarse sand ($K = 9 \cdot 10^{-10}\,\mathrm{m}^2$) with a block heterogeneity ($K = 6 \cdot 10^{-12}\,\mathrm{m}^2$) and a residual mesethylen contamination is set up (see Figure 4.10). The domain is confined by no-flow boundaries at top and bottom. At the left hand side boundary, air is injected at a rate of $26.3\,\mathrm{kg/s}$ while the right hand side boundary is of Dirichlet type with a constant pressure of $101300\,\mathrm{Pa}$. The simulation is run twice: in the first run, the injected air is water saturated with a mass fraction of $X_g^W = 0.02$; in the second run, pure air is injected. The results after 13 hours of injection are displayed in Figure 4.11. Due to the low permeability of the heterogeneity, air flows preferentially around it. Hence, the contaminant is better removed in the area on top of the heterogeneity. It can be seen that the same amount of NAPL is removed in both examples (The drying front moved the same distance).Obviously, the remediation of mesethylen is not affected by the water content of the injected air. In fact, the air has the same water content as it reaches the contamination, since it gets saturated by the water

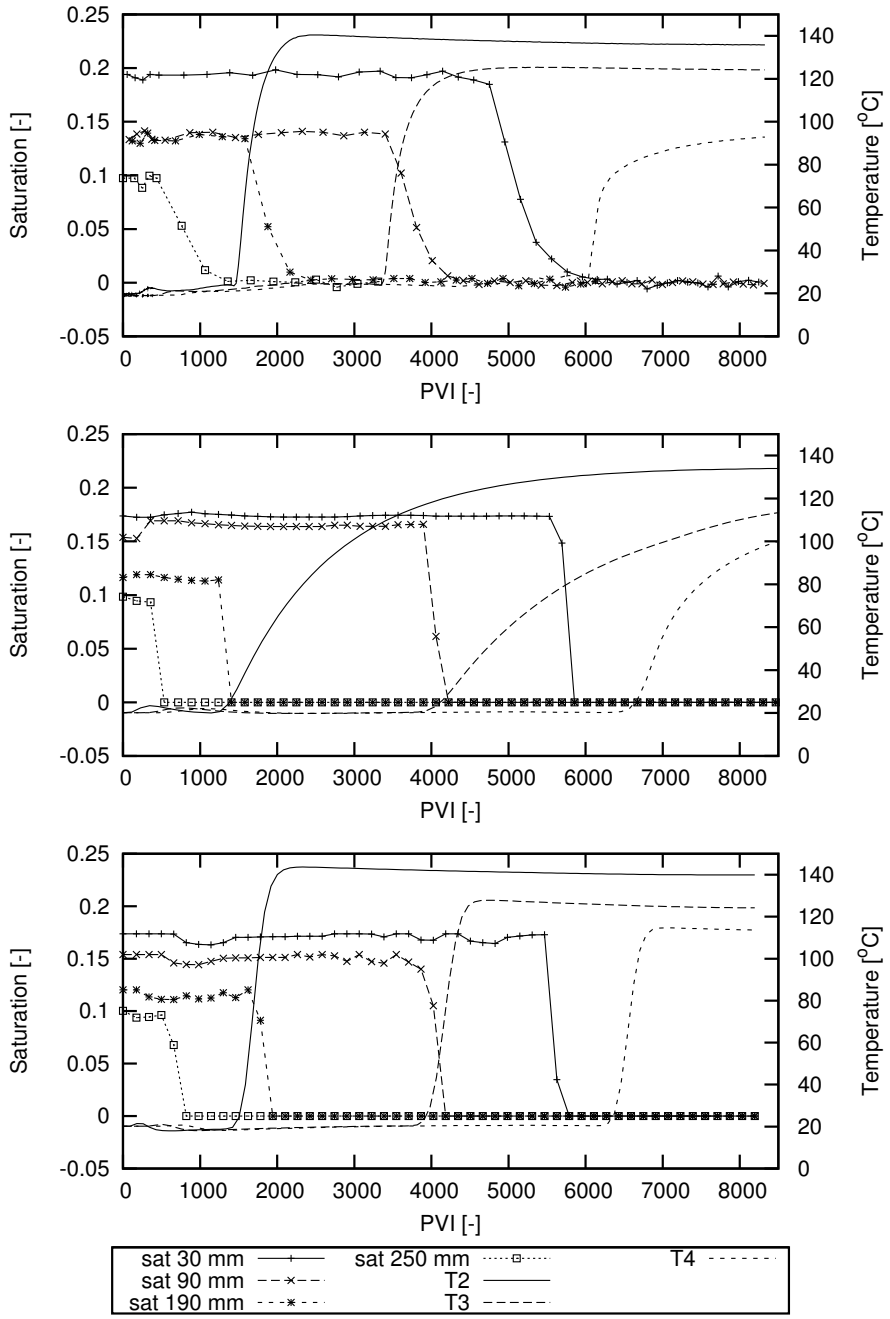

Figure 4.9: Measurements and simulation results for injection of hot air into residually saturated sand column. Top: experimental results according to Färber [1997]. Middle: simulation with original parameters. Bottom: simulation without heat conduction.

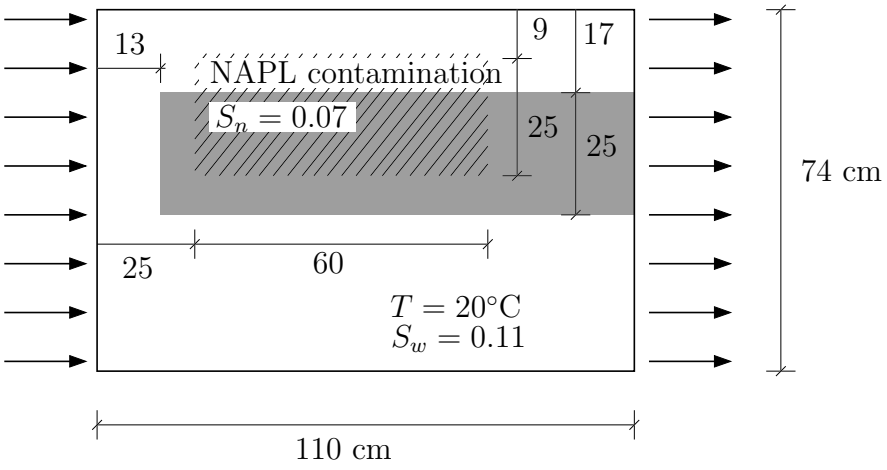

Figure 4.10: Setup of 3p3c soil vapor extraction example.

present in the porous medium. This also results in the drying front which is marked by grey isolines in Figure 4.11, right. The results in Class [2001], predict higher rates of mesethylen removement. This is because there, a random permeability distribution is used which distorts the permeability field sketched in Figure 4.10. It causes higher permeabilities in the upper part of the domain and. Thus, more air flows through the areas on top of the block heterogeneity causing more contaminant to be evaporated. However, the results match qualitatively which basically proofs the applicability of the presented model to compositional three-phase flow processes.

4.5 Discussion - Model applicability and oscillating pressures

The test cases presented in this chapter show a good agreement of the non-isothermal DuMuX model with the results of experiments and the HYDROTHERM simulator. However, the applicability of the model is restricted. Especially steam injection into dry as well as into liquid-saturated soils is a very hard benchmark example for which unconditional stability of the model can not be guaranteed at present state. This is mainly due to two phenomena which are inherent to the presented formulation. Both phenomena arise at the condensation front, i.e. at the control volume where steam flows in and condenses because the temperature lies below the boiling point. To ease the explanation, water and air are considered as components and when speaking of the boiling point, the one of water is meant. However, these considerations are general and can also be applied to other components.

Consider a control volume at a temperature below the boiling point which is fully saturated with gas. Steam flows into this control volume from an adjacent cell or

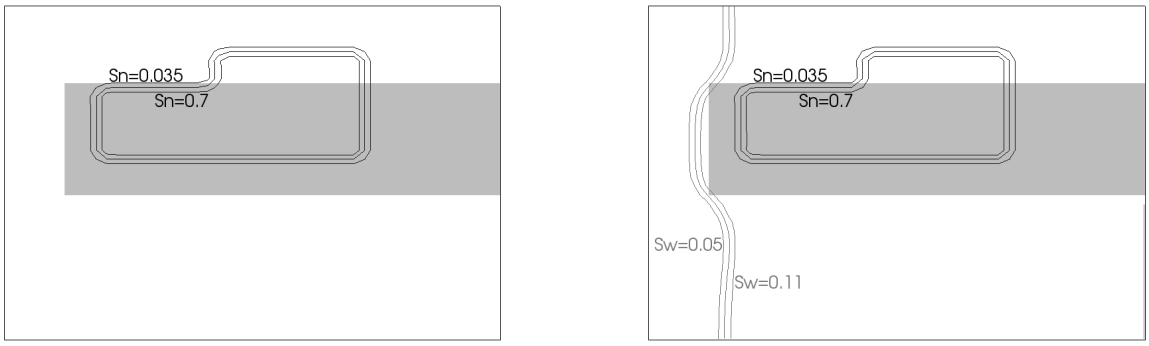

Figure 4.11: Simulation results of 3p3c soil vapor extraction after 13 hours. Left: injection of water saturated air. Right: injection of pure air.

boundary or from a source. This means that water and a high amount of energy flow into the cell. When determining the volume derivatives for the pressure equation, the change in mass of water without regarding the change of internal energy is considered and vice versa. When the derivative of fluid volume with respect to water is determined, a certain amount of water is added to the current mixture and a flash calculation at constant internal energy is performed. This will predict that most of the water forms a liquid phase and that a small amount evaporates. The same procedure for increased energy and a dry control volume will predict increasing temperature and an expanded gas phase. Compared to the actual steam injection, these derivatives overestimate the change in temperature and underestimate the change in fluid volume (since too much water is considered to be in the dense, liquid phase). Consequently, this will lead to a wrong prediction of the volume change over the next time step and therefore to considerable volumetric errors. This effect is dampened by the heat capacity of the solid matrix. A high heat capacity leads to low temperature changes due to the internal energy of the steam and therefore to the condensation of most of the steam. Hence, the actual change of fluid volume approaches the volume derivatives for increasing heat capacities.

Consider now a control volume saturated with liquid water. Again, steam flows into this control volume and condenses causing the temperature to rise until it nearly reaches the boiling point. The transport equation in the pre-step predicts that enough energy will flow into the cell to reach the boiling point and vaporize some water. Accordingly, the derivative of fluid volume with respect to energy will be considerably high. This, in turn, means that liquid water must be displaced to fulfill the volume constraint (Equation (2.65)). This is achieved by an increased pressure which causes a higher fluid flux out of the cell. At a higher pressure, however, also the boiling temperature is

higher and therefore the energy added during the following time step may not be enough to heat the control volume to boiling conditions. Hence, water was pressed out of the control volume to produce space for a steam phase that does not develop which results in a negative volume error. In the next timestep, this error is compensated by a decreased pressure which will in turn result in more vaporized water than predicted and so on. This effect is also observed when the control volume is only heated without adding any mass. In fact, the effect on the stability of the simulation is even worse since the system is not affected by a pressure gradient originating from this cell before the boiling starts. Especially this effect is the main reason for the oscillating pressures which were observed in all steam injection examples and which can be particularly seen in Figure 4.8, bottom. Attempts to solve this problem by iterating the pressure equation did not lead to success. The result then only jumps between two pressure distributions. The effects is, however, influenced by several parameters. The pressure influences the steam density and hence also the density contrast between steam and liquid. The contrast decreases with increasing absolute pressure as does the derivative of fluid volume with respect to internal energy at boiling conditions. Thus, high pressure levels make the model more stable at boiling conditions. High pressure gradients enforce a clear flow direction. At low pressure gradients, the volume errors may cause reversal flow. If large parts of the domain are at a high temperature, the pressure drop which causes reversal flow may cause a drop below the vapor pressure. This leads to a sudden (unphysical) vaporization of water inside large parts of the domain. The accordingly occurring high volume errors certainly cause an unsolvable system of equations in the next timestep. The compressibility, however, has the highest influence on the volume errors occurring at the condensation front. A high compressibility causes a high influence of the first term of the pressure equation (3.67). For the limit of an infinite compressibility, the pressure equation becomes

$$p^t = p^{t-\Delta t}\,,$$

hence, to a constant pressure. Thus, a high compressibility dampens fast pressure changes and stabilizes the model. This explains the importance to determine the derivative $\partial v_t/\partial p$ at boiling point conditions according to Equation (3.82). The value of the derivative according to this equation is typically two to four orders of magnitude higher than the compressibility of a gas.

5 Examples for applications

In this section, two applications of the multiphysics models are presented. This is, on the one hand, to demonstrate the practical applicability of the models, and on the other, to quantify the benefits in using the multiphysics schemes at concrete examples. First, the isothermal and second, the non-isothermal case will be considered.

5.1 Injection of CO_2 into the Johansen formation

The Johansen formation, located near the Norwegian coast, was discovered as a potential site for the geological storage of carbon dioxide (see e.g. IPCC [2005]). This gave reason to set up a benchmark problem in order to test and compare different commercial and academic codes capable of handling the respective physics (Class et al. [2007/2008], Eigestad et al. [2009]). Although the results of the models introduced in this work lie within the range of the other results discussed in the comparative study Class et al. [2009], they are not further discussed in this context. This example is rather chosen to validate the results of the multiphysics model against the globally applied decoupled 2p2c model. The specified model domain has a horizontal extend of approximately 9600 m by 8900 m. The highest point lies 2510 m below sea level, the lowest 3240 m. The formation thickness varies between 90 m and 140 m. The domain is discretized by 54756 elements which are strongly stretched in the horizontal directions. Figure 5.1 shows the permeability and porosity distributions in the formation. The domain is initially fully saturated by brine with a mass fraction of salt of $X_w^s = 0.1$. The layers confining the formation to the top and bottom are assumed to be impermeable while a hydrostatic pressure distribution defines the boundary condition to the sides. Furthermore, a constant geothermal gradient of 0.03 K/m and a temperature of 100 °C at a depth of 3000 m are given. The temperatures are assumed to stay constant, which is confirmed by several non-isothermal simulations which did not predict significant deviations from the initial temperatures. Over a period of 25 years, carbon dioxide is injected at a rate of 15 kg/s. The full 2p2c-model solved the given problem for the period of injection in 9540 timesteps. The multiphysics model needed four more steps. Figure 5.2, left shows the saturation calculated with the global 2p2c-model after 25 years of injection. The result of the multiphysics scheme is not displayed here since it looks perfectly the same. In Figure 5.2, right the extend of the 2p2c-subdomain inside the model domain is marked by the white grid. To compare the results of the full

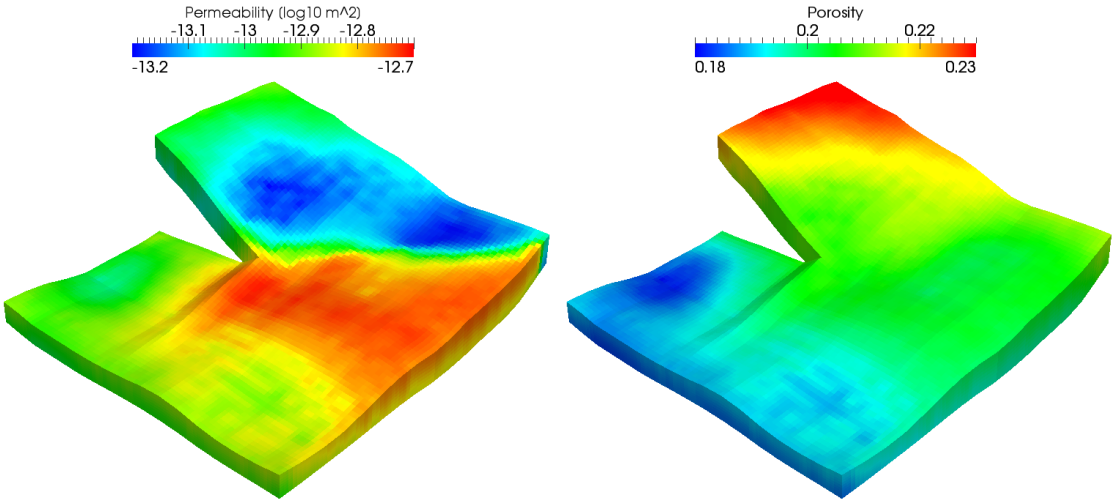

Figure 5.1: Permeability and porosity inside the Johansen formation.

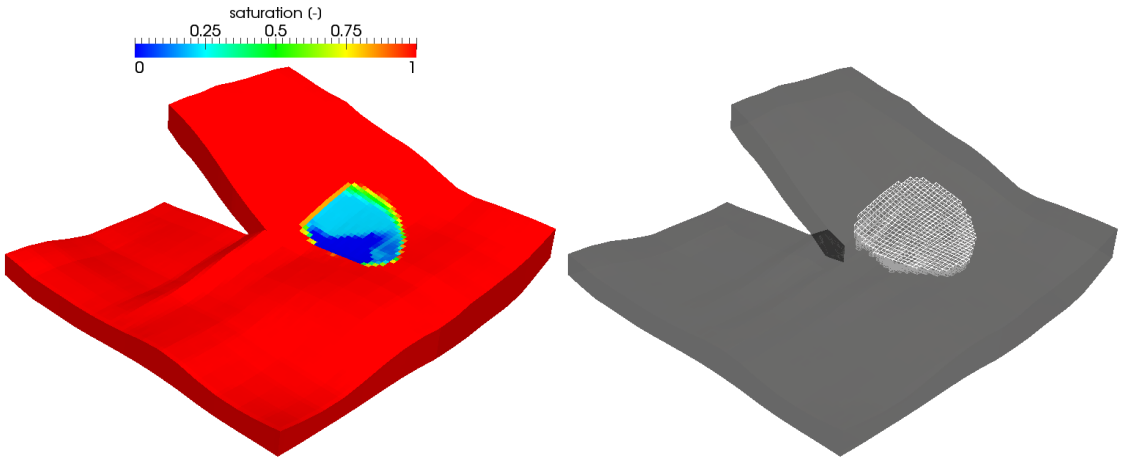

Figure 5.2: Model results after 25 years of carbon dioxide injection into the Johansen formation. Left: saturation of carbon dioxide in phase. Right: extend of the 2p2c-subdomain.

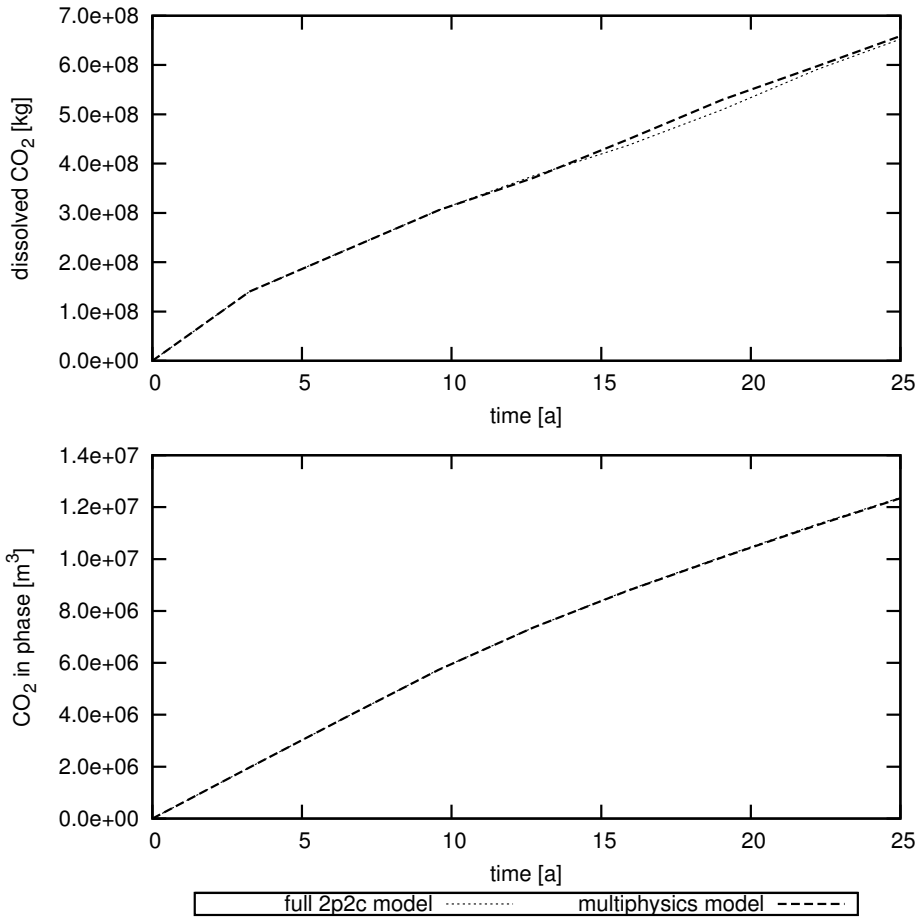

Figure 5.3: Transient model results of full 2p2c-model and multiphysics model for carbon dioxide injection into the Johansen formation. Top: total amount of dissolved carbon dioxide. Bottom: Total amount of carbon dioxide in phase.

compositional model and the multiphysics model also quantitatively, the total mass of dissolved carbon dioxide and the total volume of carbon dioxide in phase of both models are plotted in Figure 5.3. Except of small deviations of the mass of dissolved CO_2, both models yield the same results. These are probably due to the assumption of pressure independent density of the brine phase in the 1p-subdomain. At the end of the simulation, the 2p2c-subdomain covered only 5.4 % of the whole model domain. The total number of flash calculations in the multiphysics model during the whole run was reduced by a factor of 46 as compared to the full 2p2c-model. Although only a rather low speedup of around 20% could be achieved, the huge reduction of phase equilibrium calculations is very promising. As discussed in Section 3.3, the determination of phase equilibrium ratios is rather simple. The incorporation of a thermodynamically sound concept including equations of state and concentration-dependent K-values would considerably increase the CPU-time needed for these calculations. In fact, in Stenby and

Wang [1993], the authors report that in EOS-simulators up to 70% of the total time consumption are spent for phase equilibrium calculations. The possibility of saving a large part of these calculations makes the use of the presented multiphysics concept highly attractive.

5.2 Enhanced remediation of subsurface contaminations

As already mentioned in Section 2.8, subsurface contaminations and enhanced remediation techniques are common problems for the application of compositional multiphase flow models. As an example for the application of the decoupled 2p2cni-model and the non-isothermal multiphysics model presented in Section 2.8.2, a square domain of 20 m×20 m×3 m with a random geostatistical permeability distribution and a xylene contamination is considered. Figure 5.4 shows the permeability field, the initial contamination and the placement of wells and heat sources. The grey field in the middle of the domain marks the initially contaminated area with the NAPL phase in residual saturation ($S_n = 0.1$). It has an approximate paraboloid shape and reaches a maximum depth of 1.5 m. The soil vapor extraction well with an extraction rate of about 140 m^2/h is marked by the red arrow. The three wells marked by blue arrows together inject air at a total rate of 160 m^2/h. The injection wells and the extraction well reach to a depth of 2 m. Finally, the four heat wells are marked by the red cylinders. They reach to a depth of 1.5 m and have a maximum output of 5000 W each, where they heat to a maximum temperature of 300 °C.

The domain is discretized by $31 \times 31 \times 10 = 9610$ cells and a time period of 72 hours is simulated. Both models solved the problem with some 94000 timesteps. Figure 5.5 plots the results of the global 2p2cni model and the multiphysics model: the total mass inside the model domain is associated to the left y-axis, while the size of the subdomains in the multiphysics model is associated to the right y-axis. The total extracted mass of the contaminant is predicted nearly identically as plotted in Figure 5.5. The deviations between both models stay below one percent. The Figure also shows the extend of the subdomains in the domain. Initially, only the 2p2c and the 1p2c subdomains are present. Around the heat wells, however, temperatures increase fast during the first timesteps and the area between them is heated due to advection towards the extraction well. By that, the temperature exceeds the threshold of $\Delta T_{thresh} = 2\,\mathrm{K}$ inside increasing parts of the initial 2p2c-subdomain. Consequently, the 2p2c-subdomain becomes smaller in favor of an increasing 2p2cni-subdomain. With increasing amounts of contaminant being vaporized, the NAPL vanishes and the 2p2cni-subdomain shrinks again until it only covers some 0.4 % of the model domain after 72 hours. Figure 5.6 examplarily shows the extend of the subdomains after 34 and 63 hours which corresponds to 40,000 and 80,000 timesteps, respectively. The maximum extend of the

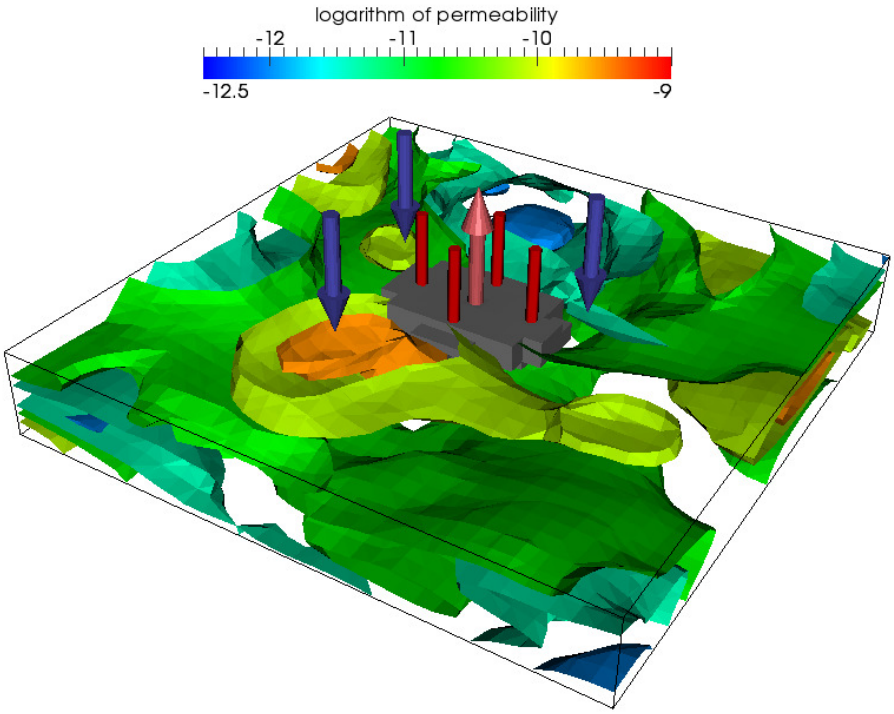

Figure 5.4: Isosurfaces of permeability, initial contamination (grey, middle of domain) and position of wells and heat wells for enhanced subsurface remediation example. Injection wells: blue downward pointing arrows, extraction well: red upward pointing arrow. Heat wells: red cylinders.

2p2cni-subdomain during the whole simulation run does not exceed 3.5% of the model domain, meaning that a huge amount of iterative non-isothermal flash calculations can be saved. In fact, the non-isothermal flash calculations were reduced by a factor of 22. The speedup of the multiphysics model compared to the 2p2cni-model consequently reaches a factor of 1.7 although computationally cheap material laws for xylene and air were used. Apart from the speedup by avoidance of flash calculations, considerable savings could be made by omitting the solution of the transport equation for the single phase subdomains. It has to be emphasized once more, that the total possible speedup depends on the complexity of the phase equilibrium calculations as pointed out in the preceding section. Additionally, the choice of complex (and computationally expensive) material laws increases the differences in CPU-time between a full non-isothermal, compositional two-phase model and the proposed multiphysics method. Hence, the benefits in applying the method increase with the desired physical accuracy of the simulation.

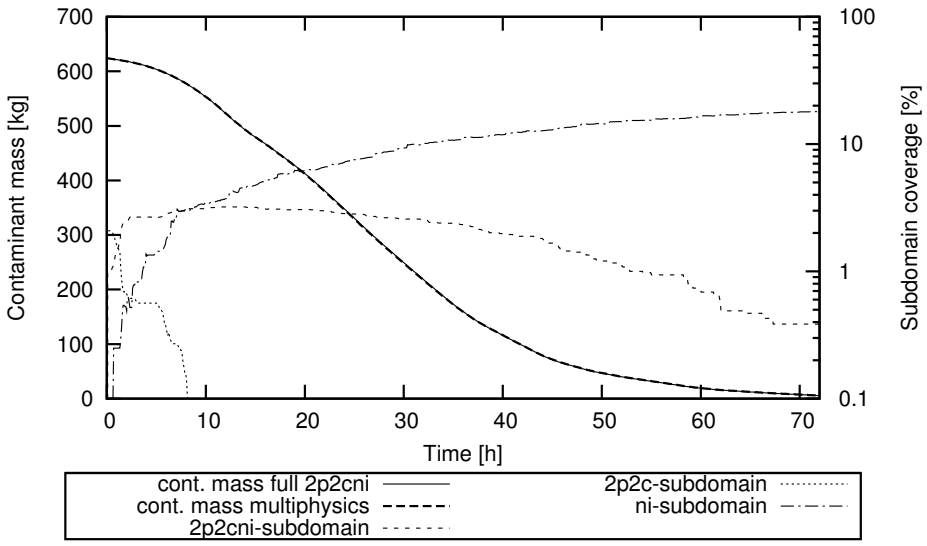

Figure 5.5: Contaminant mass and extend of subdomains in course of simulation of enhanced subsurface remediation example.

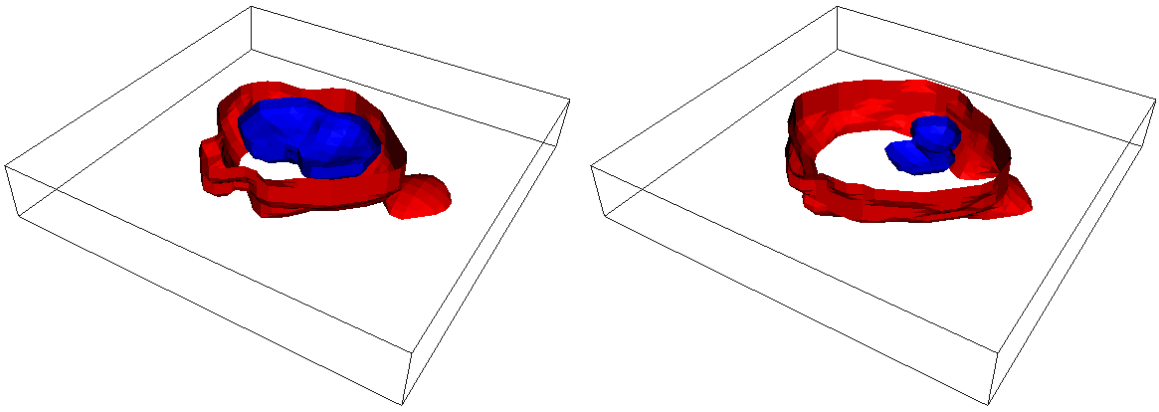

Figure 5.6: Extend of subdomains during the simulation of enhanced subsurface remediation example with the non-isothermal multiphysics model. Left: extend after 34 hours. Right: extend after 63 hours. Volume surrounded by red surface: 2p2cni-subdomain. Volume between blue and red surface: 1p2cni-subdomain.

6 Summary and Outlook

The applicability of complex models to large systems is limited by the availability of computational power and the possibility to obtain sufficiently accurate input parameters. This causes a trade-off between physical accuracy of a model and its computational and conceptual demands. Although a model should always be chosen such that the most complex physical process occurring in the model domain can be captured, this might exceed the capabilities of computational resources or the accessibility of measurements. In many practical applications of porous media flow simulators, the most complex processes are confined to a small part of the model domain. Possible options are thus to either neglect high complexities in favor of a slim model or to capture all processes with a complex model which is superfluous in large parts of the domain. To overcome the disadvantages of both options, a *multiphysics* scheme is proposed. It is meant to adapt the model to the complexity of occurring processes and provide a slim *as well as* accurate simulation method.

As basis for such a model, mathematical formulations for all occurring flow and transport processes have to be provided. The available formulations for the simulation of flow and transport in porous media can basically be divided into two categories: *fully coupled* (also called *fully implicit*) and *decoupled* (also called *sequential*) formulations. Fully coupled solution methods are generally more flexible in the incorporation of new physical processes into the mathematical formulation since the partial differential equations involved are solved iteratively. In contrary, decoupled methods require much more effort in the formulation of the mathematical model. It is therefore not surprising that simulators readily applicable to non-isothermal compositional flow in porous media only exist in a fully coupled form. Due to their solution method, however, fully coupled methods have much higher computational demands. For large systems involving complex physical processes, this may result in huge differences between the CPU time required by fully coupled and decoupled methods. A readily applicable, decoupled method for the three-dimensional simulation of non-isothermal compositional flow processes in porous media under realistic conditions does not exist thus far. This work takes a step towards the development of such a model.

Formulation of a decoupled model for compositional multiphase flow An applicable mathematical model for the description of non-isothermal multiphase flow in porous media incorporating dissolution effects is developed.

- The relevant physical processes are studied and established concepts for their mathematical description are introduced.
- Balance equations for mass and energy are derived. The systems of partial differential equations describing isothermal and non-isothermal flow and transport in porous media are set up and the fractional flow formulation is introduced.
- Phase changes and dissolution effects strongly affect the volume of a fluid mixture. The induced volume changes can not be captured mathematically by the fractional flow formulation.
- In order to overcome the shortcomings of the fractional flow formulation, a decoupled formulation for isothermal and non-isothermal compositional flow based on the local conservation of total fluid volume is presented. It relates the change of the pressure distribution to the local volumetric influence of phase formation by the introduction of derivatives of the total fluid volume.

Numerical implementation of the decoupled model To be able to solve the introduced mathematical model numerically, a robust discretization method is derived and implementation issues are discussed.

- The spatial discretization of the decoupled model for non-isothermal compositional multiphase flow in porous media in a finite volume method is derived.
- The concept of flash calculations for the cell-wise determination of saturations and phase compositions is introduced. The determination of the required parameters is discussed and the implementation of flash calculations for several isothermal and non-isothermal problems is considered.
- The assessment of the necessary coefficients for the pressure and transport equations is discussed. Special emphasis is put on the consistent upwinding of the coefficients of Darcy's law and a modification of the control volume surface integral in order to correctly describe the influence of gravity. Furthermore, the numerical evaluation of the derivatives of total volume is discussed.
- A modified IMPES time discretization is introduced and stability criteria for timestep control are formulated.

Development of multiphysics schemes for isothermal and non-isothermal two-phase two-component flow processes A general concept for the transition of complexities within a porous media domain is presented. Based on that, two multiphysics models for isothermal and non-isothermal two-phase two-component flow and transport are developed.

- The relation of decoupled formulations for immiscible multiphase flow and for compositional multiphase flow are discussed.

- A concept for the interface coupling of two-phase compositional flow and single-phase flow is presented. It is extended to the incorporation of non-isothermal processes and a simplified model for the description of low temperature changes is introduced.
- The implementation of both models into the existing finite volume discretization for non-isothermal compositional flow is discussed.
- The appropriate choice of the subdomains is crucial for the validity of the multiphysics models, since certain processes can only be represented in certain subdomains. The areas and times at which certain processes occur cannot be determined a priori. Therefore, a method is presented which optimally adapts the subdomains of the multiphysics models to the actual physical conditions.

Model validation and application to realistic examples Using the results of experimental investigations and of a published simulator, the presented non-isothermal two-phase two-component model is validated. The applicability and accuracy of the presented multiphysics models were demonstrated on realistic examples.

- Starting with a flume experiment for two-dimensional advectional and convectional heat transport in a single phase, the non-isothermal compositional model is compared to experimental and computational results of increasing complexity. The model showed good qualitative and – as far as measurements were available – quantitative accordance with the used experiments and the HYDROTHERM model.
- The results of an isothermal three-phase three-component implementation of the presented decoupled model are shown and discussed. They show qualitative good results and a stable behavior of the model. However, more effort is required for the proper quantitative description of compositional three-phase flow.
- Pressure oscillations occurring as a numerical artefact during the simulation of systems with boiling fluids limit the applicability of the presented model. The mechanisms causing these problems are discussed. A solution to the current problems could, however, not be found.
- The multiphysics models are tested at two examples. An isothermal example considers injection of carbon dioxide into a geologic formation. A non-isothermal example simulates the remediation of soil contaminations by static heat sources. Both show the applicability and the accuracy of the multiphysics methods. Although the total savings of CPU time are moderate, the methods become increasingly interesting with the incorporation of complex material laws and equation-of-state flash calculations.

Outlook The applicability of the horizontal coupling concept for the transition of complexity inside a porous media domain was demonstrated. It shows the similarities of the fractional flow and the volume conservation decoupled formulations for flow in porous media and forms the foundations to further investigations. Future efforts and scientific investigations should be made in the further development of the decoupled non-isothermal model as well as in the development of other multiphysics strategies for the transition of complexity in porous media domains.

- Additional efforts are required for the development of the compositional three-phase model, for its validation has not yet been achieved.
- A consequent extension to a decoupled formulation for non-isothermal compositional three-phase flow is necessary to be able to simulate general environmental and industrial problems.
- The current implementation has to be made flexible for the consideration of an arbitrary number of components. This also involves an interface to external flash calculation algorithms in order to combine the expertise in multiphase porous media flow with the expertise of other scientific disciplines as thermodynamics and chemical engineering.
- The three-phase three-component model already forms a basis for further investigations of horizontal multiphysics schemes. An example for the remediation of a NAPL contaminant from a residually saturated soil was shown. In this example, the amount of air dissolved in water and vice versa is not of interest, since the dissolution and remediation of the contaminant is the relevant process. The actual dissolution process of the contaminant in the water and gas phase occurs in the near field of the contamination. Here, dissolved water and air may also interact with the contaminant. Thus, the three-phase three-component model may be confined to the area with free-phase NAPL. In the rest of the domain, the mixing of water and air may be neglected in favor of a fractional flow model where the distribution of contaminant to the phases can be considered with a single equilibrium ratio.
- In Niessner and Helmig [2007], a multiscale, multiphysics model was presented in which the subdomain where complex processes happen is discretized by a fine grid. The rest of the domain is represented by upscaled equations on a coarse grid. It used vertical coupling of the different physical processes which is only possible because a divergence-free total velocity was assumed in all parts of the domain. Since this is not valid under general conditions, the merging of the multiscale method with the multiphysics method presented in this work would be a considerable progress towards general applicability. As a prerequisite, a consistent incorporation of hanging nodes into the discretization of the decoupled model has to be developed.

Bibliography

G. Acs, S. Doleschall, and E. Farkas. General Purpose Compositional Model. *Society of Petroleum Engineers Journal*, 25:543–552, 1985.

R.K. Agarwal, Y.-K. Li, L.X. Nghiem, and D.A. Coombe. Multiphase Multicomponent Isenthalpic Flash Calculations. *Journal of Canadian Petroleum Technology*, 30(3), 1991.

C. Albon, J. Jaffre, J.E. Roberts, X. Wang, and C. Serres. Domain Decompositioning for Some Transition Problems in Flow in Porous Media. In Z. Chen, R.E. Ewing, and Z.-C. Shi, editors, *Numerical Treatment of Multiphase Flow in Porous Media*, Lecture Notes in Physics. Springer, 1999.

P.W. Atkins. *Physical Chemsitry*. Oxford University Press, fifth edition, 1994.

K. Aziz and A. Settari. *Petroleum Reservoir Simulation*. Elsevier Science Publishers, 1979.

K. Aziz and T.W. Wong. Considerations in the Development of MUltipurpose Reservoir Simulation Models. In *Proceedings First and Second International Forum on Reservoir Simulation*, pages 77–208. Steiner, P., 1989.

G.I. Barenblatt, I. Zheltov, and I. Kochina. Basic Concepts in the Theory of Seepage of Homogeneous Liquids in Fissured Rocks. *Journal of Applied Mathematics and Mechanics*, 24:1286–1303, 1960.

P. Bastian, M. Blatt, A. Dedner, C. Engwer, R. Klöfkorn, M. Ohlberger, and O. Sander. A Generic Grid Interface for Parallel and Adaptive Scientific Computing. Part I: Abstract Framework. *Computing*, 82(2-3):103–119, 2008a.

P. Bastian, M. Blatt, A. Dedner, C. Engwer, R. Klöfkorn, M. Ohlberger, and O. Sander. A Generic Grid Interface for Parallel and Adaptive Scientific Computing. Part II: Implementation and Tests in DUNE. *Computing*, 82(2-3):121–183, 2008b.

J. Bear. *Dynamics of Fluids in Porous Media*. Environmental Sciences. American Elsevier Pub. Co., 1972.

J. Bear. *Hydraulics of Groundwater*. Dover Publications, 1979.

J. Bear and Y. Bachmat. *Introduction to Modeling of Transport Phenomena in Porous Media*. Kluwer Academic Publishers, 1990.

G. Beavers and D. Joseph. Boundary Condition at a Naturally Impermeable Wall. *Journal of Fluid Mechanics*, 30:197–207, 1967.

P. Binning and M. Celia. Practical Implementation of the Fractional Flow Approach to Multi-phase Flow Simulation. *Advances in Water Resources*, 22(5), 1999.

Leopold Böswirth. *Technische Strömungslehre*. Viehweg & Sohn Verlag, 2005.

B. Buchter. *Untersuchung des Wasserhaushaltes in einem inhomogenen, anisotropen Sickersystem, dargestellt an einem Rendzina-Boden*. PhD thesis, ETH Zürich, 1984.

Y. Cao, B. Eikemo, and R. Helmig. Fractional Flow Formulation for Two-Phase Flow in Porous Media. *http://www.nupus.uni-stuttgart.de/media/publications/NUPUS_2007-01_online.pdf*, 2007.

G. Chavent. A new Formulation of Diphasic Incompressible Flows in Porous Media. In *Applications of Methods of Functional Analysis to Problems in Mechanics*, Lecture Notes in Mathematics, pages 258–270. Springer, 1976.

Z. Chen and R.E. Ewing. Comparison of various Formulations of Three-Phase Flow in Porous Media. *Journal of Computational Physics*, 132:362–373, 1997.

Z. Chen, Q. Guan, and R.E. Ewing. Analysis of a Compositional Model for Fluid Flow in Porous Media. *SIAM Journal on Applied Mathematics*, 60(3):747–777, 2000.

H. Class. *Theorie und numerische Modellierung nichtisothermer Mehrphasenprozesse in NAPL-kontaminierten porösen Medien*. PhD thesis, Universität Stuttgart, 2001.

H. Class, R. Helmig, and P. Bastian. Numerical Simulation of Non-Isothermal Multiphase Multicomponent Processes in Porous Media. 1. An Efficient Solution Technique. *Advances in Water Resources*, 25:533–550, 2002.

H. Class, H. Dahle, F. Riis, A. Ebigbo, and G. Eigestad. Numerical Investigations of CO2 Sequestration in Geological Formations: Problem-Oriented Benchmarks; Problem 3: Estimation of the CO2 Storage Capacity of a Geological Formation. http://www.hydrosys.uni-stuttgart.de/co2-workshop/correctedProblem3.pdf, 2007/2008.

H. Class, A. Ebigbo, R. Helmig, H.K. Dahle, J.M. Nordbotten, M.A. Celia, P. Audigane, M. Darcis, J. Ennis-King, Y. Fan, B. Flemisch, S.E. Gasda, M. Jin, S. Krug, D. Labregere, A.N. Beni, R.J. Pawar, A. Sbai, S.G. Thomas, L. Trenty, and L. Wei. A Benchmark Study on Problems Related to CO2 Storage in Geologic Formations. *Computational Geosciences*, 13(4):409–434, 2009.

D. Coumou. *Numerical Simulation of Fluid Flow in Mid-Ocean Ridge Hydrothermal Systems*. PhD thesis, ETH Zürich, 2008.

R. Courant, K. Friedrichs, and H. Lewy. Über die partiellen Differenzengleichungen der mathematischen Physik. *Mathematische Annalen*, 100(1):32–74, 1928.

P. Deuflhard and A. Hohmann. *Numerische Mathematik II*. de Gruyter, 2002.

P. Dietrich, R. Helmig, M. Sauter, H. Hötzl, J. Köngeter, and G. Teutsch, editors. *Flow and Transport in Fractured Porous Media*. Springer, 2005.

M. Discacciati, E. Miglio, and A. Quarteroni. Mathematical and Numerical Models for Coupling Surface and Groundwater Flows. *Applied Numerical Mathematics*, 43 (1-2):57–74, 2002.

M.O. Dogan, H. Class, and R. Helmig. Different Concepts for the Coupling of Porous-Media Flow in Lower-dimensional Pipe Flow. *Computer Modeling in Engineering & Sciences*, Special Issue 2010, accepted.

B. Dverstorp and J. Andersson. Application of the Discrete Fracture Network Concept with Field Data: Possibilities of Model Calibration and Validation. *Water Resources Research*, 25(3):540–550, 1989.

G.T. Eigestad, H.K. Dahle, B. Hellevang, F. Riis, W.T. Johansen, and E. Oian. Geological Modeling and Simulation of CO2 Injection in the Johansen Formation. *Computational Geosciences*, 13(4):435–450, 2009.

M.S. Espedal and K.H. Karlsen. Numerical Solution of Reservoir Flow Models Based on Large Time Step Operator Splitting Algorithms. In M.S. Espedal, A. Fasano, and A. Miselic, editors, *Filtration in Porous Media and Industrial Application*. Springer, 1998.

A. Färber. *Wärmetransport in der ungesättigten Bodenzone: Entwicklung einer thermischen in-situ Sanierungstechnologie*. PhD thesis, Universität Stuttgart, 1997.

B. Flemisch, J. Fritz, R. Helmig, J. Niessner, and B. Wohlmuth. DuMuX: A multi-scale multi-physics toolbox for flow and transport processes in porous media. In *Multi-scale Computational Methods for Solids and Fluids*, pages 69–74. European Community on Computational Methods in Applied Sciences, 2007.

R.A. Freeze and J.A. Cherry. *Groundwater*. Prentice Hall, 1979.

A. Grant and L. Sorey. The Compressibility and Hydraulic Diffusivity of a Water-Steam Flow. *Water Resources Research*, 15(3):684–686, 1979.

H. Haegland, A. Assteerawatt, H.K. Dahle, G.T. Eigestad, and R. Helmig. Comparison of Cell- and Vertex-Centered Discretization Methods for Flow in a Two-Dimensional Discrete Fracture-Matrix System. *Advances in Water Resources*, 32(12):1740–1755, 2009.

A. Hartmann, V. Rath, and C. Clauser. Thermal Conductivity From Core and Well Log Data. *International Journal of Rock Mechanics and Mining Sciences*, 42(7-8): 1042–1055, 2005.

S.M. Hassanizadeh and W.G. Gray. General Conservation Equations for Multi-phase Systems 2. Mass, Momenta, Energy, and Entropy Equations. *Advances in Water Resources*, 2:191–203, 1979.

R. Helmig. *Gekoppelte Strömungs- und Transportprozesse im Untergrund - Ein Beitrag zur Hydrosystemmodellierung*. Universität Stuttgart, 1998.

R. Helmig, B. Flemisch, J. Niessner, M. Wolff, and J. Fritz. Efficient Modelling of Flow and Transport in Porous Media using Multi-Physics and Multi-Scale Approaches. In W. Freeden, Z. Nashed, and T. Sonar, editors, *Handbook of Geomathematics*. Springer, submitted.

F. Herning and L. Zipperer. Beitrag zur Berechnung der Zähigkeit technischer Gasgemische aus den Zähigkeitswerten der Einzelbestandteile. *Gas- und Wasserfach*, 79:49–69, 1936.

D. Hristopulos and G. Christakos. An Analysis of Hydrocarbon Conductivity Upscaling. *Nonlinear Analysis*, 30(8):4979–4989, 1997.

R. Huber and R. Helmig. Node-centered Finite Volume Discretizations for the Numerical Simulation of Multiphase Flow in Heterogeneous Porous Media. *Computational Geosciences*, 4(2), 2000.

R.U. Huber. *Compositional Multiphase Flow and Transport in Heterogeneous Porous Media*. PhD thesis, Universität Stuttgart, 2000.

IPCC. Carbon Dioxide Capture and Storage. Special Report of the Intergovernmental Panel on Climate Change. Technical report, 2005.

K.L.Jr. Kipp, P.A. Hsieh, and S.R. Charlton. *Guide to the Revised Ground-Water Flow and Heat Transport Simulator: HYDROTHERM – Version 3*. US Geological Survey, 2008. http://wwwbrr.cr.usgs.gov/projects/GW_Solute/hydrotherm/.

W. Layton, F. Schieweck, and I. Yotov. Coupling Fluid Flow with Porous Media Flow. *SIAM Journal on Numerical Analysis*, 40(6):2195–2218, 2003.

C. Lüdecke and D. Lüdecke. *Thermodynamik*. Springer, 2000.

W.D.Jr. McCain. *The Properties of Petroleum Fluids*. Pennwell Pub, 1990.

M.L. Michelsen and J.M. Mollerup. *Thermodynamic Models: Fundamentals & Computational Aspects*. Tie-Line Publications, 2007.

A. Moench. Double-Porosity Models for a Fissured Groundwater Reservoir With Fracture Skin. *Water Resources Research*, 27(7):831–846, 1984.

J. Niessner. *Multi-Scale Modeling of Multi-Phase-Multi-Component Processes in Heterogeneous Porous Media*. PhD thesis, Universität Stuttgart, 2006.

J. Niessner and R. Helmig. Multi-Scale Modeling of Two-Phase - Two-Component Processes in Heterogeneous Porous Media. *Numerical Linear Algebra with Applications*, 13(9):699–715, 2006.

J. Niessner and R. Helmig. Multi-physics Modeling of Flow and Transport in Porous Media using a Downscaling Approach. *Advances in Water Resources*, 32(6):845–850, 2009.

J. Niessner and R Helmig. Multi-Scale Modeling of Three-Phase–Three-Component Processes in Heterogeneous Porous Media. *Advances in Water Resources*, 30(11): 2309–2325, 2007.

M. Peszynska. Multiphysics Coupling for Two Phase Flow in Degenerate Conditions. In J. Chadam, A. Cunningham, R.E. Ewing, P. Ortoleva, and M.F. Wheeler, editors, *Resource Recovery, Confinement, and Remediation of Environmental Hazards*. Springer, 2002.

K. Pruess. Brief Guide to the MINC-Method for Modeling Flow and Transport in Fractured Media. Technical report, U.S. Department of Energy, 1992.

K. Pruess and T.N. Narasimhan. On Fluid Reserves and the Production of Superheated Steam from Fractured, Vapor-Dominated Geothermal Reservoirs. *Journal Geophysical Research*, 87(B11):9329–9339, 1982.

K. Pruess and T.N. Narasimhan. A Practical Method for Modeling Fluid and Heat Flow in Fractured Porous Media. *Society of Petroleum Engineers Journal*, 25(1): 14–26, 1985.

V. Reichenberger, H. Jakobs, P. Bastian, and R. Helmig. A Mixed-Dimensional Finite Volume Method for Two-Phase Flow in Fractured Porous Media. *Advances in Water Resources*, 29(7):1020–1036, 2006.

H. Römpp, J. Falbe, and E. Amelingmeier. *Römpp - Lexikon Chemie*. Thieme Verlag, Stuttgart, 1999.

S. Saha and J.J. Caroll. The isoenergetic–isochoric flash. *Fluid Phase Equilibria*, 138: 23–41, 1997.

R. Sander. Compilation of Henry's Law Constants for Inorganic and Organic Species of Potential Importance in Environmental Chemistry. http://www.mpch-mainz.mpg.de/ sander/res/henry.html, 1999.

J.W. Sheldon, B. Zondek, and W.T. Cardwell. One-Dimensional, Incompressible, Non-Capillary, Two-phase Fluid Flow in a Porous Medium. *Trans. SPE of AIME*, 216: 290–296, 1959.

B.E. Sleep and J.F. Sykes. Computational Simulation of Groundwater Contamination by Organic Compounds 1. Model Development and Verification. *Water Resources Research*, 29(6):1697–1708, 1993.

W.H. Somerton, A.H. El-Shaarani, and S.M. Mobarak. High Temperature Behaviour of Rocks Associated with Geothermal Type Reservoirs. *SPE 4897*, 1974.

E.H. Stenby and P. Wang. Noniterative Phase Equilibrium Calculation in Compositional Reservoir Simulation. *SPE 26641*, 1993.

R. Therrien and E. A. Sudicky. Three-dimensional Analysis of Variably-Saturated Flow and Solute Transport in Discretely-Fractured Porous Media. *Journal of Contaminant Hydrology*, 23(1-2):1–44, 1996.

J.A. Trangenstein and J.B. Bell. Mathematical Structure of Compositional Reservoir Simulation. *SIAM J. Sci. Stat. Comput.*, 10(5):817–845, 1989.

D.E.A. van Odyck, J.B. Bell, F. Monmont, and N. Nikiforakis. The Mathematical Structure of Multiphase Thermal Models of Flow in Porous Media. *Proceeding of the Royal Society A*, 465:523–549, 2009.

D. Vassilev and I. Yotov. Coupling Stokes-Darcy Flow with Transport. *SIAM Journal on Scientific Computing*, 31(5):3661–3684, 2009.

J.S.Y. Wang. Flow and Transport in Fractured Rocks. *Review of Geophysics*, (29): 254–262, 1991.

J.S.Y. Wang and T.N Narasimhan. Hydrologic Mechanisms Governing Fluid Flow in a Partially Saturated, Fractured, Porous Medium. *Water Resources Research*, 21(12): 1861–1874, 1985.

M.F. Wheeler, T. Arbogast, S. Bryant, J. Eaton, Q. Lu, M. Peszynska, and I. Yotov. A Parallel Multiblock/Multidomain Approach for Reservoir Simulation. *SPE 51884*, 1999.

C.F. Wiesepape, H.T. Kennedy, and P.B. Crawford. A Crude Oil - Natural Gas system Vapor-Liquid Equilibrium Ratios. *Journal of Chemical and Engineering Data*, 22, 1977.

L.C. Young and R.E. Stephenson. A Generalized Compositional Approach for Reservoir Simulation. *Society of Petroleum Engineers Journal*, 23:727–742, 1983.

W. Zhao. Numerical and Experimental Investigations on Thermally Induced Buoyancy Flow in Porous Media. Master's thesis, Universität Stuttgart, 2006.

Das ist es nun: gedruckt, gebunden und im Schrank verschwunden. – H. Budelmann

Lebenslauf

Persönliche Daten

Name:	Jochen Andreas Johannes Georg Fritz
Geburt:	19.02.1983 in Tübingen
Anschrift:	Schmiedstraße 2 61440 Oberursel jochen.fritz@iws.uni-stuttgart.de
Nationalität:	deutsch
Familienstand:	verheiratet mit Lina-Luisa Fritz, 1 Kind: Emma Helene Fritz

Ausbildung

1994–2002	Graf-Eberhardt-Gymnasium Bad Urach Abschluss: Abitur
2002–2006	Studium Bauingenieurwesen an der Universität Stuttgart Abschluss: Diplom
2006	Diplomarbeit am Institut für Wasserbau, Lehrstuhl für Hydromechanik und Hydrosystemmodellierung Titel: *Efficient Spectral Methods for Geostatistical Interpolation*
2007–2010	Mitglied im Internationalen Graduiertenkolleg *Nonlinearities and Upscaling in Porous Media (NUPUS)*
2007–2010	Doktorand am Institut für Wasserbau, Lehrstuhl für Hydromechanik und Hydrosystemmodellierung, Universität Stuttgart

Tätigkeiten

2007–2010	Wissenschaftlicher Mitarbeiter am Institut für Wasserbau, Lehrstuhl für Hydromechanik und Hydrosystemmodellierung, Universität Stuttgart

Institut für Wasserbau
Universität Stuttgart

Pfaffenwaldring 61
70569 Stuttgart (Vaihingen)
Telefon (0711) 685 - 64717/64749/64752/64679
Telefax (0711) 685 - 67020 o. 64746 o. 64681
E-Mail: iws@iws.uni-stuttgart.de
http://www.iws.uni-stuttgart.de

Verzeichnis der Mitteilungshefte

1 Röhnisch, Arthur: *Die Bemühungen um eine Wasserbauliche Versuchsanstalt an der Technischen Hochschule Stuttgart*, und
Fattah Abouleid, Abdel: *Beitrag zur Berechnung einer in lockeren Sand gerammten, zweifach verankerten Spundwand*, 1963

2 Marotz, Günter: *Beitrag zur Frage der Standfestigkeit von dichten Asphaltbelägen im Großwasserbau*, 1964

3 Gurr, Siegfried: *Beitrag zur Berechnung zusammengesetzter ebener Flächentragwerke unter besonderer Berücksichtigung ebener Stauwände, mit Hilfe von Randwert- und Lastwertmatrizen*, 1965

4 Plica, Peter: *Ein Beitrag zur Anwendung von Schalenkonstruktionen im Stahlwasserbau*, und Petrikat, Kurt: *Möglichkeiten und Grenzen des wasserbaulichen Versuchswesens*, 1966

5 Plate, Erich: *Beitrag zur Bestimmung der Windgeschwindigkeitsverteilung in der durch eine Wand gestörten bodennahen Luftschicht*,
und
Röhnisch, Arthur; Marotz, Günter: *Neue Baustoffe und Bauausführungen für den Schutz der Böschungen und der Sohle von Kanälen, Flüssen und Häfen; Gestehungskosten und jeweilige Vorteile*, sowie Unny, T.E.: *Schwingungsuntersuchungen am Kegelstrahlschieber*, 1967

6 Seiler, Erich: *Die Ermittlung des Anlagenwertes der bundeseigenen Binnenschiffahrtsstraßen und Talsperren und des Anteils der Binnenschiffahrt an diesem Wert*, 1967

7 *Sonderheft anläßlich des 65. Geburtstages von Prof. Arthur Röhnisch mit Beiträgen von* Benk, Dieter; Breitling, J.; Gurr, Siegfried; Haberhauer, Robert; Honekamp, Hermann; Kuz, Klaus Dieter; Marotz, Günter; Mayer-Vorfelder, Hans-Jörg; Miller, Rudolf; Plate, Erich J.; Radomski, Helge; Schwarz, Helmut; Vollmer, Ernst; Wildenhahn, Eberhard; 1967

8 Jumikis, Alfred: *Beitrag zur experimentellen Untersuchung des Wassernachschubs in einem gefrierenden Boden und die Beurteilung der Ergebnisse*, 1968

9 Marotz, Günter: *Technische Grundlagen einer Wasserspeicherung im natürlichen Untergrund*, 1968

10 Radomski, Helge: *Untersuchungen über den Einfluß der Querschnittsform wellenförmiger Spundwände auf die statischen und rammtechnischen Eigenschaften*, 1968

11 Schwarz, Helmut: *Die Grenztragfähigkeit des Baugrundes bei Einwirkung vertikal gezogener Ankerplatten als zweidimensionales Bruchproblem*, 1969

12 Erbel, Klaus: *Ein Beitrag zur Untersuchung der Metamorphose von Mittelgebirgsschneedecken unter besonderer Berücksichtigung eines Verfahrens zur Bestimmung der thermischen Schneequalität*, 1969

13 Westhaus, Karl-Heinz: *Der Strukturwandel in der Binnenschiffahrt und sein Einfluß auf den Ausbau der Binnenschiffskanäle*, 1969

14 Mayer-Vorfelder, Hans-Jörg: *Ein Beitrag zur Berechnung des Erdwiderstandes unter Ansatz der logarithmischen Spirale als Gleitflächenfunktion*, 1970

15 Schulz, Manfred: *Berechnung des räumlichen Erddruckes auf die Wandung kreiszylindrischer Körper*, 1970

16 Mobasseri, Manoutschehr: *Die Rippenstützmauer. Konstruktion und Grenzen ihrer Standsicherheit*, 1970

17 Benk, Dieter: *Ein Beitrag zum Betrieb und zur Bemessung von Hochwasserrückhaltebecken*, 1970

18 Gàl, Attila: *Bestimmung der mitschwingenden Wassermasse bei überströmten Fischbauchklappen mit kreiszylindrischem Staublech*, 1971, vergriffen

19 Kuz, Klaus Dieter: *Ein Beitrag zur Frage des Einsetzens von Kavitationserscheinungen in einer Düsenströmung bei Berücksichtigung der im Wasser gelösten Gase*, 1971, vergriffen

20 Schaak, Hartmut: *Verteilleitungen von Wasserkraftanlagen*, 1971

21 *Sonderheft zur Eröffnung der neuen Versuchsanstalt des Instituts für Wasserbau der Universität Stuttgart mit Beiträgen von* Brombach, Hansjörg; Dirksen, Wolfram; Gàl, Attila; Gerlach, Reinhard; Giesecke, Jürgen; Holthoff, Franz-Josef; Kuz, Klaus Dieter; Marotz, Günter; Minor, Hans-Erwin; Petrikat, Kurt; Röhnisch, Arthur; Rueff, Helge; Schwarz, Helmut; Vollmer, Ernst; Wildenhahn, Eberhard; 1972

22 Wang, Chung-su: *Ein Beitrag zur Berechnung der Schwingungen an Kegelstrahlschiebern*, 1972

23 Mayer-Vorfelder, Hans-Jörg: *Erdwiderstandsbeiwerte nach dem Ohde-Variationsverfahren*, 1972

24 Minor, Hans-Erwin: *Beitrag zur Bestimmung der Schwingungsanfachungsfunktionen überströmter Stauklappen*, 1972, vergriffen

25 Brombach, Hansjörg: *Untersuchung strömungsmechanischer Elemente (Fluidik) und die Möglichkeit der Anwendung von Wirbelkammerelementen im Wasserbau*, 1972, vergriffen

26 Wildenhahn, Eberhard: *Beitrag zur Berechnung von Horizontalfilterbrunnen*, 1972

27 Steinlein, Helmut: *Die Eliminierung der Schwebstoffe aus Flußwasser zum Zweck der unterirdischen Wasserspeicherung, gezeigt am Beispiel der Iller*, 1972

28 Holthoff, Franz Josef: *Die Überwindung großer Hubhöhen in der Binnenschiffahrt durch Schwimmerhebewerke*, 1973

29 Röder, Karl: *Einwirkungen aus Baugrundbewegungen auf trog- und kastenförmige Konstruktionen des Wasser- und Tunnelbaues*, 1973

30 Kretschmer, Heinz: *Die Bemessung von Bogenstaumauern in Abhängigkeit von der Talform*, 1973

31 Honekamp, Hermann: *Beitrag zur Berechnung der Montage von Unterwasserpipelines*, 1973

32 Giesecke, Jürgen: *Die Wirbelkammertriode als neuartiges Steuerorgan im Wasserbau*, und Brombach, Hansjörg: *Entwicklung, Bauformen, Wirkungsweise und Steuereigenschaften von Wirbelkammerverstärkern*, 1974

33 Rueff, Helge: *Untersuchung der schwingungserregenden Kräfte an zwei hintereinander angeordneten Tiefschützen unter besonderer Berücksichtigung von Kavitation*, 1974

34 Röhnisch, Arthur: *Einpreßversuche mit Zementmörtel für Spannbeton - Vergleich der Ergebnisse von Modellversuchen mit Ausführungen in Hüllwellrohren*, 1975

35 *Sonderheft anläßlich des 65. Geburtstages von Prof. Dr.-Ing. Kurt Petrikat mit Beiträgen von*: Brombach, Hansjörg; Erbel, Klaus; Flinspach, Dieter; Fischer jr., Richard; Gàl, Attila; Gerlach, Reinhard; Giesecke, Jürgen; Haberhauer, Robert; Hafner Edzard; Hausenblas, Bernhard; Horlacher, Hans-Burkhard; Hutarew, Andreas; Knoll, Manfred; Krummet, Ralph; Marotz, Günter; Merkle, Theodor; Miller, Christoph; Minor, Hans-Erwin; Neumayer, Hans; Rao, Syamala; Rath, Paul; Rueff, Helge; Ruppert, Jürgen; Schwarz, Wolfgang; Topal-Gökceli, Mehmet; Vollmer, Ernst; Wang, Chung-su; Weber, Hans-Georg; 1975

36 Berger, Jochum: *Beitrag zur Berechnung des Spannungszustandes in rotationssymmetrisch belasteten Kugelschalen veränderlicher Wandstärke unter Gas- und Flüssigkeitsdruck durch Integration schwach singulärer Differentialgleichungen*, 1975

37 Dirksen, Wolfram: *Berechnung instationärer Abflußvorgänge in gestauten Gerinnen mittels Differenzenverfahren und die Anwendung auf Hochwasserrückhaltebecken*, 1976

38 Horlacher, Hans-Burkhard: *Berechnung instationärer Temperatur- und Wärmespannungsfelder in langen mehrschichtigen Hohlzylindern*, 1976

39 Hafner, Edzard: *Untersuchung der hydrodynamischen Kräfte auf Baukörper im Tiefwasserbereich des Meeres*, 1977, ISBN 3-921694-39-6

40 Ruppert, Jürgen: *Über den Axialwirbelkammerverstärker für den Einsatz im Wasserbau*, 1977, ISBN 3-921694-40-X

41 Hutarew, Andreas: *Beitrag zur Beeinflußbarkeit des Sauerstoffgehalts in Fließgewässern an Abstürzen und Wehren*, 1977, ISBN 3-921694-41-8, vergriffen

42 Miller, Christoph: *Ein Beitrag zur Bestimmung der schwingungserregenden Kräfte an unterströmten Wehren*, 1977, ISBN 3-921694-42-6

43 Schwarz, Wolfgang: *Druckstoßberechnung unter Berücksichtigung der Radial- und Längsverschiebungen der Rohrwandung*, 1978, ISBN 3-921694-43-4

44 Kinzelbach, Wolfgang: *Numerische Untersuchungen über den optimalen Einsatz variabler Kühlsysteme einer Kraftwerkskette am Beispiel Oberrhein*, 1978, ISBN 3-921694-44-2

45 Barczewski, Baldur: *Neue Meßmethoden für Wasser-Luftgemische und deren Anwendung auf zweiphasige Auftriebsstrahlen*, 1979, ISBN 3-921694-45-0

46 Neumayer, Hans: *Untersuchung der Strömungsvorgänge in radialen Wirbelkammerverstärkern*, 1979, ISBN 3-921694-46-9

47 Elalfy, Youssef-Elhassan: *Untersuchung der Strömungsvorgänge in Wirbelkammerdioden und -drosseln*, 1979, ISBN 3-921694-47-7

48 Brombach, Hansjörg: *Automatisierung der Bewirtschaftung von Wasserspeichern*, 1981, ISBN 3-921694-48-5

49 Geldner, Peter: *Deterministische und stochastische Methoden zur Bestimmung der Selbstdichtung von Gewässern*, 1981, ISBN 3-921694-49-3, vergriffen

50 Mehlhorn, Hans: *Temperaturveränderungen im Grundwasser durch Brauchwassereinleitungen*, 1982, ISBN 3-921694-50-7, vergriffen

51 Hafner, Edzard: *Rohrleitungen und Behälter im Meer*, 1983, ISBN 3-921694-51-5

52 Rinnert, Bernd: *Hydrodynamische Dispersion in porösen Medien: Einfluß von Dichteunterschieden auf die Vertikalvermischung in horizontaler Strömung*, 1983, ISBN 3-921694-52-3, vergriffen

53 Lindner, Wulf: *Steuerung von Grundwasserentnahmen unter Einhaltung ökologischer Kriterien*, 1983, ISBN 3-921694-53-1, vergriffen

54 Herr, Michael; Herzer, Jörg; Kinzelbach, Wolfgang; Kobus, Helmut; Rinnert, Bernd: *Methoden zur rechnerischen Erfassung und hydraulischen Sanierung von Grundwasserkontaminationen*, 1983, ISBN 3-921694-54-X

55 Schmitt, Paul: *Wege zur Automatisierung der Niederschlagsermittlung*, 1984, ISBN 3-921694-55-8, vergriffen

56 Müller, Peter: *Transport und selektive Sedimentation von Schwebstoffen bei gestautem Abfluß*, 1985, ISBN 3-921694-56-6

57 El-Qawasmeh, Fuad: *Möglichkeiten und Grenzen der Tropfbewässerung unter besonderer Berücksichtigung der Verstopfungsanfälligkeit der Tropfelemente*, 1985, ISBN 3-921694-57-4, vergriffen

58 Kirchenbaur, Klaus: *Mikroprozessorgesteuerte Erfassung instationärer Druckfelder am Beispiel seegangsbelasteter Baukörper*, 1985, ISBN 3-921694-58-2

59 Kobus, Helmut (Hrsg.): *Modellierung des großräumigen Wärme- und Schadstofftransports im Grundwasser*, Tätigkeitsbericht 1984/85 (DFG-Forschergruppe an den Universitäten Hohenheim, Karlsruhe und Stuttgart), 1985, ISBN 3-921694-59-0, vergriffen

60 Spitz, Karlheinz: *Dispersion in porösen Medien: Einfluß von Inhomogenitäten und Dichteunterschieden*, 1985, ISBN 3-921694-60-4, vergriffen

61 Kobus, Helmut: *An Introduction to Air-Water Flows in Hydraulics*, 1985, ISBN 3-921694-61-2

62 Kaleris, Vassilios: *Erfassung des Austausches von Oberflächen- und Grundwasser in horizontalebenen Grundwassermodellen*, 1986, ISBN 3-921694-62-0

63 Herr, Michael: *Grundlagen der hydraulischen Sanierung verunreinigter Porengrundwasserleiter*, 1987, ISBN 3-921694-63-9

64 Marx, Walter: *Berechnung von Temperatur und Spannung in Massenbeton infolge Hydratation*, 1987, ISBN 3-921694-64-7

65 Koschitzky, Hans-Peter: *Dimensionierungskonzept für Sohlbelüfter in Schußrinnen zur Vermeidung von Kavitationsschäden*, 1987, ISBN 3-921694-65-5

66 Kobus, Helmut (Hrsg.): *Modellierung des großräumigen Wärme- und Schadstofftransports im Grundwasser*, Tätigkeitsbericht 1986/87 (DFG-Forschergruppe an den Universitäten Hohenheim, Karlsruhe und Stuttgart) 1987, ISBN 3-921694-66-3

67 Söll, Thomas: *Berechnungsverfahren zur Abschätzung anthropogener Temperaturanomalien im Grundwasser*, 1988, ISBN 3-921694-67-1

68 Dittrich, Andreas; Westrich, Bernd: *Bodenseeufererosion, Bestandsaufnahme und Bewertung*, 1988, ISBN 3-921694-68-X, vergriffen

69 Huwe, Bernd; van der Ploeg, Rienk R.: *Modelle zur Simulation des Stickstoffhaushaltes von Standorten mit unterschiedlicher landwirtschaftlicher Nutzung*, 1988, ISBN 3-921694-69-8, vergriffen

70 Stephan, Karl: *Integration elliptischer Funktionen*, 1988, ISBN 3-921694-70-1

71 Kobus, Helmut; Zilliox, Lothaire (Hrsg.): *Nitratbelastung des Grundwassers, Auswirkungen der Landwirtschaft auf die Grundwasser- und Rohwasserbeschaffenheit und Maßnahmen zum Schutz des Grundwassers*. Vorträge des deutsch-französischen Kolloquiums am 6. Oktober 1988, Universitäten Stuttgart und Louis Pasteur Strasbourg (Vorträge in deutsch oder französisch, Kurzfassungen zweisprachig), 1988, ISBN 3-921694-71-X

72 Soyeaux, Renald: *Unterströmung von Stauanlagen auf klüftigem Untergrund unter Berücksichtigung laminarer und turbulenter Fließzustände*,1991, ISBN 3-921694-72-8

73 Kohane, Roberto: *Berechnungsmethoden für Hochwasserabfluß in Fließgewässern mit überströmten Vorländern*, 1991, ISBN 3-921694-73-6

74 Hassinger, Reinhard: *Beitrag zur Hydraulik und Bemessung von Blocksteinrampen in flexibler Bauweise*, 1991, ISBN 3-921694-74-4, vergriffen

75 Schäfer, Gerhard: *Einfluß von Schichtenstrukturen und lokalen Einlagerungen auf die Längsdispersion in Porengrundwasserleitern*, 1991, ISBN 3-921694-75-2

76 Giesecke, Jürgen: *Vorträge, Wasserwirtschaft in stark besiedelten Regionen; Umweltforschung mit Schwerpunkt Wasserwirtschaft*, 1991, ISBN 3-921694-76-0

77 Huwe, Bernd: *Deterministische und stochastische Ansätze zur Modellierung des Stickstoffhaushalts landwirtschaftlich genutzter Flächen auf unterschiedlichem Skalenniveau*, 1992, ISBN 3-921694-77-9, vergriffen

78 Rommel, Michael: *Verwendung von Kluftdaten zur realitätsnahen Generierung von Kluftnetzen mit anschließender laminar-turbulenter Strömungsberechnung*, 1993, ISBN 3-92 1694-78-7

79 Marschall, Paul: *Die Ermittlung lokaler Stofffrachten im Grundwasser mit Hilfe von Einbohrloch-Meßverfahren*, 1993, ISBN 3-921694-79-5, vergriffen

80 Ptak, Thomas: *Stofftransport in heterogenen Porenaquiferen: Felduntersuchungen und stochastische Modellierung*, 1993, ISBN 3-921694-80-9, vergriffen

81 Haakh, Frieder: *Transientes Strömungsverhalten in Wirbelkammern,* 1993, ISBN 3-921694-81-7

82 Kobus, Helmut; Cirpka, Olaf; Barczewski, Baldur; Koschitzky, Hans-Peter: *Versucheinrichtung zur Grundwasser und Altlastensanierung VEGAS, Konzeption und Programmrahmen*, 1993, ISBN 3-921694-82-5

83 Zang, Weidong: *Optimaler Echtzeit-Betrieb eines Speichers mit aktueller Abflußregenerierung*, 1994, ISBN 3-921694-83-3, vergriffen

84 Franke, Hans-Jörg: *Stochastische Modellierung eines flächenhaften Stoffeintrages und Transports in Grundwasser am Beispiel der Pflanzenschutzmittelproblematik*, 1995, ISBN 3-921694-84-1

85 Lang, Ulrich: *Simulation regionaler Strömungs- und Transportvorgänge in Karstaquiferen mit Hilfe des Doppelkontinuum-Ansatzes: Methodenentwicklung und Parameteridentifikation*, 1995, ISBN 3-921694-85-X, vergriffen

86 Helmig, Rainer: *Einführung in die Numerischen Methoden der Hydromechanik*, 1996, ISBN 3-921694-86-8, vergriffen

87 Cirpka, Olaf: *CONTRACT: A Numerical Tool for Contaminant Transport and Chemical Transformations - Theory and Program Documentation* -, 1996, ISBN 3-921694-87-6

88 Haberlandt, Uwe: *Stochastische Synthese und Regionalisierung des Niederschlages für Schmutzfrachtberechnungen*, 1996, ISBN 3-921694-88-4

89 Croisé, Jean: *Extraktion von flüchtigen Chemikalien aus natürlichen Lockergesteinen mittels erzwungener Luftströmung*, 1996, ISBN 3-921694-89-2, vergriffen

90 Jorde, Klaus: *Ökologisch begründete, dynamische Mindestwasserregelungen bei Ausleitungskraftwerken*, 1997, ISBN 3-921694-90-6, vergriffen

91 Helmig, Rainer: *Gekoppelte Strömungs- und Transportprozesse im Untergrund - Ein Beitrag zur Hydrosystemmodellierung*-, 1998, ISBN 3-921694-91-4, vergriffen

92 Emmert, Martin: *Numerische Modellierung nichtisothermer Gas-Wasser Systeme in porösen Medien,* 1997, ISBN 3-921694-92-2

93 Kern, Ulrich: *Transport von Schweb- und Schadstoffen in staugeregelten Fließgewässern am Beispiel des Neckars*, 1997, ISBN 3-921694-93-0, vergriffen

94 Förster, Georg: *Druckstoßdämpfung durch große Luftblasen in Hochpunkten von Rohrleitungen 1997*, ISBN 3-921694-94-9

95 Cirpka, Olaf: *Numerische Methoden zur Simulation des reaktiven Mehrkomponententransports im Grundwasser*, 1997, ISBN 3-921694-95-7, vergriffen

96 Färber, Arne: *Wärmetransport in der ungesättigten Bodenzone: Entwicklung einer thermischen In-situ-Sanierungstechnologie*, 1997, ISBN 3-921694-96-5

97 Betz, Christoph: *Wasserdampfdestillation von Schadstoffen im porösen Medium: Entwicklung einer thermischen In-situ-Sanierungstechnologie*, 1998, ISBN 3-921694-97-3

98 Xu, Yichun: *Numerical Modeling of Suspended Sediment Transport in Rivers*, 1998, ISBN 3-921694-98-1, vergriffen

99 Wüst, Wolfgang: *Geochemische Untersuchungen zur Sanierung CKW-kontaminierter Aquifere mit Fe(0)-Reaktionswänden,* 2000, ISBN 3-933761-02-2

100 Sheta, Hussam: *Simulation von Mehrphasenvorgängen in porösen Medien unter Einbeziehung von Hysterese-Effekten*, 2000, ISBN 3-933761-03-4

101 Ayros, Edwin: *Regionalisierung extremer Abflüsse auf der Grundlage statistischer Verfahren*, 2000, ISBN 3-933761-04-2, vergriffen

102 Huber, Ralf: *Compositional Multiphase Flow and Transport in Heterogeneous Porous Media*, 2000, ISBN 3-933761-05-0

103 Braun, Christopherus: *Ein Upscaling-Verfahren für Mehrphasenströmungen in porösen Medien*, 2000, ISBN 3-933761-06-9

104 Hofmann, Bernd: *Entwicklung eines rechnergestützten Managementsystems zur Beurteilung von Grundwasserschadensfällen*, 2000, ISBN 3-933761-07-7

105 Class, Holger: *Theorie und numerische Modellierung nichtisothermer Mehrphasenprozesse in NAPL-kontaminierten porösen Medien,* 2001, ISBN 3-933761-08-5

106 Schmidt, Reinhard: *Wasserdampf- und Heißluftinjektion zur thermischen Sanierung kontaminierter Standorte*, 2001, ISBN 3-933761-09-3

107 Josef, Reinhold:, *Schadstoffextraktion mit hydraulischen Sanierungsverfahren unter Anwendung von grenzflächenaktiven Stoffen*, 2001, ISBN 3-933761-10-7

108 Schneider, Matthias: *Habitat- und Abflussmodellierung für Fließgewässer mit unscharfen Berechnungsansätzen*, 2001, ISBN 3-933761-11-5

109 Rathgeb, Andreas: *Hydrodynamische Bemessungsgrundlagen für Lockerdeckwerke an überströmbaren Erddämmen*, 2001, ISBN 3-933761-12-3

110 Lang, Stefan: *Parallele numerische Simulation instätionärer Probleme mit adaptiven Methoden auf unstrukturierten Gittern*, 2001, ISBN 3-933761-13-1

111 Appt, Jochen; Stumpp Simone: *Die Bodensee-Messkampagne 2001, IWS/CWR Lake Constance Measurement Program 2001*, 2002, ISBN 3-933761-14-X

112 Heimerl, Stephan: *Systematische Beurteilung von Wasserkraftprojekten,* 2002, ISBN 3-933761-15-8

113 Iqbal, Amin: *On the Management and Salinity Control of Drip Irrigation,* 2002, ISBN 3-933761-16-6

114 Silberhorn-Hemminger, Annette: *Modellierung von Kluftaquifersystemen: Geostatistische Analyse und deterministisch-stochastische Kluftgenerierung,* 2002, ISBN 3-933761-17-4

115 Winkler, Angela: *Prozesse des Wärme- und Stofftransports bei der In-situ-Sanierung mit festen Wärmequellen,* 2003, ISBN 3-933761-18-2

116 Marx, Walter: *Wasserkraft, Bewässerung, Umwelt - Planungs- und Bewertungsschwerpunkte der Wasserbewirtschaftung,* 2003, ISBN 3-933761-19-0

117 Hinkelmann, Reinhard: *Efficient Numerical Methods and Information-Processing Techniques in Environment Water,* 2003, ISBN 3-933761-20-4

118 Samaniego-Eguiguren, Luis Eduardo: *Hydrological Consequences of Land Use / Land Cover and Climatic Changes in Mesoscale Catchments*, 2003, ISBN 3-933761-21-2

119 Neunhäuserer, Lina: *Diskretisierungsansätze zur Modellierung von Strömungs- und Transportprozessen in geklüftet-porösen Medien*, 2003, ISBN 3-933761-22-0

120 Paul, Maren: *Simulation of Two-Phase Flow in Heterogeneous Poros Media with Adaptive Methods*, 2003, ISBN 3-933761-23-9

121 Ehret, Uwe: *Rainfall and Flood Nowcasting in Small Catchments using Weather Radar*, 2003, ISBN 3-933761-24-7

122 Haag, Ingo: *Der Sauerstoffhaushalt staugeregelter Flüsse am Beispiel des Neckars - Analysen, Experimente, Simulationen -,* 2003, ISBN 3-933761-25-5

123 Appt, Jochen: *Analysis of Basin-Scale Internal Waves in Upper Lake Constance,* 2003, ISBN 3-933761-26-3

124 Hrsg.: Schrenk, Volker; Batereau, Katrin; Barczewski, Baldur; Weber, Karolin und Koschitzky, Hans-Peter: *Symposium Ressource Fläche und VEGAS - Statuskolloquium 2003, 30. September und 1. Oktober 2003,* 2003, ISBN 3-933761-27-1

125 Omar Khalil Ouda: *Optimisation of Agricultural Water Use: A Decision Support System for the Gaza Strip,* 2003, ISBN 3-933761-28-0

126 Batereau, Katrin: *Sensorbasierte Bodenluftmessung zur Vor-Ort-Erkundung von Schadensherden im Untergrund*, 2004, ISBN 3-933761-29-8

127 Witt, Oliver: *Erosionsstabilität von Gewässersedimenten mit Auswirkung auf den Stofftransport bei Hochwasser am Beispiel ausgewählter Stauhaltungen des Oberrheins*, 2004, ISBN 3-933761-30-1

128 Jakobs, Hartmut: *Simulation nicht-isothermer Gas-Wasser-Prozesse in komplexen Kluft-Matrix-Systemen*, 2004, ISBN 3-933761-31-X

129 Li, Chen-Chien: *Deterministisch-stochastisches Berechnungskonzept zur Beurteilung der Auswirkungen erosiver Hochwasserereignisse in Flussstauhaltungen,* 2004, ISBN 3-933761-32-8

130 Reichenberger, Volker; Helmig, Rainer; Jakobs, Hartmut; Bastian, Peter; Niessner, Jennifer: *Complex Gas-Water Processes in Discrete Fracture-Matrix Systems: Upscaling, Mass-Conservative Discretization and Efficient Multilevel Solution,* 2004, ISBN 3-933761-33-6

131 Hrsg.: Barczewski, Baldur; Koschitzky, Hans-Peter; Weber, Karolin; Wege, Ralf: *VEGAS - Statuskolloquium 2004,* Tagungsband zur Veranstaltung am 05. Oktober 2004 an der Universität Stuttgart, Campus Stuttgart-Vaihingen, 2004, ISBN 3-933761-34-4

132 Asie, Kemal Jabir: *Finite Volume Models for Multiphase Multicomponent Flow through Porous Media*. 2005, ISBN 3-933761-35-2

133 Jacoub, George: *Development of a 2-D Numerical Module for Particulate Contaminant Transport in Flood Retention Reservoirs and Impounded Rivers,* 2004, ISBN 3-933761-36-0

134 Nowak, Wolfgang: *Geostatistical Methods for the Identification of Flow and Transport Parameters in the Subsurface,* 2005, ISBN 3-933761-37-9

135 Süß, Mia: *Analysis of the influence of structures and boundaries on flow and transport processes in fractured porous media*, 2005, ISBN 3-933761-38-7

136 Jose, Surabhin Chackiath: *Experimental Investigations on Longitudinal Dispersive Mixing in Heterogeneous Aquifers,* 2005, ISBN: 3-933761-39-5

137 Filiz, Fulya: *Linking Large-Scale Meteorological Conditions to Floods in Mesoscale Catchments,* 2005, ISBN 3-933761-40-9

138 Qin, Minghao: *Wirklichkeitsnahe und recheneffiziente Ermittlung von Temperatur und Spannungen bei großen RCC-Staumauern*, 2005, ISBN 3-933761-41-7

139 Kobayashi, Kenichiro: *Optimization Methods for Multiphase Systems in the Subsurface - Application to Methane Migration in Coal Mining Areas*, 2005, ISBN 3-933761-42-5

140 Rahman, Md. Arifur: *Experimental Investigations on Transverse Dispersive Mixing in Heterogeneous Porous Media,* 2005, ISBN 3-933761-43-3

141 Schrenk, Volker: *Ökobilanzen zur Bewertung von Altlastensanierungsmaßnahmen,* 2005, ISBN 3-933761-44-1

142 Hundecha, Hirpa Yeshewatesfa: *Regionalization of Parameters of a Conceptual Rainfall-Runoff Model*, 2005, ISBN: 3-933761-45-X

143 Wege, Ralf: *Untersuchungs- und Überwachungsmethoden für die Beurteilung natürlicher Selbstreinigungsprozesse im Grundwasser,* 2005, ISBN 3-933761-46-8

144 Breiting, Thomas: *Techniken und Methoden der Hydroinformatik - Modellierung von komplexen Hydrosystemen im Untergrund*, 2006, 3-933761-47-6

145 Hrsg.: Braun, Jürgen; Koschitzky, Hans-Peter; Müller, Martin: *Ressource Untergrund: 10 Jahre VEGAS: Forschung und Technologieentwicklung zum Schutz von Grundwasser und Boden,* Tagungsband zur Veranstaltung am 28. und 29. September 2005 an der Universität Stuttgart, Campus Stuttgart-Vaihingen, 2005, ISBN 3-933761-48-4

146 Rojanschi, Vlad: *Abflusskonzentration in mesoskaligen Einzugsgebieten unter Berücksichtigung des Sickerraumes,* 2006, ISBN 3-933761-49-2

147 Winkler, Nina Simone: *Optimierung der Steuerung von Hochwasserrückhaltebecken-systemen,* 2006, ISBN 3-933761-50-6

148 Wolf, Jens: *Räumlich differenzierte Modellierung der Grundwasserströmung alluvialer Aquifere für mesoskalige Einzugsgebiete*, 2006, ISBN: 3-933761-51-4

149 Kohler, Beate: *Externe Effekte der Laufwasserkraftnutzung*, 2006, ISBN 3-933761-52-2

150 Hrsg.: Braun, Jürgen; Koschitzky, Hans-Peter; Stuhrmann, Matthias: *VEGAS-Statuskolloquium 2006,* Tagungsband zur Veranstaltung am 28. September 2006 an der Universität Stuttgart, Campus Stuttgart-Vaihingen, 2006, ISBN 3-933761-53-0

151 Niessner, Jennifer: *Multi-Scale Modeling of Multi-Phase - Multi-Component Processes in Heterogeneous Porous Media*, 2006, ISBN 3-933761-54-9

152 Fischer, Markus: *Beanspruchung eingeerdeter Rohrleitungen infolge Austrocknung bindiger Böden,* 2006, ISBN 3-933761-55-7

153 Schneck, Alexander: *Optimierung der Grundwasserbewirtschaftung unter Berücksichtigung der Belange der Wasserversorgung, der Landwirtschaft und des Naturschutzes*, 2006, ISBN 3-933761-56-5

154 Das, Tapash: *The Impact of Spatial Variability of Precipitation on the Predictive Uncertainty of Hydrological Models,* 2006, ISBN 3-933761-57-3

155 Bielinski, Andreas: *Numerical Simulation of CO_2 sequestration in geological formations*, 2007, ISBN 3-933761-58-1

156 Mödinger, Jens: *Entwicklung eines Bewertungs- und Entscheidungsunterstützungssystems für eine nachhaltige regionale Grundwasserbewirtschaftung*, 2006, ISBN 3-933761-60-3

157 Manthey, Sabine: *Two-phase flow processes with dynamic effects in porous media - parameter estimation and simulation,* 2007, ISBN 3-933761-61-1

158 Pozos Estrada, Oscar: *Investigation on the Effects of Entrained Air in Pipelines,* 2007, ISBN 3-933761-62-X

159 Ochs, Steffen Oliver: *Steam injection into saturated porous media – process analysis including experimental and numerical investigations*, 2007, ISBN 3-933761-63-8

160 Marx, Andreas: *Einsatz gekoppelter Modelle und Wetterradar zur Abschätzung von Niederschlagsintensitäten und zur Abflussvorhersage, 2007,* ISBN 3-933761-64-6

161 Hartmann, Gabriele Maria: *Investigation of Evapotranspiration Concepts in Hydrological Modelling for Climate Change Impact Assessment*, 2007, ISBN 3-933761-65-4

162 Kebede Gurmessa, Tesfaye: *Numerical Investigation on Flow and Transport Characteristics to Improve Long-Term Simulation of Reservoir Sedimentation*, 2007, ISBN 3-933761-66-2

163 Trifković, Aleksandar: *Multi-objective and Risk-based Modelling Methodology for Planning, Design and Operation of Water Supply Systems*, 2007, ISBN 3-933761-67-0

164 Götzinger, Jens: *Distributed Conceptual Hydrological Modelling - Simulation of Climate, Land Use Change Impact and Uncertainty Analysis*, 2007, ISBN 3-933761-68-9

165 Hrsg.: Braun, Jürgen; Koschitzky, Hans-Peter; Stuhrmann, Matthias: *VEGAS – Kolloquium 2007,* Tagungsband zur Veranstaltung am 26. September 2007 an der Universität Stuttgart, Campus Stuttgart-Vaihingen, 2007, ISBN 3-933761-69-7

166 Freeman, Beau: *Modernization Criteria Assessment for Water Resources Planning; Klamath Irrigation Project, U.S.*, 2008, ISBN 3-933761-70-0

167 Dreher, Thomas: *Selektive Sedimentation von Feinstschwebstoffen in Wechselwirkung mit wandnahen turbulenten Strömungsbedingungen*, 2008, ISBN 3-933761-71-9

168 Yang, Wei: *Discrete-Continuous Downscaling Model for Generating Daily Precipitation Time Series*, 2008, ISBN 3-933761-72-7

169 Kopecki, Ianina: *Calculational Approach to FST-Hemispheres for Multiparametrical Benthos Habitat Modelling,* 2008*,* ISBN 3-933761-73-5

170 Brommundt, Jürgen: *Stochastische Generierung räumlich zusammenhängender Niederschlagszeitreihen*, 2008, ISBN 3-933761-74-3

171 Papafotiou, *Alexandros: Numerical Investigations of the Role of Hysteresis in Heterogeneous Two-Phase Flow Systems*, 2008, ISBN 3-933761-75-1

172 He, Yi: *Application of a Non-Parametric Classification Scheme to Catchment Hydrology*, 2008, ISBN 978-3-933761-76-7

173 Wagner, Sven: *Water Balance in a Poorly Gauged Basin in West Africa Using Atmospheric Modelling and Remote Sensing Information*, 2008, ISBN 978-3-933761-77-4

174 Hrsg.: Braun, Jürgen; Koschitzky, Hans-Peter; Stuhrmann, Matthias; Schrenk, Volker: *VEGAS-Kolloquium 2008 Ressource Fläche III*, Tagungsband zur Veranstaltung am 01. Oktober 2008 an der Universität Stuttgart, Campus Stuttgart-Vaihingen, 2008, ISBN 978-3-933761-78-1

175 Patil, Sachin: *Regionalization of an Event Based Nash Cascade Model for Flood Predictions in Ungauged Basins*, 2008, ISBN 978-3-933761-79-8

176 Assteerawatt, Anongnart: *Flow and Transport Modelling of Fractured Aquifers based on a Geostatistical Approach,* 2008, ISBN 978-3-933761-80-4

177 Karnahl, Joachim Alexander: *2D numerische Modellierung von multifraktionalem Schwebstoff- und Schadstofftransport in Flüssen*, 2008, ISBN 978-3-933761-81-1

178 Hiester, Uwe: *Technologieentwicklung zur In-situ-Sanierung der ungesättigten Bodenzone mit festen Wärmequellen,* 2009, ISBN 978-3-933761-82-8

179 Laux, Patrick: *Statistical Modeling of Precipitation for Agricultural Planning in the Volta Basin of West Africa,* 2009, ISBN 978-3-933761-83-5

180 Ehsan, Saqib: *Evaluation of Life Safety Risks Related to Severe Flooding,* 2009, ISBN 978-3-933761-84-2

181 Prohaska, Sandra: *Development and Application of a 1D Multi-Strip Fine Sediment Transport Model for Regulated Rivers,* 2009, ISBN 978-3-933761-85-9

182 Kopp, Andreas: *Evaluation of CO_2 Injection Processes in Geological Formations for Site Screening,* 2009, ISBN 978-3-933761-86-6

183 Ebigbo, Anozie: *Modelling of biofilm growth and its influence on CO_2 and water (two-phase) flow in porous media,* 2009, ISBN 978-3-933761-87-3

184 Freiboth, Sandra: *A phenomenological model for the numerical simulation of multiphase multicomponent processes considering structural alterations of porous media*, 2009, ISBN 978-3-933761-88-0

185 Zöllner, Frank: *Implementierung und Anwendung netzfreier Methoden im Konstruktiven Wasserbau und in der Hydromechanik*, 2009, ISBN 978-3-933761-89-7

186 Vasin, Milos: *Influence of the soil structure and property contrast on flow and transport in the unsaturated zone*, 2010, ISBN 978-3-933761-90-3

187 Li, Jing: *Application of Copulas as a New Geostatistical Tool*, 2010, ISBN 978-3-933761-91-0

188 AghaKouchak, Amir: *Simulation of Remotely Sensed Rainfall Fields Using Copulas*, 2010, ISBN 978-3-933761-92-7

189 Thapa, Pawan Kumar: *Physically-based spatially distributed rainfall runoff modelling for soil erosion estimation*, 2010, ISBN 978-3-933761-93-4

190 Wurms, Sven: *Numerische Modellierung der Sedimentationsprozesse in Retentionsanlagen zur Steuerung von Stoffströmen bei extremen Hochwasserabflussereignissen*, 2010, ISBN 978-3-933761-94-1

191 Merkel, Uwe: *Unsicherheitsanalyse hydraulischer Einwirkungen auf Hochwasserschutzdeiche und Steigerung der Leistungsfähigkeit durch adaptive Strömungsmodellierung*, 2010, ISBN 978-3-933761-95-8

192 Fritz, Jochen: *A Decoupled Model for Compositional Non-Isothermal Multiphase Flow in Porous Media and Multiphysics Approaches for Two-Phase Flow*, 2010, ISBN 978-3-933761-96-5

Die Mitteilungshefte ab der Nr. 134 (Jg. 2005) stehen als pdf-Datei über die Homepage des Instituts: www.iws.uni-stuttgart.de zur Verfügung.